WADC TR 54-120 Part 2 APRIL 1955

AN INVESTIGATION OF INTERGRANULAR OXIDATION IN STAINLESS STEELS AND HIGH-NICKEL ALLOYS

Clarence A. Siebert
Maurice J. Sinnott
Lynn H. DeSmyter
Robert E. Keith

University of Michigan

Engineering Research Institute Project No. 2110-5-F
Materials Laboratory
Contract No. AF 33(616)-353
Project No. 7351
Task No. 73512

United States Air Force
Wright Air Development Center
Air Research and Development Command
Wright-Patterson Air Force Base, Ohio

FOREWORD

This report was prepared by the University of Michigan, under USAF Contract No. AF 33(616)-353. The contract was initiated under Project No. 7351, "Metallic Materials", Task No. 73512, "High Temperature Alloys", formerly RDO No. 615-13, "High Temperature Alloys", and was administered under the direction of the Materials Laboratory, Directorate of Research, Wright Air Development Center with Lt J. R. Miller acting as project engineer.

ABSTRACT

Chromel alloys ASM, ARM, and D, and type 310 stainless steels were oxidized for 100-hour periods in the stressed condition. The above alloys and Inconel were oxidized for times up to 500 hours in the unstressed condition. Intergranular oxidation measurements were obtained microscopically. The influence of stress was to cause an increase in the intergranular penetration when a minimum stress was reached. In general, the intergranular penetration increased with increasing time and temperature. Increasing the water-vapor content of the air increased the intergranular penetration slightly. The effect of a preferred orientation decreased the intergranular penetration slightly. The weight gained during oxidation was determined. It was found that in the alloys tested that a plot of the square of the specific weight gain versus temperature resulted in a straight-line relationship. Visual and magnetic examinations were made on the oxidized specimens and their oxides. No correlation between these observations and oxidation properties could be determined. X-ray diffraction patterns were made on representative oxides. This analysis showed the scales encountered to be of a protective nature by Randall and Robbs criteria of the presence of Cr_2O_3 or high-parameter spinel. Electron diffraction examination of the subsurface structure was performed on type 310 stainless steels oxidized in the unstressed condition. It was found that the oxidation products in the subsurface region were substantially the same as the surface oxides as determined by x-ray diffraction techniques.

PUBLICATION REVIEW

This report has been reviewed and is approved.

FOR THE COMMANDER:

M. R. WHITMORE
Technical Director
Materials Laboratory
Directorate of Research

TABLE OF CONTENTS

LIST OF ILLUSTRATIONS

LIST OF ILLUSTRATIONS
(continued)

LIST OF TABLES

INTRODUCTION

It has been established by numerous investigators that grain-boundary diffusion can be greater than the lattice or volume diffusion. Since the oxidation process is primarily controlled by diffusion rates, it is not surprising that the oxidation rates of the grain boundary can be greater than that of the metal matrix. This report is primarily concerned with this grain-boundary oxidation although the volume or lattice oxidation rate will affect the measured grain-boundary oxidation rate and therefore must be considered as well.

Compared with the total volume of literature concerning the subject of oxidation, the portion concerned with intergranular oxidation is small. Intergranular oxidation becomes an important factor when thin sections are exposed to an oxidizing medium, since under these conditions the portion of the metal influenced by these oxide fissures is a significant percentage of the whole. Because of these facts the program outlined below used materials of about 0.05 of an inch thick.

The present program arose from the need of the U. S. Air Force for information concerning intergranular oxidation in the temperature range of 1600° to 2000°F. There were six objectives in this research program:

1. to determine the effect of temperatures between 1600° and 2000°F on intergranular oxidation,
2. to examine the effects of alloy composition on intergranular oxidation,
3. to determine the nature of the penetrating material in areas of intergranular attack,
4. to determine the effect of stress on intergranular oxidation,
5. to determine the effect of moisture content of air on intergranular oxidation, and
6. to determine the effect of a preferred orientation on intergranular oxidation.

During the past year the major efforts have been concentrated on objectives through 4.

EQUIPMENT

In addition to the unstressed oxidation equipment used during the previous year (1) the oxidation equipment consisted of stressed oxidation units, progressive weight-gain equipment, and apparatus for humid atmosphere generation.

Stressed Oxidation Equipment

The stressed oxidation equipment consisted of three direct load units as shown schematically in Fig. 1. This type of unit was considered more applicable than a beam-loaded unit because the loads used were small, and because the in-line

suspension resulted in less eccentricity in the sample. The sample and suspension were entirely suspended on ball and socket joints as shown in Fig. 2. To determine the eccentricity of the system a 1/8- x 1- x 18-inch flatground stock was made into a standard sheet specimen and equipped with SR4-A12 strain gauges attached to both flat surfaces of the test specimen. The stress-strain curve, which was obtained by progressively loading the system, had essentially the same slope for each gauge position. This system was a considerable improvement over the clamp-type grips tested. The ground stock was used to assure that the suspension was being tested and not the specimen flatness.

The vertical-stress oxidation furnaces, although shorter, were similar to the horizontal furnaces used in the previous work with the following two exceptions: (1) more windings were placed on the bottom and top of the furnace to correct for draft effects; and (2) the furnace core consisted of Chromel wire covered inside and out with alundum cement. A temperature survey showed the 2-inch oxidation zone to be essentially flat (± 3°F) and little variation for the next inch above and below this zone. The furnaces were controlled from a control thermocouple placed close to the furnace windings. This type of control demonstrated no thermal cycling on a recorder sensitive to a temperature change of 3°F. It was estimated that natural convection in the furnace roughly corresponded to the low flow rates used in the horizontal furnace. Since no variation in intergranular penetration was observed with varying flow rates (1) this natural convection was considered adequate.

Humidifying Equipment

A humidifier was constructed for producing air of various dewpoints. The air was humidified by passing it countercurrently through heated water sprayed over a column packed with porcelain saddles as shown in Fig. 3. It was found that humidity could be controlled to ± 2°F over a 100-hour run, and maintained at any mean value from minus 60°F to plus 120°F by mixing the humidified air with dry air.

Weight-Gain Equipment

The equipment for the determination of the increase in weight of a material while it is being oxidized consists principally of a vertical furnace, an analytical balance, a sample suspension, and an atmosphere system, as shown in Fig. 4. The furnace was duplicate of the furnaces used in unstressed oxidation studies previously described (1). The specimen to be oxidized was suspended from the balance by the platinum wire, and dry air was metered through the furnace, being heated by the porcelain chips in the lower portion.

This method of obtaining oxidation data has been criticized in the past since scale may flake off during the test. The scales encountered in the alloys used in this investigation were very adherent at the testing temperature. Since no significant jumps were encountered in the weight-gain data, this factor was considered to be a minor one.

Specimen Preparation

The specimens for the unstressed oxidation and electron diffraction tests were standard 1-1/2-inch samples of the type used during the previous investigation (1). Stressed oxidation specimens were prepared as standard strip specimens, as illustrated in Fig. 2. Special care was used to keep foreign materials and scratches from the 1/2- x 2-inch gauge portion of the specimen since the samples for intergranular penetration measurements were taken from this section.

Texture specimens for work on preferred orientation were prepared by cold-rolling the 310 RA alloy 97-98%, and shearing the material into standard, unstressed oxidation specimens. In order to indicate the oxidation in specimens without a texture, control samples were made by cutting the 1/2-inch as-received stock lengthwise and cold-working about 10% to produce a material with a surface similar to that of the textured specimens. This resulted in samples about 3/16-inch thick in the 10% reduced reference material and 1/32 inch in thickness in the 97% reduced material. Both samples were given a 2000°F anneal for 4-1/2 hours in dry argon (dewpoint, minus 60°F) in an attempt to produce an annealing texture in the highly reduced material.

The specimens for the weight-gain measurements were 2- x 1-inch rectangles of the as-received material containing a 1/64-inch hole near the top for the insertion of the platinum suspension wire.

Equipment Operation

When the furnaces had reached thermal equilibrium the specimens were loaded into the furnace. At the conclusion of the run the stressed and unstressed samples were quenched in distilled water. This was done to help preserve the high-temperature phases for x-ray and electron diffraction studies. After the samples were quenched, the contents were filtered through coarse filter paper and washed with acetone and then ether to accelerate the drying of the loose scale which flaked off on quenching. When the filter paper had dried, the contents were bottled along with any scale which could be removed by gentle scraping with a surgical scalpel. The total elapsed time between quenching and bottling was about 45 minutes. The visual appearance of the samples was recorded.

The percentage elongation which occurred during the test, was determined by measuring the extension of gauge punch marks placed 2 inches apart in the reduced section of the specimen.

The samples used for penetration evaluation were sectioned as shown in Fig. 5, and bent 90° to assure perpendicularity in mounting. The bent samples were given a qualitative magnetic test (1), mounted in bakelite, and polished on a water-cooled belt sander using 120- and 240-grit silicon carbide paper. This was followed by a semifinal polish on 1-micron diamond paste which resulted in a sample with a good edge, retained inclusions and oxide stringers, and was reasonably free of scratches. A final polish consisting of Linde A (levigated alumna) paste, of sufficient thick-

ness to avoid contact with the polishing cloth, removed the remaining scratches and did not tear out inclusions or oxide stringers.

Evaluation of Specimens

The mounted and polished samples were measured to determine the extent of intergranular penetration. The mean depth ($\bar{X}$)and the total number of penetrations (N) were then determined from the penetration measurements. A complete description of the method of taking penetration data as well as a development of the penetration parameters is given in the previous year's report (1).

In brief, the method consisted of examining the polished specimen at 500 diameters using a calibrated, No. 6 grain-size eye piece. The grid, containing 6 squares on the side was aligned with the specimen edge, and the number of penetrations and their depths were obtained by traversing the edge over a distance of approximately 2 inches. As was expected, the greatest uncertainty was encountered in the very small penetrations, that is, those less than 1 grid in depth. Repeated measurements by various operators indicated that individual variability, considering the first grid penetrations, was approximately 20% in samples extremely difficult to evaluate, and about 10% in the more easily counted samples. The variability encountered in penetrations extending deeper (those in the second, third, etc., grids) was approximately 5%.

After the penetration measurements were completed, the specimens were given a careful metallographic examination in the etched and unetched conditions. Unusual or significant areas were examined under oblique, polarized, and dark field illumination. Some of the specimens exhibited fissures throughout the matrix, as shown in Fig. 6, which made it impossible to determine intergranular penetrations due to oxidation.

Evaluation of Oxide Scales

The oxide scale was examined visually and tested for magnetism (1). Powdered oxide samples were prepared for x-ray examination, and diffraction patterns obtained using either a 57.5- or 114-mm camera. The values of interplaner spacings were obtained from the film by use of a transparent Nelson Nies x-ray diffraction scale. The values obtained with this method compared favorably with the values obtained by the more laborious direct reading of the film using a comparator, or by the use of a photometer trace.

Electron Diffraction

In an effort to determine the nature of the intergranular compounds, a technique was developed for examining the subsurface regions of oxidized specimens by means of reflection electron diffraction, a method well suited for the study of solid surface layers. The procedure which was followed on previously oxidized specimens consisted of the following steps:

1. All the external scale possible was removed by scraping, without

actually disturbing the metal surface itself. The scale thus collected was powdered and analyzed by x-ray diffraction.

2. Thickness measurements were made on the specimen at two points on the surface. One of these points was later to be subject to etching action while the other was to be protected from etching by Scotch tape, and thus, served as a reference standard for later thickness measurements. These measurements were made on a Pratt and Whitney supermicrometer accurate to 0.0001 inch. The assumption was that the etching attack on the exposed underside of the specimen was essentially uniform.
3. An electron diffraction pattern was made of the specimen surface, using an RCA Type EMD-2 electron diffraction apparatus.
4. The specimen was electrolytically etched for 15 to 30 sec in a mixture of 10% perchloric and 90% glacial acetic acids at a temperature of 15°C and a current density of 6 amp/in.^{2} This etching treatment has the property of removing the metal without disturbing the intergranular compounds (2).
5. An electron diffraction pattern was made of the exposed compounds.
6. The exposed compounds were brushed off the surface using a rotary wire brush on a hand-power tool. The brush did not damage the surface, and in addition, was much less likely to cause contamination than was an abrasive compound. The Scotch tape covering the unetched portion of the specimen was then removed.
7. Thickness measurements were made of the etched and unetched portions of the specimen as described in Step 2. By appropriate subtractions, the amount of metal removed in the etching operation could then be determined. A fresh piece of Scotch tape was then applied to the unetched portion of the surface and Steps 4 through 7 were repeated as many times as necessary to reach the depth in the specimen where diffraction patterns from the intergranular compounds no longer appeared.

The electron diffraction procedure outlined above made it possible to show any changes in the overall composition of the intergranular compounds resulting from oxidation as a function of their depth below the metal-oxide interface. For this part of the program, six heats were selected from the nine studied in the oxidation runs. In the case of the type 309 plus Nb and type 310, heats 64177 and 64270, specimens were studied following 100 hours of oxidation at 1600°, 1700°, 1800°, and 1900°F. For the heats X11306, X11338, and X27258, 2000°F specimens were studied in addition to the other four temperatures.

In connection with the electron diffraction studies, it should be mentioned that this method also has its limitations, although it is capable of use with extremely small amounts of materials, and is especially useful for thin films. The smallest uncertainty in interplanar spacing which can be expected using the reflection, electron diffraction technique is about 2%. Since this uncertainty is of the same order as the change in interplanar spacing between the diffraction patterns of Fe_2O_3 and Cr_2O_3, and between spinels having low and high lattice parameters, the electron diffraction studies can do little more in the present case than to indicate the presence or absence of the rhombohedral or cubic phases.

In evaluating the diffraction patterns obtained, the relative proportions of

spinel and rhombohedral phases shown in individual patterns were indicated by specifying whether the patterns of specific phases were strong (S), medium (M), weak (W), very weak (VW), or very, very weak (VVW) [see Table 5]. In addition, a qualitative attempt was made to show the diminution of diffracted intensity from intergranular oxides on individual specimens accompanying successive etches by referring intensities to those obtained in patterns taken prior to etching. It must be remembered, however, that comparison of relative intensities obtained in different exposures can be misleading, since many factors related to exposure and specimen surface preparation and alignment can influence the intensity obtained in a given pattern; and these factors vary among exposures.

MATERIAL

The material for this investigation (Table 1) was received in sheet and strip form and tested as described below:

1. Type 310 alloy, heats 64177, 64270, X11306, X11338, and X27258; and type 309 plus Nb.—This material was oxidized in the unstressed condition in horizontal tube furnaces and used for electron diffraction studies.
2. Type 310 alloy, heats X27258, X46572, 31372, J10, Vt-5, Vt-7; Inconel; and Chromel alloys ARM (heats A and B), ASM, and D.—These alloys were oxidized in the unstressed condition in horizontal tube furnaces and under stress in the stress units, and the intergranular penetration determined.
3. Type 310 alloy, heats X46572, J10, Vt-5, and Vt-7; and Chromel alloys ARM (heat A), ASM, and D.—These alloys were tested in the progressive weight-gain equipment.

RESULTS AND DISCUSSION

For the purposes of discussion the results of this investigation are divided into three parts, namely: (1) weight-gain investigation, (2) effect of stress, and (3) unstressed studies.

Weight-Gain Investigation

Since an apparently low rate of intergranular penetration may result from a small difference in the rates of grain-boundary and volume oxidation, it was necessary to determine a measure of the volume oxidation. The progressive weight-gain equipment was assembled to give an answer to this problem.

Table 2 indicates the progressive gain in weight per square inch of sample with increasing time. The experimental data were plotted as conventional weight-gain vs. time curves, and the data shown in Table 3 were taken from these curves. In general these curves follow the parabolic law of oxidation as is evidenced by the straight

lines obtained in plots of the square of the specific weight gained vs. time shown in Figs. 31 through 37. Alloy ASM showed a considerable deviation from this relationship at 2000°F. The line drawn through the 2000°F points is admittedly only a rough estimation of the weight gained, but it is useful for weight-gain rate comparisons with other alloys. Most samples show some deviation from the parabolic oxidation in the early stages. This initial deviation is to be expected for a number of reasons, some of which have been listed by Gulbransen (3); they are:

1. the effect of the decrease in roughness or surface area as the reaction proceeds,
2. the effect of the heat evolved in the reaction on the rate of reaction,
3. the effect of the solution of oxygen in the metal on the rate of reaction,
4. the effect of the concentration of impurities in the oxide during the early stages of the reaction,
5. the change in oxide composition, and
6. the influence of potential fields at the gas interface due to absorbed oxygen ions.

In addition to these theoretical deviations there were also some experimental variables which influenced the initial stages of the process, such as speed of loading, and the fact that a finite time is necessary to bring the metal to temperature. Because of these and other related factors the parabolic rate constant (slope of ΔW^2 vs. time curve) is probably a better indication of the volume oxidation than the other parameters. A slight inaccuracy is involved by ascribing all the weight gain to volume oxidation since the intergranular oxidation will also increase the weight of the sample, although this is thought to be a slight factor. Figure 38 is a rating of the alloys tested on the basis of the parabolic rate constant. A small value of this constant is indicative of a slow rate of oxidation. It is notable that the ASM alloy is significantly superior to the other alloys tested at all the temperatures used in this investigation. This difference is especially pronounced at 2000°F. Heat X46572, a commercial heat of type 310 stainless steel, showed the highest rate of oxidation at 1800° and 1900°F while its oxidation resistance is better than some of the other alloys at 2000°F.

Effect of Stress

In this phase of the work it was desired to determine the effect of stress on intergranular oxidation. Since each material has its own characteristic attributes, the alloys will be considered individually. All the data obtained for the stressed studies are summarized in Table 4; the key to the symbols used is given in Table 3. Included in this table are the results of the visual observations and magnetic measurements made on the oxidized samples and on the oxides which were removed from these samples. As in the previous investigation no correlation between these data and oxidation characteristics could be found.

Commercial Type 310 Alloys, Heats X27258 and X46572

Heat X27258 was the first material investigated under stressed conditions.

Unstressed studies during the previous year showed that this heat had comparatively good intergranular oxidation resistance, and subsequent tests showed it to have exceptional high-temperature properties. The highest stresses used are approximately the 100-hour rupture strength listed in the ASTM publication concerning the high-temperature properties of stainless steels (4). However, this heat showed little elongation even at the higher stresses and therefore does not adequately illustrate the effect of stress. The stress region, where elongation becomes appreciable and where the effect of stress on oxidation would be expected to increase, was only roughly determined when the available supply of material was exhausted.

Figures 39 through 41 and Table 4 show the number of penetrations per inch vs. the depth curves, as well as all the other penetration-frequency vs. depth curves encountered in this investigation, are of the general decay type described in the previous yearly report (1). Figure 42 illustrates the effect of stress on the number of intergranular penetrations, and Fig. 43 shows the effect of stress on the mean depth of penetration. The mean depth curves show a decrease in the mean depth of the slightly stressed samples over the unstressed values. Although this decrease is slight, it is consistent in all samples. At present no explanation for this observation has been found. It is to be emphasized that 0.0032 inch represents the smallest mean depth which can be determined with the present counting method. Therefore the relatively straight line in the 1600°F mean depth graph as shown in Fig. 43 indicates that most of the penetrations counted were in the first grid and not necessarily of the same depth.

In an effort to determine the reproducibility of the results, samples were run at 2460 and 2480 psi, respectively. As can be seen from Figs. 42 and 43, the reproducibility of the results is quite good.

Heat X46572 showed approximately the same unstressed intergranular penetration behavior as heat X27258, but relatively poor high-temperature properties. The test temperatures of 1800° and 1900°F were used, since the previous run indicated that the effect of stress would be more noticeable at these temperatures. Figures 44 and 45 indicate the penetration frequency at various depths and stress levels, and Figs. 46 through 49 show the variation in penetration number and mean depth, with stress as well as the elongation encountered at the various stress levels. The penetration-frequency curves show a general increase in penetration depth with increasing stress, especially in the case of the deeper penetrations. The 1500-psi graph is an exception in that the sample contained considerably more penetrations; and penetrations of a greater depth on one side of the specimen compared with the other side. This persisted even after repeated polishing. When fissures of considerable depth are present there is a tendency to overlook some of the very small penetrations. This, in addition to the greater uncertainty in the small fissures, can account in part for the small number of shallow fissures counted in the 1500- and 1650-psi samples.

The mean depth graphs show a considerable increase in depth when the elongation becomes greater than approximately 15%. These depth graphs are probably more significant than the number graphs since the weighted average minimizes the effect of the small penetrations.

Figures 7 and 8 are photomicrographs illustrating the effect of stress on intergranular penetration. A comparison of Figs. 7 and 8 shows that a stress of

2480 psi increased the depth of the fissures.

The points on the graphs showing the effect of stress on the mean depth and number of penetrations, with a vertical arrow extending through the point, indicate the lowest stress of those used, at which the sample contained fissures throughout the matrix. The 1900°F, 1750-psi sample showed some of these fissures throughout as shown in Fig. 9. In general, samples which exhibited this phenomenon were not counted because these fissures are the beginning of a stress rupture failure, and would therefore be misleading in a count of intergranular oxidation penetrations. However, it was noticed that the intergranular oxidation in specimens which showed these fissures throughout had occurred to a greater depth than was the case at stress levels where fissuring throughout did not occur. An interesting characteristic of the type 310 material, which exhibited these fissures throughout, is the appearance of an excess phase as shown in Figs. 10 and 11. Microhardness impressions shown in Fig. 10 indicate that the excess phase is much harder than the matrix. Although it has not been positively established, it is thought that this phase is a high nitrogen-chromium compound. A chemical analysis on a similar phase found in creep-rupture specimens of 18-8 stainless steel by Smith (5) indicated that it was high nitrogen phase. Since this phase was only found in quantity in specimens which were fissured throughout, and therefore beyond the range of practical stresses, it was not deemed advisable to investigate the nature of this phase at the present time.

Vacuum-Melted Type 310 Alloy; Heats Vt-5, Vt-7, and J10

This material contained a considerable quantity of inclusions as can be seen from Fig. 12. All three heats have the same grain size as typified by the above figure. All the vacuum-melted stock was tested in the unstressed condition and heats Vt-5 and Vt-7 were also tested in the stressed condition. It is to be emphasized that these heats differ markedly from the commercial type 310 material, with respect to the amounts of the minor elements present, as can be seen from Table 1. This alloy is essentially an iron, chromium, nickel alloy, and it is known that the minor elements such as carbon, silicon, and nitrogen have a pronounced effect on the properties of the commercial type 310 alloy. Figures 50 through 52 indicate the effect of temperature on the penetration frequency at various depths in the unstressed condition. Figures 53 through 58 show the effect of temperature on the number and mean depth of penetrations. It can be seen that the number of penetrations per inch and the mean depth of penetrations are extremely small. The number of fissures is relatively independent of temperature, and the mean depth increases only slightly with increasing temperature. This apparently good, intergranular penetration resistance may be the result of the relatively high-volume oxidation rates in the case of heats Vt-5 and Vt-7 as indicated in Fig. 38. The J10 alloy, however, has relatively good intergranular and volume oxidation resistance.

Heats Vt-5 and Vt-7 have relatively poor properties under stress as revealed by the frequency vs. depth, and number and mean depth vs. stress graphs shown in Figs. 59 through 66. This is probably due in part to lower creep resistance caused by the extremely low-carbon contents of these alloys (Table 1). The effect of stress on the intergranular penetration is similar to that observed in heat X46572 of type 310 stainless alloy previously discussed, except that the increase in pene-

tration depth and number due to stress appears at a lower value. The sample of heat Vt-5 which was run at 1900°F and 750-psi stress was counted for intergranular penetration even though it showed a few fissures throughout the matrix. This sample showed a marked increase in the mean depth of intergranular oxidation.

Figure 13 shows the edge of a sample which contained fissures throughout. Note the completely encircled grain, a phenomenon which was occasionally observed. The photomicrograph also shows a considerable amount of thickening of the oxide at the boundary. Figure 14 illustrates a similar case, as well as some islands of metal in the oxide phase, presumed to be nickel-rich as found by other investigations (6).

Chromel Alloys D, ASM, and ARM (Heats A and B)

All these alloys were first tested in the unstressed condition. Figure 67 through 70 illustrate the variation in penetration frequency and Figs. 71 and 72 show the effect of stress on the number and mean depth of penetrations. Chromel alloys ARM (heats A and B), ASM, and D, showed a general increase in intergranular penetration resistance at 2000°F in the above order, D being the best, considering the mean depth to be the more significant measure. The number of fissures vs. temperature graphs show all alloys to have a comparatively large number of penetrations, the ASM material showing the largest number encountered in this investigation. Figure 15 shows a surface layer of small grains which could account for this large number of fissures. Although the other Chromel alloys showed a similar abnormality at the surface it is thought that the higher-volume oxidation in these alloys eliminated the affected surface region. The increased intergranular penetration resistance of the Chromel D and ASM alloys is apparently the result of a decrease in intergranular oxidation and not merely an increase in volume oxidation. This is shown by the volume-oxidation-rate constant (Fig. 38) which is low in the case of Chromel D, and extremely low in the case of the ASM alloy.

Chromel D, ARM (heat A), and ASM alloys were also tested in the stressed condition. Figures 73 through 81 show the effect of stress on the penetration frequency, and Figs. 82 through 99 show the effect of stress on the number of penetrations and mean depth. In general the penetration-frequency curves show an increase in fissure frequency at the greater depths as the stress is increased. The ARM (heat A) material was tested at more frequent stress intervals than the other Chromel alloys and therefore more completely illustrates the effect of low stresses. The mean depth graphs (Figs. 83, 85, and 87) show a decrease in depth in the slightly stressed samples over the unstressed values in every instance. This phenomenon was also noticed in type 310 alloy, heat X27258. As mentioned previously no explanation for this decrease has been found. When the elongation becomes appreciable the mean depth increases, and as the point at which fissures are observed throughout the matrix is approached, the depth increases greatly. This increase in depth is due in part to the appearance of some deep fissures which occur in the highly stressed samples. Figure 16 shows one of these fissures which occurred in the 1900°F, 500-psi Chromel ARM (heat A) material, and Fig. 17 shows the normal penetrations which occurred in the 1900°F, 250-psi sample of the same material. The latter penetrations are typical of the unstressed material. Samples which exhibited these fissures throughout also contain an excess phase, although not in the quantities or form encountered in the type 310 material. Figure 18 shows this phase in the Chromel material. It can be seen by comparing Fig. 18 with Figs. 10 and 11 of type 310 alloy that the phase

is more agglomerated and widely dispersed in the Chromel material than in the type 310 alloys.

Unstressed Studies

In addition to the runs used for electron diffraction, weight gain, and stress studies previously discussed, unstressed runs were made to obtain unstressed data on type 310 alloy (heat J10) and Inconel, and to test the effect of increased humidity, extended time, and preferred orientation on intergranular penetration. The J10 material was discussed in connection with the other vacuum-melted alloys in the stressed section of the results.

Inconel.—Inconel was subjected to unstressed oxidation for times of 10, 30, and 100 hours at temperatures of 1600° through 2000°F at 100° increments, using dried air having a velocity of 30 ft/sec. The number of penetrations increases at the higher temperatures as can be seen from penetration-frequency vs. temperature graphs shown in Figs. 100 through 102. These penetrations are shallow, however, as shown by Figs. 103 and 104. Increasing the oxidation times from 10 to 100 hours has little effect on the mean depth. This small dependency of depth on oxidation time from 10 to 100 hours was also found in studies on type 310 alloys in work done during the previous year (1).

Effect of Time.—Since little variation in intergranular penetration was encountered with variation in oxidation time from 10 to 100 hours, a 500-hour test was performed on type 310 alloy (heat X27258), Chromel ARM material (heat A), and Inconel to determine the effect of a fivefold increase in time over the longest previous run. The temperature used was 1900°F and the air velocity was 30 ft/min. Figure 105 shows the frequency vs. depth curves for the 500-hour run. Since some of the number of small penetrations were off the scale in Fig. 105, the number of penetrations at various depths, the mean depth, and the total number of penetrations in the above materials for the 100- and 500-hour runs are given in Table 5. As can be seen from this table the 500-hour treatment on the type 310 alloy, heat X27258, resulted in a much greater number of penetrations and a greater mean depth than a 100-hour exposure. Figures 19 and 20 show the microstructure of the intergranular penetration in the 100- and 500-hour test for the type 310 material. In general the 500-hour treatment resulted in a much thicker scale layer and in wider penetrations than those observed for the 100-hour test. This increased thickness of the fissures is probably due to lateral volume oxidation from existing intergranular penetrations. The 500-hour treatment also forms a deeper and more continuous penetration.

The greater number of fissures in the 500-hour test is due in part to the fact that in the 100-hour run some very small entries may be considered surface imperfections and therefore not counted. However, after a 500-hour exposure these slight penetrations were deep enough to remove any doubt that they are real. Table 5 also shows a fewer number of very small penetrations in the 500-hour run. This is probably a result of initial entries progressing to the medium depths. The Chromel alloy acts similarly to the type 310 alloy just described. The Inconel alloy acts differently as can be seen from Fig. 105 and Table 5. The mean depth of the penetrations is not altered appreciably by increasing the time of exposure to 500 hours, although the number has increased.

Effect of Humidity.—The great majority of the unstressed oxidation runs made during this investigation were done in air with the dewpoint close to minus 60°F. To check the effect of a higher humidity on intergranular oxidation, type 310 alloy, heats X46572 and J10, and Chromel alloy ASM were tested in air having a dewpoint of plus 60°F. The temperatures used during the 100-hour test were 1700°, 1800°, 1900°, and 2000°F, and the air velocity was the standard 30 ft/min. Figures 106 through 110 show penetration frequency vs. depth graphs and the mean depth and number vs. temperature graphs. By comparing these curves with those obtained in the dry air test shown in Figs. 50, 53, and 54, and Table 6, it can be seen that the general effect of a high dewpoint is to increase the number and depths of penetrations. This increase in number is considerable, being of the order of 25%, while the increase in mean depth is very small in the Chromel ASM and J10 alloy, and of the order of 15% in the type 310 alloy, heat X46572.

Texture Studies.—From theoretical considerations it seems likely that if it were possible to introduce a very strong preferred orientation into the stainless steel, a profound decrease in intergranular oxidation should result. The line of reasoning behind this argument is as follows: intergranular oxidation is apparently a manifestation of preferential diffusion of O ions along grain boundaries. From recent studies of grain-boundary diffusion, it is known that the ratio of the grain-boundary diffusion coefficient to the volume diffusion coefficient is strongly dependent on the relative orientation of the grains on either side of the boundary in question, this ratio decreasing to approximately unity for small angular misalignments between grains. The criterion of a strong preferred orientation is the existence of just such small angular misalignments among a majority of the grains of the metal. If, therefore, a thermally stable, strong preferred orientation could be introduced, intergranular oxidation should be significantly decreased in amount.

The requirement of thermal stability of the preferred orientation rules out the consideration of rolling textures, leaving only the possibility of recrystallization textures. Of the possible recrystallization textures which can occur, the well-known "cube" texture, which is formed in face-centered-cubic metals under suitable conditions, is outstanding for its high degree of orientation. The cube, or (100) [100], texture, in those metals in which it can be caused to form, results from a high-temperature anneal following an extremely heavy cold-working operation. It is also known that in some cases the presence of small amounts of impurities, such as As in Cu, will prevent the formation of a cube texture.

An attempt was made to produce an annealing texture in the type 310 alloy, heat 31372, as described in the procedure section. Forward-reflection Debye x-ray patterns were made of the material in the as-rolled and the rolled and annealed conditions. These patterns appear in Figs. 21 and 22. A strong rolling texture was developed, but this texture failed to transform to a strong recrystallization texture on annealing. Recrystallization did take place during the anneal, however, as is evidenced by the discrete spots; some degree of preferred orientation resulted.

Runs were made at temperatures of 1600°, 1700°, 1800°, 1900°, and 2000°F for 100 hours, in which each furnace was at a different temperature and contained a 97% cold-worked and annealed reference specimen and a 10% reduced and annealed reference specimen. Following the run, the specimens were quenched, mounted, polished, and examined in the usual manner. The penetration vs. depth curves resulting from this examination are presented in Figs. 111 and 112, and the penetration-frequency

and depth-parameter curves appear in Figs. 113 and 114. As the latter pair of figures shows, there was not a great deal of difference in penetration characteristics resulting from the two treatments. It does appear that at the higher temperatures the 97% cold-worked and annealed material was superior.

It was noted that the 97% cold-worked and annealed material possessed an extremely adherent, reddish-brown oxide, which appeared to be considerably thicker than the oxides usually encountered, while the oxide produced on the reference specimens was black and very loosely adherent. This difference may have resulted in part from the difference in cooling rate encountered due to the variation in size of the two materials.

Figures 23 and 24 show the microstructures after the oxidation treatment in the 97% cold-worked and annealed material and in the 10% reduced and annealed material. The intergranular penetrations in the 10% reduced material are different from any observed in the other type 310 alloys, being considerably thicker throughout. The structure observed in the texture specimen is more typical of the other type 310 alloys.

A more extensive program to attempt to produce a more pronounced texture was not undertaken because the other phases of this investigation utilized all the available time on the project.

Electron Diffraction

One of the objectives of this investigation was an attempt to determine the nature of the intergranular material extending into the metal from the scale layer. It was desired to find the composition of this material and whether there were any significant differences between its composition and that of the external scale material. Just how this was to be done experimentally was a problem, since the intergranular material was well dispersed and extremely thin. The method ultimately adopted was described in the procedure section of this report and utilized reflection electron diffraction following successive etching treatments. Using this technique, it was possible to obtain data on the composition of the intergranular material as a function of depth below the metal-oxide interface. The results obtained by this method are presented in Table 6. Six heats of material were selected for examination: type 309 plus Nb; and type 310, heats 64177, 64270, X11306, X11338, and X27258. Specimens from the latter three heats were examined at all temperatures of oxidation, while the first three heats were examined only at the four lower temperatures. The program was restricted to an oxidation time of 100 hours.

As was noted previously, the accuracy obtainable with the reflection electron diffraction technique is of the order of 1 or 2% error in interplanar spacing, the same order as the changes in lattice parameters between Cr_2O_3 and Fe_2O_3 and between spinels having the highest and lowest possible lattice parameters. Therefore, the phases shown to be present in the electron diffraction patterns could be identified only as "rhombohedral" or "spinel". Examples of these two patterns are presented in Figs. 25 and 26. Identification was made on the basis of the (220) spinel line and several rhombohedral lines, notably the (100), (110), (120), and (200) lines. The appearance of the (100) line in the electron diffraction patterns could be due either to oriented oxide growth or to the fact that the low-angle structure factor for elec-

trons is greater than for x-rays. The latter reason is the more likely, considering the probable randomness of the surface-metal grain orientations.

The electron diffraction results showed that the same phases exist in the grain-boundary fissures as were found in the external scales. In heats 64177 and 64270 the spinel phase was rarely observed. In the other four heats both phases appeared, the spinel phase being especially prominent in the type 309 plus Nb alloy with its high Mn content (see Table 1). The relative proportions of the phases in a given specimen seemed to vary slightly with depth but the two patterns taken on each specimen at the same depth often showed similar variations. As nearly as can be determined, the intergranular material is identical to the material found in the external scale and is in general simply an inward extension of the external scale.

In order to be absolutely certain that the electron diffraction patterns obtained were not from reaction products between the metal and the etchant, a specimen was etched and allowed to dry without rinsing. The resulting electron diffraction pattern could be easily differentiated from those associated with the two oxide phases obtained by the routine process.

Figures 27 through 30 show the metallographic appearance of the specimen surfaces following successive etching treatments. The photomicrographs were taken using oblique light in order to show the oxides in relief more clearly. These photomicrographs show that electrolytic etching with 10% perchloric acid and 90% glacial acetic acid left the intergranular oxide films intact and exposed. Figures 27 through 30 also illustrate something which was observed at the time etching was carried out, namely, that the first etching usually attacked the metal only at certain points where the path through the surface scale to the metal was relatively open. Further etching undercut the scale layer adjacent to these points, and in the subsequent brushing process new metal surface was exposed. Ultimately, the scale layer could be completely removed by this process, but at the same time much of the deeper intergranular material in the areas which etched initially was probably lost. Furthermore, patterns taken while appreciable amounts of scale remained on the surface probably are not representative of intergranular material at all, since the scale would serve to block the intergranular material from the electron beam. In some specimens no difficulty was encountered with adhering scales and even the first patterns obtained are representative of intergranular material.

It will be noted from Table 6, when compared with appropriate penetration vs. depth curves, that the measured depths below which no oxide patterns were obtained were sometimes very much less than the maximum fissure depths observed metallographically. In a few cases apparent increases in thickness of the metal were observed on etching. There are two alternative conclusions that can be drawn from these facts: either the thickness measurements as made on the supermicrometer were not as reliable as they were believed to be, or the number of intergranular oxide areas in relief at the deeper levels was not sufficient to give an electron diffraction pattern. Considering the apparent thickness increases on some specimens and the sensitivity of the electron diffraction technique, the probability is that the measurements were not representative. Since the surfaces often became rather rough as a result of the etching treatment, it was difficult to devise a suitable means of making thickness measurements which would be accurate to 0.0001 inch and at the same time would be representative of the surface as a whole.

X-ray Analysis

The composition of high-alloy steels as determined by x-ray analysis has been extensively studied by a research group at Purdue University (7, 8, 9, 10). After oxidizing types 309 and 310 stainless steels for 100 hours at 1600° through 2200°F, this group found oxides consisting of Cr_2O_3 rhombohedral solid solutions of Cr_2O_3 and Fe_2O_3 having complete solid solubility, and a spinel of lattice parameter 8.310 to 8.330 KX in type 309 steel and 8.323 to 8.429 KX in the type 310 steel. The low-parameter spinel was identified as Fe-Cr oxide, and the high-parameter spinel as an Mn-Cr oxide. The individual alloys always contained a spinel except the type 309 alloy at 2200°F. The majority of the scales contained one solid solution, and a few contained two solid solutions of differing composition. Most of the scales contained either Cr_2O_3 or a solid solution high in Cr_2O_3. In alloys having a high nickel content, nickel compounds were also present in the scale.

The x-ray results obtained in the present investigation are given as part of Table 4 with a key to the symbols being given in Table 3. There did not seem to be any trends in the oxide compositions with respect to time or temperature. All the oxide contained Cr_2O_3 or a Cr_2O_3-rich solid solution, and all the oxides analyzed were of a protective nature considering Randall and Robb's criteria of the presence of Cr_2O_3, or high-parameter spinels. It is interesting to note that nickel compounds were found in the the high-nickel alloys. This is consistent with the results of the Purdue group mentioned above. It is to be emphasized here that the interplaner spacings of $NiCr_2O_4$ and $NiFe_2O_4$, as well as $FeCr_2O_4$ and $NiMn_2O_4$, are very close, differing only in the third decimal.

SUMMARY AND CONCLUSIONS

1. The weight gained at various time intervals during oxidation was determined for Chromel alloys ASM, ARM, and D, and type 310 stainless steels, in the temperature range of 1600° through 2000°F. The parabolic rate constant was determined for each specimen investigated.

2. Chromel alloys ASM, ARM, and D, type 310 stainless steels, and Inconel were subjected to oxidation in the unstressed condition in moving dry air, having a dewpoint less than minus 40°F, at temperatures of 1600°, 1700°, 1800°, 1900°, and 2000°F. The duration of the tests was 100 hours for the majority of the tests although oxidation times of 10, 30, and 500 hours were used. The oxidized samples were mounted, polished metallographically, and measured for intergranular penetration, recording the numbers of fissures and their depths. These data are presented as follows: (1) penetration frequency vs. depth, (2) penetration number [N] vs. temperature, and (3) the mean depth of penetration vs. temperature. In general, the intergranular oxidation increased with time and temperature. Increasing the testing time from 100 to 500 hours caused a marked increase in intergranular penetration in some alloys.

3. Chromel alloy ASM and type 310 stainless steels were oxidized for 100 hours at temperatures of 1700°, 1800°, 1900°, and 2000°F using moving air with a dewpoint of plus 60°F. It was found that the increased humidity of the ambient air had in general a small effect on the intergranular penetrations although it did increase

the number of penetrations somewhat and also the mean depth to a slight extent.

4. One heat of type 310 stainless steel, having some degree of preferred orientation, was studied for intergranular penetration characteristics. A slight improvement in resistance to intergranular oxidation was noted in the texture material.

5. Chromel alloys ASM, ARM, and D, and type 310 stainless steels were oxidized at various stress levels for 100-hour periods, using a temperature range of 1600° through 2000°F. Intergranular penetration measurements were made and the data presented as follows: (1) penetration frequency vs. depth, (2) penetration number [N] vs. stress, and (3) the mean depth [$\overline{X}$] vs. stress. There appears to be a minimum stress level for each material, above which a noticeable increase in intergranular oxidation is observed.

6. Visual examination and magnetic tests were performed on the oxidized specimens and the oxide itself. No correlation between these observations and oxidation characteristics could be found.

7. X-ray diffraction studies were performed on a few of the oxides resulting from the oxidation procedures. All the oxides tested were of the adherent type using Randall and Robb's criteria of the presence of Cr_2O_3 or high-parameter spinel.

8. Electron diffraction examination of the subsurface structure was performed on type 310 stainless steels oxidized in the unstressed condition. It was found that the oxidation products in the subsurface region were substantially the same as the surface oxides as determined by x-ray diffraction techniques.

BIBLIOGRAPHY

1. Siebert, C. A., Sinnott, M. J., and Keith, R. E., An Investigation of Intergranular Oxidation in Stainless Steels, WADC TR 54-120, January 1954.

2. Brockway, L. O. and Bigelow, W. C., Development of Procedure for the Identification of Minor Phases in Heat-Resistant Alloys by Electron Diffraction, Annual Summary Report on Project 2020, Eng. Res. Inst., Univ. of Mich., to Flight Research Laboratory (WCRRL), WADC, 15 January 1953.

3. Gulbransen, E. A. and Andrew, K. F., J. of Electrochemic Soc., 98, 241 (1951).

4. Simmons, W. F. and Cross, H. C., Report on the High-Temperature Properties of Stainless Steels, ASTM Spec. Tech. Pub. No. 124 (1952).

5. Smith, G. V., Dulis, E. J., and Houston, G. E., Trans. Amer. Soc. Metals, 42, 935 (1950).

6. Preece A., Richardson, G. T., and Cobb, J. W., Second Report of the Alloy Steels Research Committee, Iron and Steel Inst. Spec. Rept. No. 24, 9 (1939).

7. Yearian, H. J. and Radavich, J. F., Dept. of Physics, Purdue University, Unpublished Data.

8. Boren, H. E., Jr., M.S. Thesis, Dept. of Physics, Purdue University, August, 1950.

9. Warr, R. E., M.S. Thesis, Dept. of Physics, Purdue University, August, 1951.

10. Radavich, J. F., Ph.D. Thesis, Dept. of Physics, Purdue University, May, 1953.

TABLE 1

CHEMICAL ANALYSIS OF MATERIALS, WEIGHT PERCENT

Alloy and Heat No.	Fe	N_2	Mn	Si	Cr	Co	Cu	Ta	P	Ni	C	S	Mo	W	Nb
Type 310, 64177	Bal.	0.1	0.42	0.55	24.03	0.01	0.13	0.01	0.018	16.93	0.13	0.008	0.033	<0.01	--
Type 310, 64270	Bal.	0.06	0.50	0.43	22.30	0.01	0.10	--	0.025	19.14	0.12	0.008	0.042	<0.01	--
Type 309 plus Nb	Bal.	--	2.31	0.46	22.64	--	--	--	0.012	15.39	0.080	0.008	--	--	0.82
Type 310, X11338	Bal.	--	1.53	0.83	24.48	--	0.25	--	0.029	20.08	0.085	0.029	0.14	--	--
Type 310, X27258	Bal.	--	1.58	0.75	24.80	--	0.30	--	0.025	20.81	0.070	0.008	0.15	--	--
Type 310, J10*	Bal.	--	0.18	0.1	23.25	0.024	0.001 to 0.01	0.08	--	20.63	0.038	0.01	<0.002	0.04	<0.017
Type 310, Vt-5*	55.20	--	0.10	0.034	24.65	0.038	0.003	<0.085	--	20.39	0.014	0.019	<0.0013	0.042	<0.017
Type 310, Vt-7*	55.00	--	0.07	0.003	24.56	--	<0.00004	<0.002	--	20.30	0.008	0.008	<0.001	0.025	<0.006
Inconel	8.25	--	--	0.19	15.72	--	--	--	--	75.18	0.05	--	--	--	--
Chromel, ASM	0.37	--	0.30	1.43	19.81	--	--	--	--	77.65	0.05	--	--	--	--
Chromel ARM, heat A	0.39	--	1.60	1.00	19.86	--	--	--	--	77.01	0.04	--	--	--	--
Chromel ARM, heat B	0.42	--	1.53	1.06	19.83	--	--	--	--	77.36	0.1	--	--	--	--
Chromel D	39.76	--	0.67	1.61	21.69	--	--	--	--	35.92	0.09	--	--	--	--

*Vacuum-melted heat.

TABLE 2

SPECIFIC WEIGHT GAINED IN MILLIGRAMS PER SQUARE INCH

Alloy and Heat No.	Oxidizing Temperature, °F	Time, Minutes 1000	2000	3000	4000	5000	6000
Type 310, X46572	1800	2.60	4.10	4.90	5.70	6.50	7.30
	1900	2.90	7.30	8.90	10.10	11.00	11.80
	2000	8.00	10.30	11.80	12.20	14.20	15.10
Type 310, Vt-5	1800	1.80	2.80	3.50	4.20	4.70	5.30
	1900	3.80	5.50	6.80	7.70	8.70	9.60
	2000	8.10	9.70	14.40	16.40	18.20	19.40
Type 310, Vt-7	1800	1.00	1.70	2.50	3.20	3.80	4.60
	1900	4.10	6.10	7.40	8.60	9.60	10.70
	2000	--	--	--	--	--	--
Type 310, Ht J10	1600	0.60	0.90	1.00	1.20	1.30	1.40
	1700	0.70	1.00	1.20	1.40	1.50	1.70
	1800	1.50	2.20	2.60	3.10	3.50	3.90
	1900	2.50	3.90	5.10	6.30	7.20	8.20
	2000	5.50	7.90	9.60	11.00	12.20	13.00
Chromel ARM, heat A	1800	1.10	1.80	2.50	3.10	3.60	4.10
	1900	3.60	5.10	6.30	7.20	8.10	8.70
	2000	5.20	7.70	9.80	12.00	14.00	15.50
Chromel D	1800	3.20	4.00	4.40	4.80	5.20	5.40
	1900	4.00	4.60	5.10	5.60	6.20	6.80
	2000	6.00	8.20	10.40	12.20	13.60	15.00
Chromel ASM	1800	1.00	1.40	1.50	1.70	1.80	2.00
	1900	1.80	1.40	2.80	3.10	3.40	3.70
	2000	3.30	4.80	5.80	6.50	7.00	7.20

TABLE 3

EXPLANATION OF SYMBOLS USED IN OXIDATION DATA TABULATIONS

SPECIMEN

Appearance

- PGB - Powdery gray black
- PGB w/OS - Powdery gray black with orange substrate
- SGB - Shiny gray black
- B and S - Black and scoriated
- BP w/LG - Black pits with light gray surface (mostly pits)
- LG - Light gray surface
- LG w/BP - Light gray with black pits (mostly light gray)
- LG w/IC - Light gray with interference colors
- Gr - Green
- Br - Brown

Magnetism

- ND - Not detectable
- W - Weak
- M - Medium
- S - Strong

No. of Fissures

- FT - Fissures throughout

OXIDE SCALE

Amount

- N - None
- S - Small
- M - Medium
- L - Large

Color

- G - Gray
- B - Black
- GB - Gray-black
- Gr - Green

Flake Size

- P - Powder
- SF - Small (<1/32 in.)
- MF - Medium (1/32 - 1/8 in.)
- LF - Large (>1/8 in.)

Composition (X-ray)

- SS XQ - Cr_2O_3 - Fe_2O_3 solid solution with Q ± 10 atomic percent Cr_2O_3
- HPS - High-parameter spinel
- Insuf. - Insufficient oxide for x-ray pattern
- W - Weak pattern
- M - Medium pattern
- S - Strong pattern

TABLE 4

RESULTS OF OXIDATION TESTS

Run No.	Dewpoint, °F	Duration, hr	Temperature, °F	Stress, psi	SPECIMEN					OXIDE SCALE				
					Appearance	Magnetism	Elongation % in 2 in.	No. of Fissures/in.	Mean Depth in. x 10^3	Amount	Color	Flake Size	Magnetism	Composition (X-ray)
Type 310 Alloy, Heat 46572														
17	<-40	100	1800	0	BP w/LG LG w/BP PGB	W	-	930	0.493	M	B	P	M	-
14S	-	100	1800	1500	LG w/IC PGB	W	0.8	907	0.393	L	GB	P	S	-
14S	-	100	1800	2000	PGB	W	2.4	1132	0.519	S	GB	P	W	-
15S	-	100	1800	2250	LG w/IC PGB	W	4.7	1128	0.4907	M	GB	P	M	-
12S	-	100	1800	2480	PGB	M	13.5	1730	0.774	M	GB	P	S	-
13S	-	100	1800	3038	PGB LG	S	≈26.6	Ruptured		M	GB	P	S	-
17	<-40	100	1900	0	LG w/BP B and S LG	M	-	943	0.455	M	B	P	S	-
17S	-	100	1900	1000	PGB	M	1.6	1171	0.675	M	GB	P	M	-
16S	-	100	1900	1250	PGB	M	2.0	1480	0.557	M	GB	P	M	-
16S	-	100	1900	1500	PGB	M	3.2	812	0.667	M	GB	P	S	-
23S	-	100	1900	1650	PGB	M	6.0	681	0.789	L	GB	P	S	-
17S	-	100	1900	1750	PGB	M	22.7	1261*	1.429*	L	GB	SF	S	-
15S	-	100	1900	2000	PGB	ND	39.1	FT	FT	L	GB	P	S	-
Type 310 Alloy, Heat Vt-5														
38	<-50	100	1600	0	PGB	S	-	358	0.340	N	-	-	-	-
38	<-50	100	1700	0	LG w/BP PGB	S	-	422	0.354	S	GB	P	M	-
38	<-50	100	1800	0	PGB LG w/BP	M	-	452	0.373	M	GB	P	S	SS X75 (S)
18S	-	100	1800	750	PGB	M	1.6	386	0.502	S	GB	P	M	-
19S	-	100	1800	1000	PGB	S	3.9	388	0.624	S	GB	P	W	-
20S	-	100	1800	1150	PGB	S	4.5	397	0.672	S	GB	P	M	-
39	<-50	100	1900	0	PGB LG LG w/IC	M	-	309	0.372	M	GB	MF	M	SS X75 (S) HPS (W)
28S	-	100	1900	650	PGB	-	4.0	753	0.476	L	GB	P	S	-
18S	-	100	1900	750	PGB	M	4.7	544*	0.820*	S	GB	P	M	-
19S	-	100	1900	1000	B and S	S	16.4	FT	FT	L	GB	MF	S	-
17S	-	100	1900	1250	PGB	S	≈32.8	Ruptured		L	GB	MF	S	-
39	<-50	100	2000	0	PGB LG w/IC LG	M	-	396	0.370	M	GB	MF	M	-
Type 310 Alloy, Heat Vt-7														
38	<-50	100	1600	0	PGB	S	-	379	0.328	N	-	-	-	-
38	<-50	100	1700	0	PGB	S	-	448	0.347	S	GB	P	W	-
38	<-50	100	1800	0	LG w/BP LG w/IC LG	M	-	458	0.367	M	GB	P	M	SS X75(M) Cr_2O_3 (M)
18S	-	100	1800	750	PGB	M	1.9	386	0.522	M	GB	P	S	-
20S	-	100	1800	1000	PGB	ND	3.5	435	0.679	S	GB	P	M	-
23S	-	100	1800	1150	PGB	W	32.0	FT	FT	M	GB	P	S	-
21S	-	100	1800	1250	PGB	W	32.0	FT	FT	S	GB	P	S	-
39	<-50	100	1900	0	PGB LG LG w/IC	M	-	392	0.368	M	GB	LF	M	SS X75 (S)
28S	-	100	1900	500	PGB LG	-	1.5	792*	0.520*	M	GB	P	M	-
19S	-	100	1900	750	PGB PGB w/OS	W	6.3	FT	FT	M	GB	P	W	-
20S	-	100	1900	901	B and S PGB PGB w/OS	ND	15.5	FT	FT	L	GB	P	S	-
39	<-50	100	2000	0	PGB LG LG w/IC	M	-	404	0.373	M	GB	MF	M	-
Type 310 Alloy, Heat J10														
33	<-50	100	1600	0	PGB	M	-	249	0.320	S	GB	P	S	SS X75 (S) Fe_2O_3 (W) $NiFe_2O_4$ (W)
33	<-50	100	1700	0	B and S	W	-	246	0.322	S	GB	P	S	SS X75 (S) Fe_2O_3 (W)
33	<-50	100	1800	0	B and S	W	-	492	0.328	S	GB	P	M	-
33	<-50	100	1900	0	B and S LG w/IC	M	-	250	0.322	M	GB	P	S	SS X75 (S) $NiCr_2O_4$ (W)
33	<-50	100	2000	0	PGB	S	-	425	0.382	M	GB	MF	S	SS X75 (S) Fe_2O_3 (M) $NiFe_2O_4$ (W)
Chromel ARM Alloy, Heat B														
34	<-40	100	1600	0	Br LG PGB w/OS	ND	-	328	0.338	N	-	-	-	HPS (S) SS X75 (M)
34	<-40	100	1700	0	Br	W	-	929	0.344	N	-	-	-	-
34	<-60	100	1800	0	LG LG w/BP BP w/LG	ND	-	920	0.392	M	G	MF	W	SS X75 (S) HPS (S)
34	<-40	100	1900	0	PGB LG w/IC LG w/BP	S	-	782	0.377	-	-	-	-	SS X75 (M) HPS (M)
34	<-60	100	2000	0	Br	W	-	1342	0.581	S	GB	P	W	SS X75 (M) $NiFe_2O_4$ (S)

*Some small fissures throughout.

TABLE 4 (continued)

Run No.	Dewpoint, °F	Duration, hr	Temperature, °F	Stress, psi	SPECIMEN					OXIDE SCALE				
					Appearance	Magnetism	Elongation % in 2 in.	No. of Fissures/in.	Mean Depth in. x 10^3	Amount	Color	Flake Size	Magnetism	Composition (X-ray)
Type 310 Alloy, Heat X27258														
16	<-40	100	1600	0	BP w/LG LG w/IC	-	-	1457	0.331	M	B	P	W	Cr_2O_3 (S) HPS (W)
10S	-	100	1600	1850	PGB	ND	ND	1578	0.323	S	GB	MF	ND	-
10S	-	100	1600	3040	PGB	W	ND	1567	0.321	S	GB	MF	W	-
16	<-40	100	1700	0	LG w/BP PGB	W	-	808	0.399	L	B	MF	ND	Cr_2O_3 (S) HPS (W)
6S	-	100	1700	500	PGB	W	ND	1448	0.325	S	GB	P	W	-
6S	-	100	1700	960	PGB BP w/LG LG w/IC	W	ND	1346	0.325	S	GB	P	W	SS X75 (S) HPS (W)
7S	-	100	1700	1425	PGB PGB w/OS	W	ND	1105	0.322	S	GB	SF	W	-
8S	-	100	1700	1880	LG w/BP PGB	M	ND	1073	0.322	M	GB	MF	W	HPS (M) SS X75 (S)
16	<-40	100	1800	0	Lg w/IC	-	-	1409	0.526	L	B	MF	ND	SS x75 (S) HPS (S)
7S	-	100	1800	520	PGB	W	ND	981	0.408	L	GB	P	S	HPS (M) Fe_2O_3 (M)
7S	-	100	1800	940	PGB	W	ND	1138	0.392	M	GB	P	M	HPS (M)
8S	-	100	1800	1440	PGB	W	ND	970	0.345	L	GB	P	S	SS X75 (S) HPS (M)
10S	-	100	1800	2460	PGB	W	2.0	1089	0.457	S	GB	P	W	-
12S	-	100	1800	2460	PGB LG	W	2.5	1074	0.419	M	GB	P	S	-
16	<-40	100	1900	0	LG w/BP B and S LG w/IC	W	-	1015	0.613	M	GB	P	ND	SS X75 (S) HPS (W)
36	<-60	500	1900	0	B and S PGB w/OS	M	-	2047	0.948	L	GB	P	S	-
16	<-40	100	2000	0	LG w/BP LG w/IC	W	-	-	-	M	GB	P	ND	-
Type 310 Alloy, Heat 31372, Annealed														
33	<-60	100	1600	-	PGB	-	-	1263.4	0.350	M	GB	P	M	SS X75 (S) HPS (M)
33	<-60	100	1700	-	PGB	-	-	1713	0.351	S	GB	P	M	SS X75 (S) Fe_2O_3 (W) HPS (S)
33	<-40	100	1800	-	PGB	-	-	1510	0.421	S	GB	P	S	-
33	<-60	100	1900	-	PGB	-	-	1256	0.888	L	GB	P	S	SS X50 (S) $FeCr_2O_4$ (W) HPS (S)
33	<-40	100	2000	-	PGB, LG	-	-	1698	0.842	S	GB	P	M	-
Type 310 Alloy, Heat 31372, 97% Reduced, Annealed														
33	<-60	100	1600	-	PGB	ND	-	1758	0.320	N	-	-	-	Insuf.
33	<-60	100	1700	-	PGB	M	-	2003	0.3266	N	-	-	-	Insuf.
33	<-40	100	1800	-	LG	M	-	1658	0.540	N	-	-	-	Insuf.
33	<-60	100	1900	-	PGB	W	-	1680	0.492	N	-	-	-	Insuf.
33	<-40	100	2000	-	PGB	W	-	1488	0.651	N	-	-	-	SS X50 (S), $FeCr_2O_4$(M)
Chromel Alloy ARM, Heat A														
34	<-60	100	1600	0	BP w/LG LG w/BP	W	-	263	0.348	N	-	-	-	SS X75 (S) HPS (M)
34	<-60	100	1700	0	Br BP w/LG	ND	-	1362	0.335	N	-	-	-	SS X75 (M) HPS (M)
34	<-60	100	1800	0	Br	W	-	1238	0.464	N	-	-	-	HPS (S), Cr_2O_3(M)
1S	-	100	1800	240	PGB	W	ND	1292	0.357	N	-	-	-	-
1S	-	100	1800	500	PGB	W	ND	1222	0.384	N	-	-	-	-
1S	-	100	1800	940	PGB	W	0.5	1409	0.379	N	-	-	-	-
2S	-	100	1800	1500	PGB PGB w/OS	W	4.0	1402	0.448	S	GB	P	W	-
2S	-	100	1800	2000	PGB	ND	34.0	FT	FT	N	-	-	-	-
34	<-60	100	1900	0	Br	W	-	1510	0.524	N	-	-	-	SS X75 (W) HPS (S)
3S	-	100	1900	240	PGB PGB w/OS	ND	ND	1744	0.430	S	GB	P	W	-
3S	-	100	1900	535	PGB	W	2.0	1732	0.431	N	-	-	-	-
13S	-	100	1900	880	PGB Br	W	8.4	-	-	S	GB	P	ND	-
3S	-	100	1900	990	PGB	W	19.0	1897	0.604	N	-	-	-	-
9S	-	100	1900	1264	PGB w/OS PGB	ND	39.0	FT	FT	S	GB	P	W	-
8S	-	100	1900	1500	PGB	ND	50.0	FT	FT	S	GB	P	M	HPS ($MnCr_2O_4$) (M)
36	<-60	500	1900	0	PGB B and S	W	-	2440	1.078	L	GB	P	W	Fe_3O_4 (S) Cr_2O_3 (M), NiO (M)
34	<-60	100	2000	0	Br	W	-	1417	0.495	S	GB	P	ND	Cr_2O_3 (M) HPS (M) $NiFe_2O_4$ or $FeCr_2O_4$ (M)
4S	-	100	2000	235	Br	W	1.0	1478	0.429	M	GB	P	W	Cr_2O_3 (M) HPS (S) ($MnCr_2O_4$)
4S	-	100	2000	535	PGB PGB w/OS	W	4.1	1639	0.552	S	GB	P	W	SS X75 (M) HPS (S)
6S	-	100	2000	655	PGB PGB w/OS Gr	ND	8.5	1731	0.694	L	Gr	P	ND	HPS (S) ($MnCr_2O_4$)
13S	-	100	2000	690	PGB Br	ND	8.6	2080	0.669	S	GB	P	ND	-
5S	-	100	2000	745	PGB PGB w/OS	ND	15.0	FT	FT	M	GB	P	ND	-
5S	-	100	2000	985	PGB Gr	ND	35.0	FT	FT	S	GB	P	ND	HPS (S) ($MnCr_2O_4$)

TABLE 4 (concluded)

Run No.	Dewpoint, °F	Duration, hr	Temperature, °F	Stress, psi	SPECIMEN					OXIDE SCALE				
					Appearance	Magnetism	Elongation % in 2 in.	No. of Fissures/in.	Mean Depth in. x 10^3	Amount	Color	Flake Size	Magnetism	Composition (X-ray)
Chromel D Alloy														
34	<-40	100	1600	0	PGB w/OS BP w/LG	W	-	274	0.32	N	-	-	-	-
34	<-40	100	1700	0	LG w/BP BP w/LG	M	-	603	0.32	N	-	-	-	SS X75 HPS
34	<-60	100	1800	0	LG w/BP LG	M	-	914	0.396	M	GB	P	W	SS X75 (M) HPS (M)
22S	-	100	1800	501	LG PGB	W	3.5	2315	0.395	L	GB	P	M	-
23S	-	100	1800	750	LG w/BP LG	W	11.0	1021	0.342	L	GB	P	M	-
24S	-	100	1800	850	LG w/BP LG	W	13.0	916	0.426	L	GB	P	W	-
25S	-	100	1800	925	PGB LG Br	ND	26.0	1726	0.520	M	GB	P	W	-
21S	-	100	1800	1000	PGB	ND	40.0	FT	FT	S	GB	P	M	-
34	<-40	100	1900	0	Br	W	-	1275	0.397	N	-	-	-	SS X75 (M) HPS (M) $FeCr_2O_4$ (M)
22S	-	100	1900	500	PGB	W	4.0	3127	0.689	S	GB	P	W	-
24S	-	100	1900	650	PGB	W	9.0	3557	0.472	S	GB	P	W	-
25S	-	100	1900	700	PGB LG Br	W	14.0	2114	0.568	M	GB	P	W	-
21S	-	100	1900	750	PGB	S	32.0	FT	FT	S	GB	P	M	-
9S	-	100	1900	975	PGB	S	40.0	FT	FT	S	GB	P	ND	-
34	<-60	100	2000	0	LG w/PB LG w/IC	S	-	544	0.351	M	GB	P	W	Cr_2O_3 (S) HPS (S)
22S	-	100	2000	500	PGB Br	S	4.0	3652	0.560	M	GB	P	M	-
25S	-	100	2000	650	PGB Br	ND	13.5	FT	FT	M	GB	P	W	-
9S	-	100	2000	730	PGB PGB w/OS	ND	13.5	FT	FT	S	GB	P	S	-
11S	-	100	2000	982	PGB Br	-	36.0	FT	FT	N	-	-	-	-
Inconel Alloy														
29A	<-45	10	1600	-	SGB PGB	M	-	250	0.335	N	-	-	-	-
29A	<-45	10	1700	-	SGB	S	-	399	0.344	N	-	-	-	-
29A	<-45	10	1800	-	SGB	S	-	445	0.409	S	B	P	ND	-
30A	<-40	10	1900	-	PGB w/OS	S	-	408	0.393	S	B	P	ND	-
30A	<-40	10	2000	-	PGB w/OS	S	-	493	0.446	S	B	P	S	-
29B	<-45	30	1600	-	SGB PGB LG	M	-	269	0.324	S	B	P	ND	-
29B	<-45	30	1700	-	PGB SGB	M	-	868	0.321	N	-	-	-	-
29B	<-45	30	1800	-	PGB	S	-	991	0.320	N	-	-	-	-
30B	<-40	30	1900	-	PGB w/OS SGB	S	-	840	0.324	S	B	P	S	SS X75 (S) $NiFe_2O_4$ (S)
30B	<-40	30	2000	-	SGB	S	-	887	0.325	S	B	P	S	SS X75 (S) $NiFe_2O_4$? (S)
29C	<-45	100	1600	-	LG w/BP SGB	M	-	256	0.323	S	B	P	ND	-
29C	<-45	100	1700	-	PGB	M	-	557	0.323	N	-	-	-	-
29C	<-45	100	1800	-	PGB	M	-	427	0.326	S	B	P	W	-
30C	<-40	100	1900	-	PGB w/OS SGB	S	-	1150	0.463	M	B	P	S	Cr_2O_3 (S) $NiCr_2O_4$ (S)
36	<-60	500	1900	-	PGB w/OS B and S	S	-	2046	0.464	S	B	P	S	
30C	<-40	100	2000	-	PGB w/OS SGB	S	-	969	0.408	M	B	P	S	Cr_2O_3 (S) $FeCr_2O_4$ (S)
Chromel Alloy, ASM														
40	<-60	100	1600	0	Gr	W	-	482	0.32	N	-	-	-	-
40	<-60	100	1700	0	Gr LG	W	-	1590	0.322	N	-	-	-	-
40	<-60	100	1800	0	Gr	W	-	2396	0.344	S	Gr	P	ND	-
28S	-	100	1800	1250	Gr	ND	1.5	3078	0.321	S	Gr	P	ND	-
26S	-	100	1800	1500	Gr	ND	1.5	1620	0.320	S	Gr	P	W	-
29S	-	100	1800	1750	Gr	ND	19.0	FT	FT	N	-	-	-	-
27S	-	100	1800	2000	Gr	ND	28.0	FT	FT	S	Gr	P	W	-
40	<-60	100	1900	0	Gr LG	W	-	2037	0.384	S	Gr	P	ND	-
26S	-	100	1900	750	Gr	ND	1.0	1240	0.402	S	Gr	P	W	-
29S	-	100	1900	1000	Gr	W	6.0	1643	0.504	S	Gr	P	ND	-
30S	-	100	1900	1100	Gr	ND	6.0	1407	0.455	S	Gr	P	W	-
27S	-	100	1900	1250	Gr	ND	29.0	FT	FT	N	-	-	-	-
40	<-60	100	2000	0	LG Gr	W	-	1648	0.472	N	-	-	-	-
29S	-	100	2000	500	Gr	ND	2.5	1897	0.469	L	Gr	P	W	-
26S	-	100	2000	650	Gr	ND	6.0	1350	0.635	M	Gr	P	W	-
30S	-	100	2000	750	Gr	ND	34.0	FT	FT	M	Gr	P	W	-
27S	-	100	2000	1000	Gr	ND	55.0	FT	FT	S	Gr	P	M	-

TABLE 5

PENETRATION DISTRIBUTION

Alloy and Heat No.	Time, hr	Run No.	Penetration Depth in 0.001"							Total No.	Mean Depth in 0.001"
			0 to 0.64	0.64 to 1.28	1.28 to 1.92	1.92 to 2.56	2.56 to 3.20	3.20 to 3.74	3.74 up		
Chromel ARM, heat A	100	34	1049*	434	24.8	1.8				1510	0.524
Chromel ARM, heat A	500	36	438	1342	473	127	41	16	3.5	2440	1.078
Type 310, X27258	100	16	510	418	27					1015	0.623
Type 310 X27258	500	36	673	951	261	99	45	18		2047	0.948
Inconel	100	30C	896	247	7.1	7				1150	0.463
Inconel	500	36	1642	348	49					2046	0.464

*The numbers in these columns represent number of penetrations per inch.

TABLE 6

ANALYSES OF INTERGRANULAR OXIDES OF STAINLESS STEELS OBTAINED BY ELECTRON DIFFRACTION

Etch	Oxidizing Temperature, °F: 1600 Measured Depth, in.	1600 Analysis	1700 Measured Depth, in.	1700 Analysis	1800 Measured Depth, in.	1800 Analysis	1900 Measured Depth, in.	1900 Analysis	2000 Measured Depth, in.	2000 Analysis
TYPE 309 PLUS Nb ALLOY, Run 20										
Scale (x-ray)		Cr_2O_3(S) HPS (S)		Cr_2O_3(S) Fe_2O_3(S) HPS (W)		Cr_2O_3(S) Fe_2O_3(M) HPS (M)		Cr_2O_3(S) Fe_2O_3(M) HPS (M)	-	-
Surface	0	Sp (S) Rh (S)	0	Sp (S) Rh (S)	0	Sp (S) Rh (M)	0	Sp (S)	-	-
I	-	Sp (S) Rh (S)	-	Sp (S) Rh (S)	0.0002	Sp (S) Rh (M)	0.0004	Sp (S) Rh (VW)?	-	-
II	-	$M_{23}C_6$?	-	Sp (S) Rh (S)	0.0002	Sp (S) Rh (M)	0.0006		-	-
III	-	-	-	Sp (M) Rh (M)	0.0001	Sp (W) Rh (W)	0.0007	Sp (VW) Rh (VW)	-	-
IV	-	-	-	-	0.0004	Sp (W) Rh (W)	0.0007	Sp (VVW) Rh (VW)	-	-
TYPE 310 ALLOY, HEAT 64177, Run 20										
Scale (x-ray)		Cr_2O_3		Insuf.		X 50		X 50		-
Surface	0	Rh (S)	0	Rh (S)	0	Rh (S)	0	Rh (S)	-	-
I	-	Rh (S)	-	Rh (S)	-0.0003	Rh (S)	0.0000	Rh (S) Sp (VVW)?	-	-
II	-	Rh (S)	-	Rh (S)	0.0000	Rh (S) Sp (VVW)?	-0.0003	Rh (S)	-	-
III	-	-	-	-	-0.0001	Rh (W)	-0.0006	Rh (S)	-	-
IV	-	-	-	-	-0.0003	No Pattern	-0.0007	Metal	-	-
TYPE 310 ALLOY, HEAT 64270, Run 20										
Scale (x-ray)		X 50		Fe_2O_3(S) LPS (M)		X 50 (S) LPS (W)		X 50 (S) Fe_2O_3(W)?		-
Surface	0	Rh (S)	0	Rh (S) Sp (VW)?	0	Rh (S)	0	Rh (S) Sp (VVW)	-	-
I	-	-	-0.0002	Rh (S)	0.0000	Rh (S)	0.0000	Rh (S) Sp (VVW)	-	-
II	-	-	0.0000	Rh (W)	0.0004	Rh (S)	0.0001	Rh (S) Sp (VVW)?	-	-
III	-	-	-0.0001	No Pattern	0.0006	Rh (M)	0.0003	Rh (M) Sp (VVW)?	-	-
IV	-	-	-	-	0.0007	Metal	0.0001	Metal	-	-
TYPE 310 ALLOY, HEAT X11306										
Scale (x-ray)		Fe_2O_3(S) HPS (M)		Fe_2O_3(S) LPS (M)		Cr_2O_3(S) HPS (S)		Cr_2O_3(S) HPS (S) LPS (W)		X 75 (S) LPS (S) HPS (M)
Surface	0	Sp (S) Rh (M)	0	Sp (S) Rh (M)	0	Sp (S) Rh (W)	0	Sp (S) -	0	Sp (S) Rh (VW)?
I	0.0002	Sp (S) Rh (VW)?	0.0000	Sp (S) Rh (M)	0.0000	Contam. -	0.0003	Sp (S) -	0.0002	Sp (S) Rh (VW)?
II	0.0001	Sp (S)	0.0000	Sp (S) Rh (M)	0.0000	Sp (M) Rh (VW)?	0.0003	Sp (S) Rh (S)	-0.0001	Sp (W) Rh(VVW)?
III	0.0001	Sp (S)	0.0001	Sp (M) Rh (M)	0.0002	Sp (S) Rh (M)	0.0004	Sp (M) Rh (M)	-0.0002	Sp(VVW)? Rh (VW)
IV	0.0002	Metal	0.0001	Sp (M) Rh (M)	0.0000	-	0.0004	Sp (W) Rh (W)	-0.0003	Sp(VVVW) Rh (VVW)
V	-	-	0.0001	Sp (VVW) Rh (VVW)	0.0000	Sp (M) Rh (W)	0.0002	Sp (M) Rh (M)	-	-
VI	-	-	-	-	0.0001	Sp (W) Rh (VW)?	0.0000	Sp (M) Rh (W)	-	-
VII	-	-	-	-	0.0001	Sp (W) Rh (VW)?	0.0003	Sp (W) Rh (W)	-	-
VIII	-	-	-	-	0.0001	Sp (VW) Rh (VVW)?	0.0007	Sp (VVW) Rh (VVW)?	-	-
TYPE 310 ALLOY, HEAT X11338										
Scale (x-ray)		Cr_2O_3(S) HPS (S)		Cr_2O_3(S) HPS (S) LPS (W)		Cr_2O_3(S) HPS (S) LPS (W)		X 25 (S) LPS (M)		X 25 (S) LPS (M)
Surface	0	Sp (S) Rh (S)	0	Sp (S) Rh (S)	0	Sp (S) Rh (W)	0	Sp (S)	0	Sp (S) Rh (VW)
I	0.0001	Sp (S) Rh (S)	0.0002	Sp (S) Rh (S)	0.0001	Contam.	0.0002	Sp (S)	0.003	Sp (S) Rh (W)
II	0.0001	Sp (S) Rh (S)	0.0002	Sp (S) Rh (S)	0.0001	No Pattern	0.0002	Sp (S) Rh (S)	0.0003	Rh (M)
III	0.0001	Sp (W) Rh (M)	0.0003	Sp (M) Rh (VW)?	0.0004	No Pattern	0.0002	Sp (M) Rh (M)	0.0005	Sp (M) Rh (M)
IV	0.0001	No Pattern	0.0002	Sp (W) Rh (VVW)?	-	-	0.0004	Sp (S) Rh (S)	0.0004	Sp (M) Rh (M)
V	-	-	-	-	-	-	0.0002	Sp (M) Rh (M)	0.0004	Sp (VW) Rh (VW)
VI	-	-	-	-	-	-	0.0002	Sp (M) Rh (W)	0.0004	Sp (VW) Rh(VVW)?
VII	-	-	-	-	-	-	0.0002	Sp (M) Rh (W)	-	-
VIII	-	-	-	-	-	-	0.0002	Sp (VVW) Rh (VVW)?	-	-
TYPE 310 ALLOY, HEAT X27258										
Scale (x-ray)		Cr_2O_3(S) HPS (S)		X 75 (S) HPS (S) LPS (W)		Cr_2O_3(S) HPS (S) LPS (W)?		X 50 (S) HPS (S)		Cr_2O_3(S) HPS (S)
Surface	0	Sp (S) Rh (S)	0	Sp (S) Rh (M)	0	Sp (S) Rh (W)	0	Sp (S) Rh (W)?	0	Sp (S) Rh (W)
I	0.0000	Sp (S) Rh (M)	0.0002	Sp (S) Rh (M)	-0.0001	Sp (S) Rh (W)?	0.0001	Sp (S)	-0.0001	Sp (S) Rh (W)
II	0.0000	Sp (S) Rh (S)	0.0005	Sp (S) Rh (M)	0.0002	Sp (M) Rh (W)	0.0003	Sp (S) Rh (W)	0.0001	Sp (M) Rh (M)
III	0.0001	No Pattern	0.0006	Sp (S) Rh (M)	0.0005	Sp (S) Rh (M)	0.0006	Sp (S) Rh (S)	0.0000	Sp (VW) Rh (W)
IV	0.0002	No Pattern	0.0008	No Pattern	0.005	Sp (S) Rh (M)	0.0005	Contam.	0.0001	Sp (VW) Rh (VW)
V	-	-	0.0007	No Pattern	0.0003	Sp (M) Rh (W)	0.0005	Sp (S) Rh (S)	0.0000	Sp (VW) Rh (VW)
VI	-	-	-	-	0.0004	Sp (W) Rh (VW)?	0.0007	No Pattern	-0.0001	Sp (VW) Rh(VVW)?
VII	-	-	-	-	0.0005	No Pattern	-	-	-	-

HPS - High-parameter spinel
LPS - Low-parameter spinel
Sp - Spinel phase
Rh - Rhombohedral phase

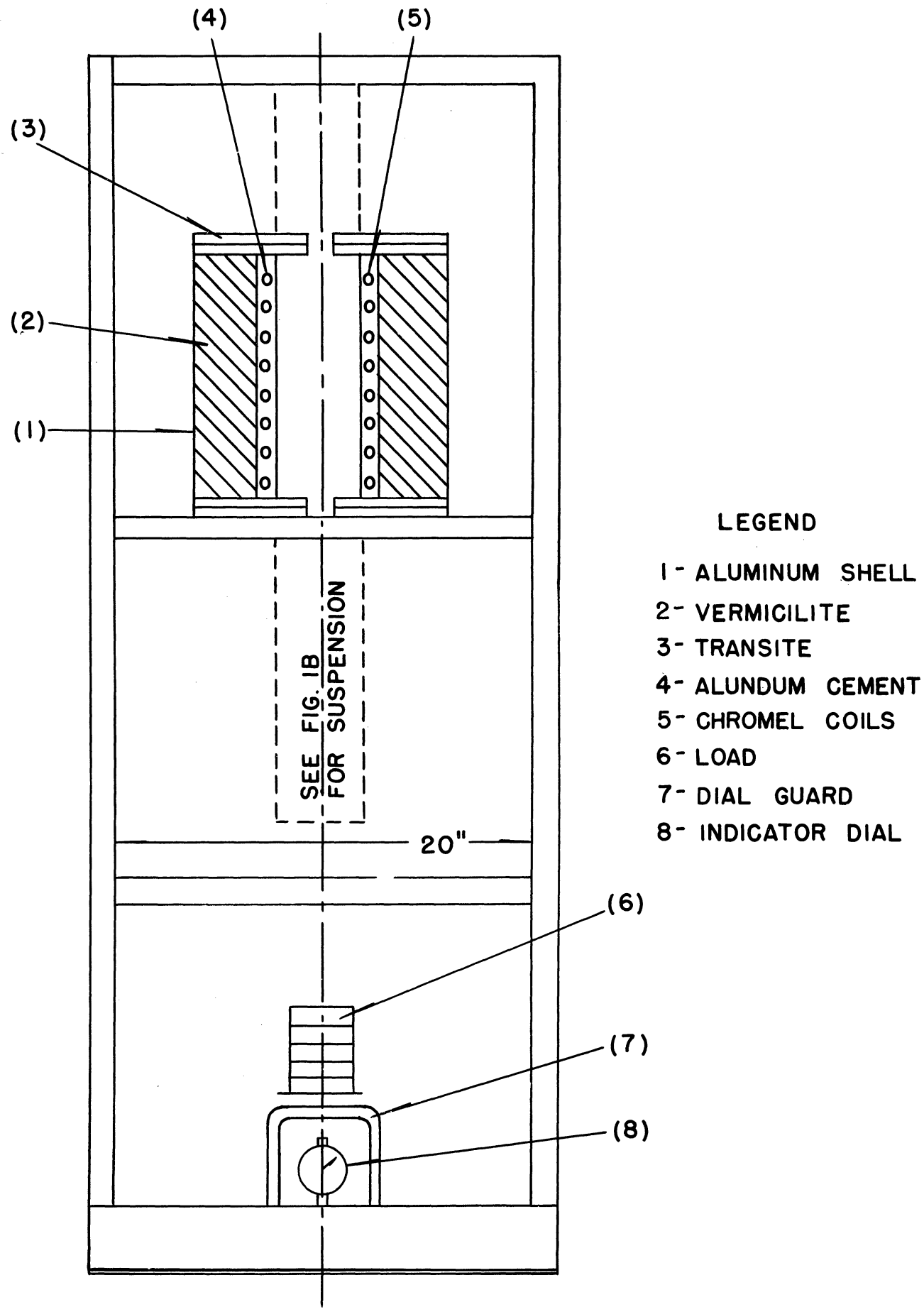

Fig. 1. Schematic Drawing of Stress Oxidation Unit.

Fig. 2. Assembly of Suspension Mechanism

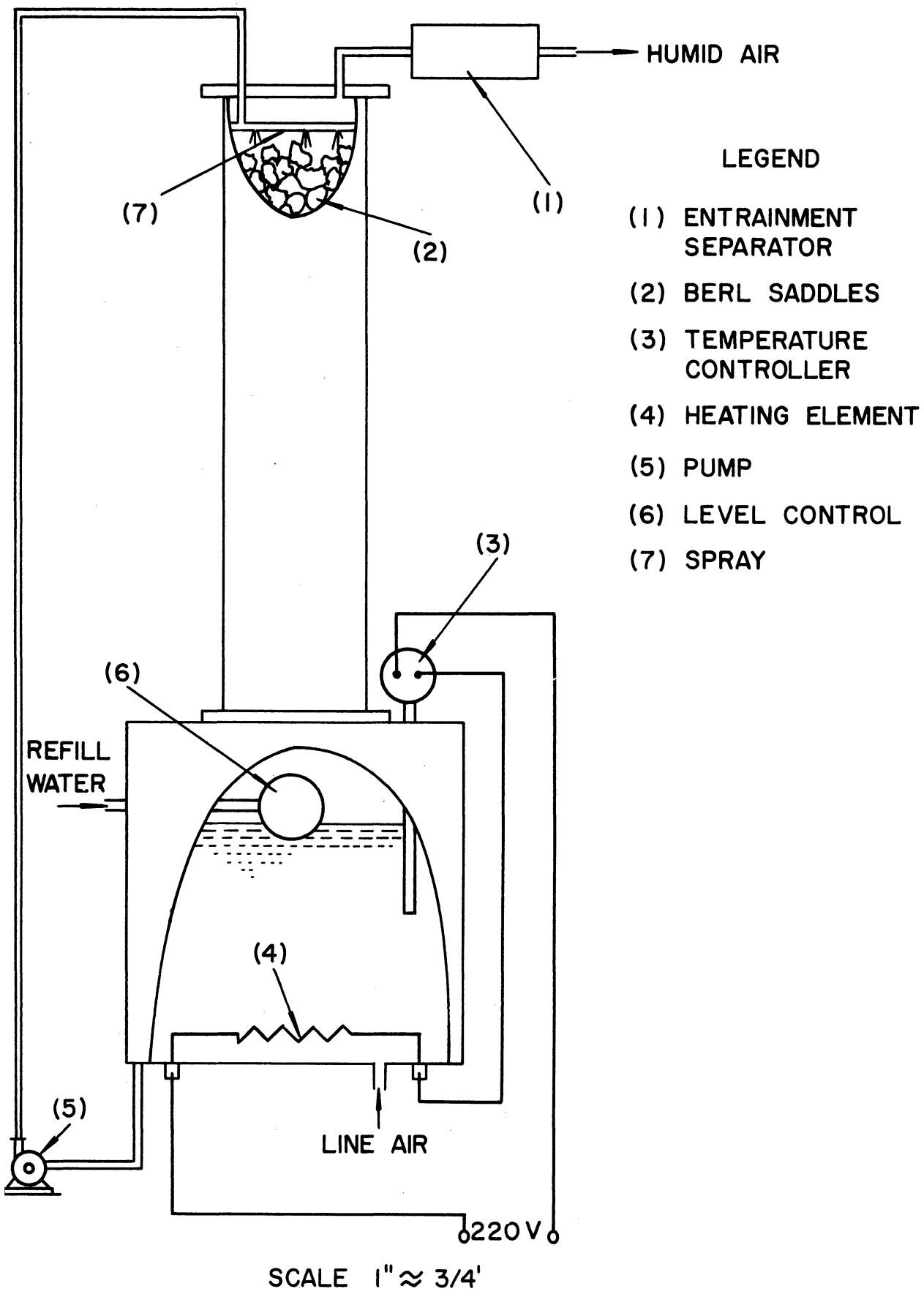

Fig. 3. Schematic Drawing of Humidifier Unit.

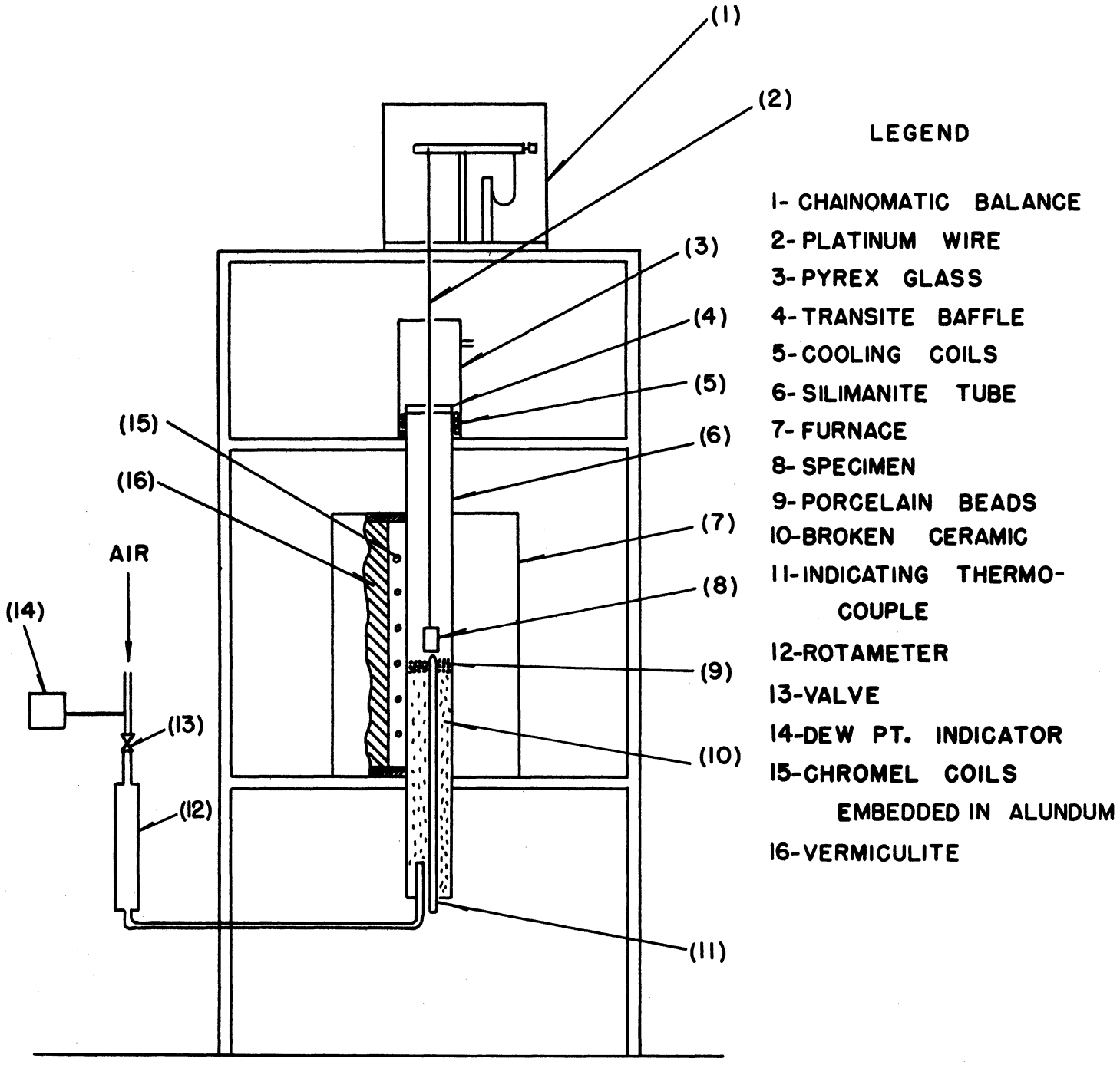

Fig. 4. Schematic Drawing of Weight-Gain Unit.

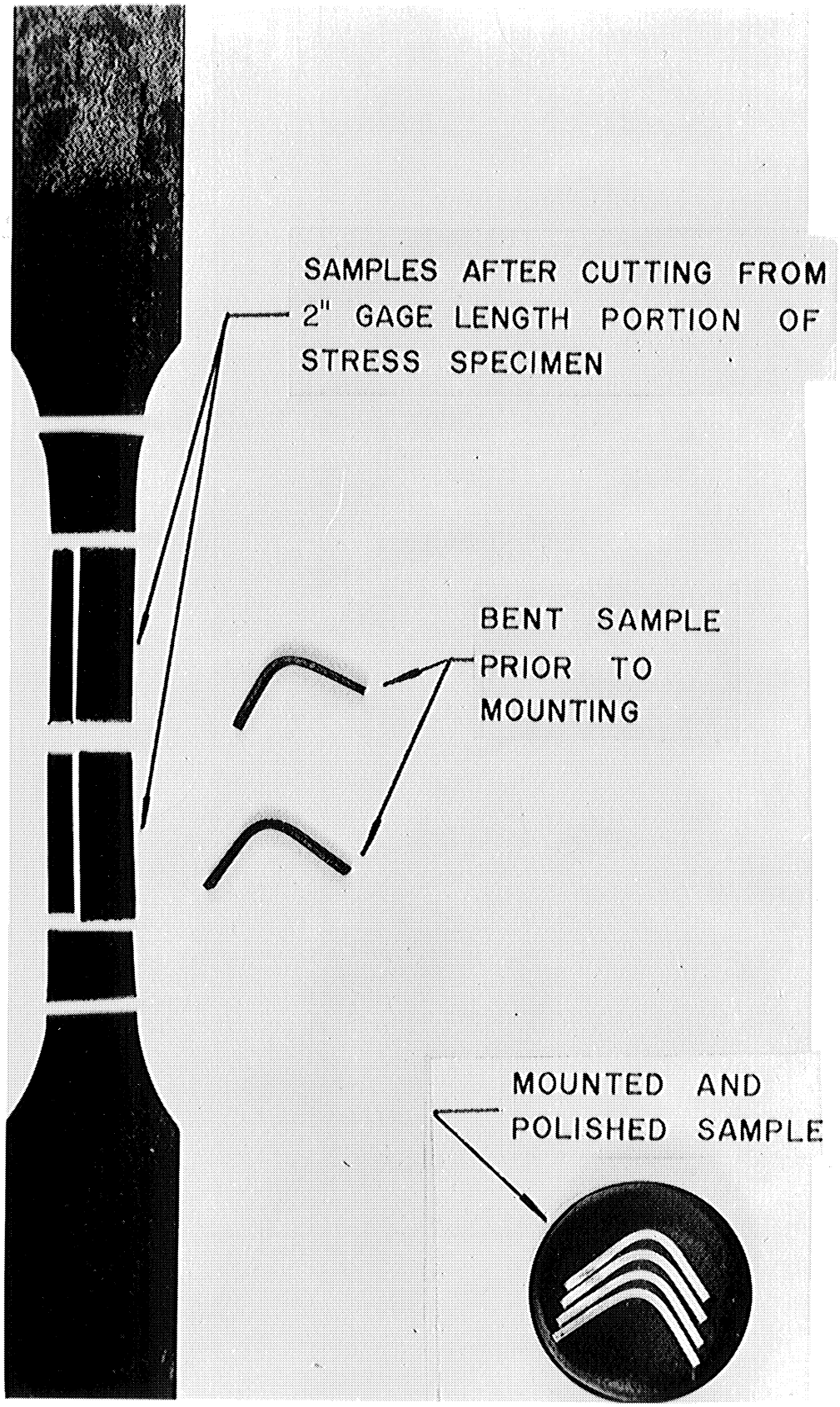

Fig. 5. Specimen Before and After Mounting.

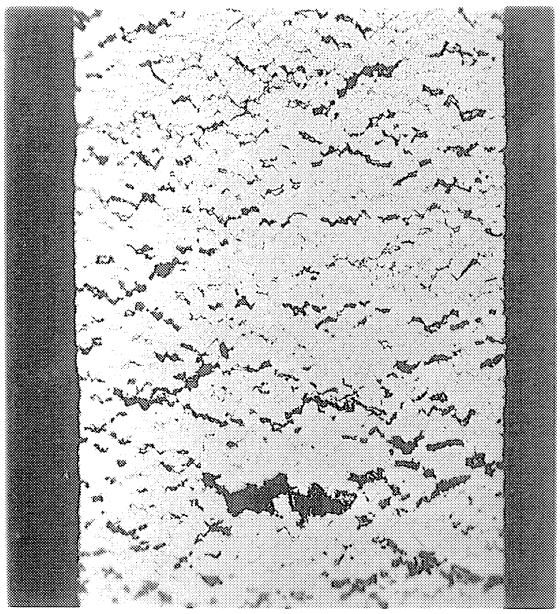

Fig. 6. Pre-rupture Fissures; Chromel ARM Alloy, Heat A, 1800°F, 100 Hours, Stress 2000 Psi, 50X; Cross Section, Unetched, Oblique Light.

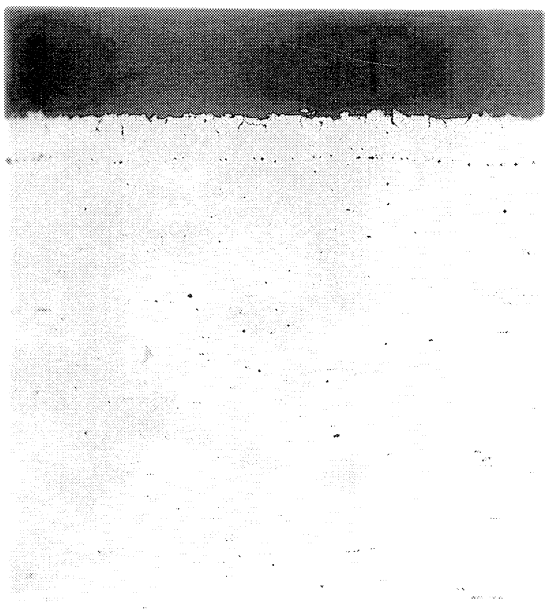

Fig. 7. Intergranular Penetrations; Type 310 Alloy, Heat X46572, 1800°F, 100 Hours, No Stress, 100X; Cross Section, Unetched.

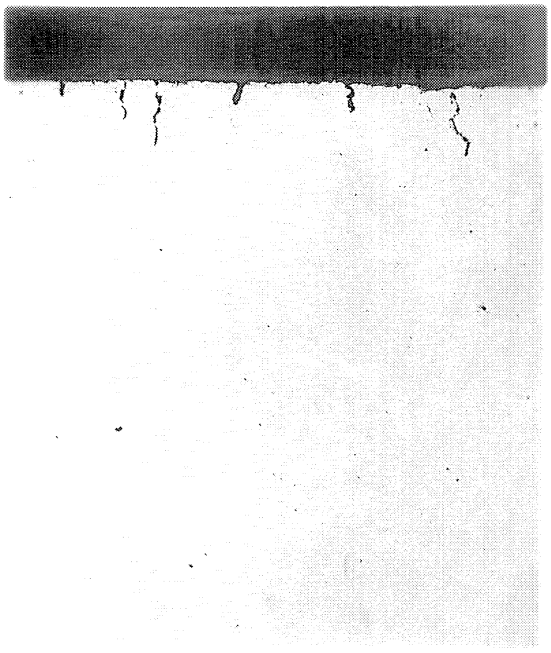

Fig. 8. Intergranular Penetrations; Type 310 Alloy, Heat X46572, 1800°F, 100 Hours, Stress 2480 Psi, 100X; Cross Section, Unetched.

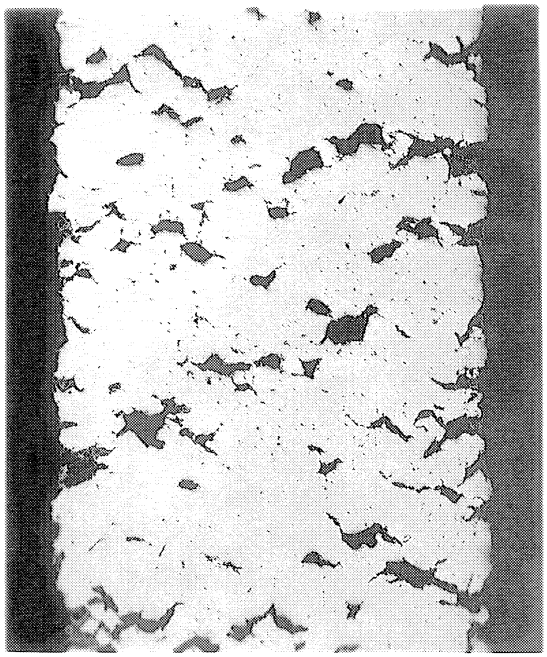

Fig. 9. Pre-rupture Fissures; Type 310 Alloy, Heat X46572, 1900°F, 100 Hours, Stress 2000 Psi, 50X; Cross Section, Unetched.

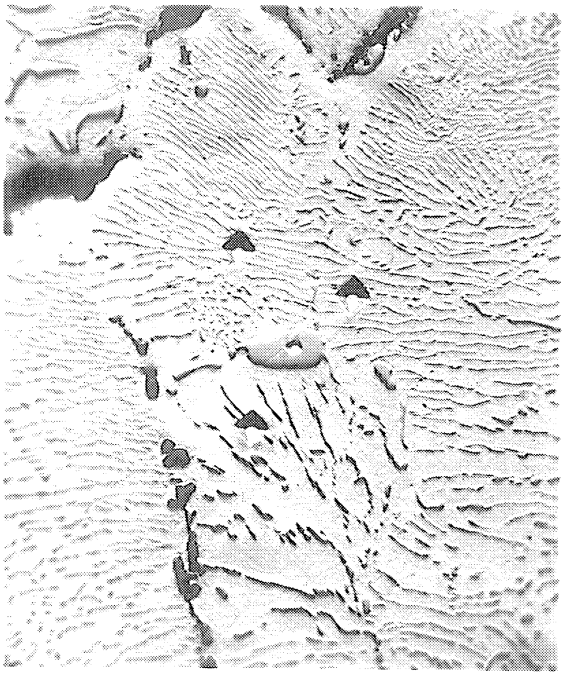

Fig. 10. Excess Constituent Pre-rupture Fissures and Knoop Microhardness Indentations; 10-Gram Load, Type 310 Alloy, Heat Vt-5, 1900°F, 100 Hours, Stress 1250 Psi, 750X; Cross Section, Unetched, Oblique Light.

Fig. 11. Excess Constituent and Pre-rupture Fissures; Type 310 Alloy, Heat X46572, 1900°F, 100 Hours, Stress 1000 Psi, 750X; Cross Section, Unetched, Oblique Light.

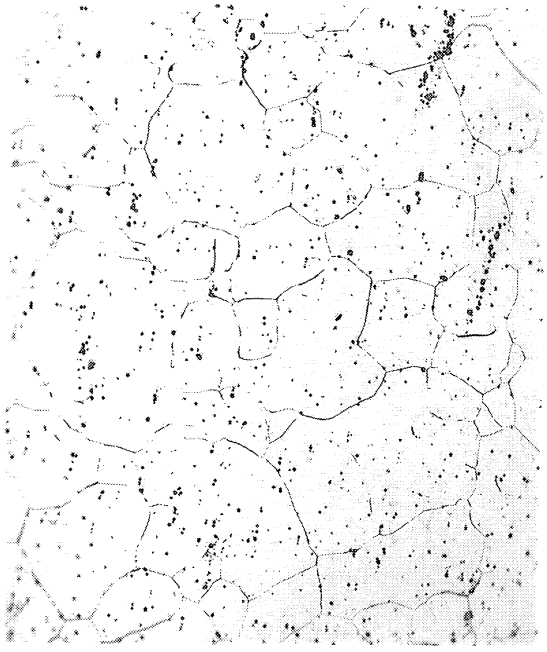

Fig. 12. Inclusions and Grain Size in As-Received Type 310 Alloy, Heat Vt-7, 250X; Cross Section, Etched Electrolytically in 10% Chromic Acid.

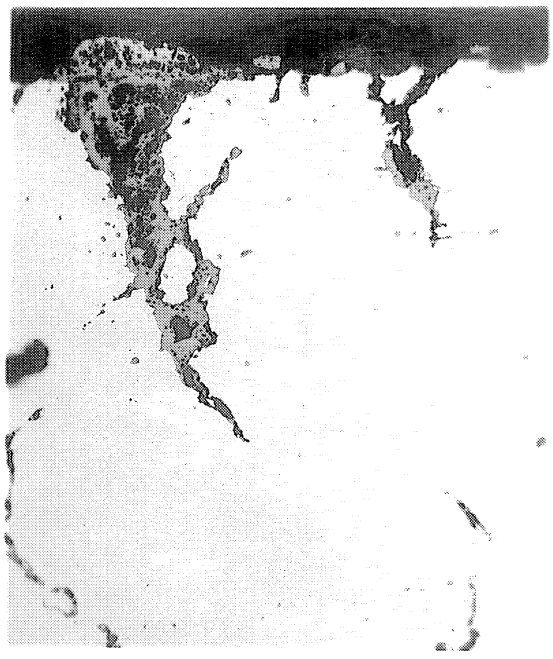

Fig. 13. Edge of Sample Containing Pre-rupture Fissures; Type 310 Alloy, Heat Vt-7, 1900°F, 100 Hours, Stress 900 Psi, 750X; Cross Section, Unetched.

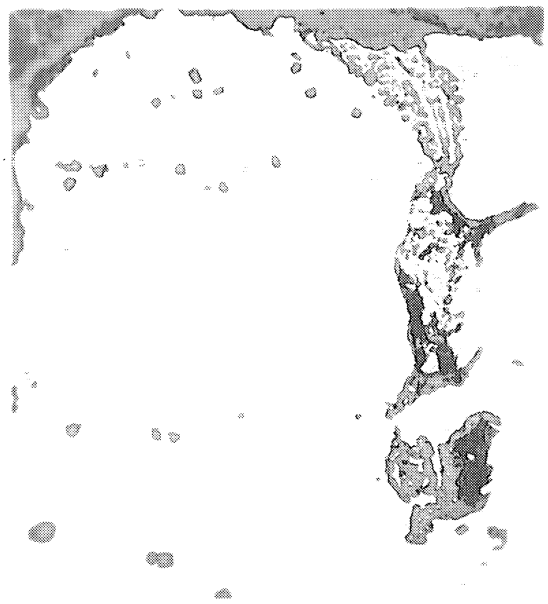

Fig. 14. Edge of Sample Containing Pre-rupture Fissures; Type 310 Alloy, Heat Vt-7, 1900°F, 100 Hours, Stress 900 Psi, 750X; Cross Section, Unetched.

Fig. 15. Surface Grains of Chromel Alloy ASM, 250X; Cross Section, Etched Electrolytically in 1-1-5 HCl, HNO_3, H_2O Solution.

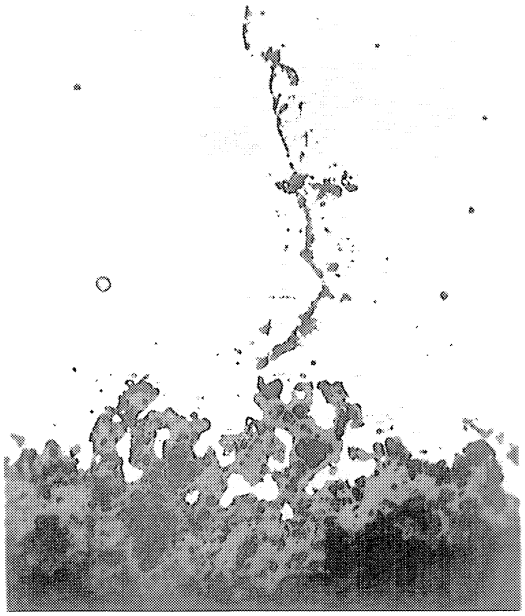

Fig. 16. Intergranular Penetrations; Chromel Alloy ARM, Heat A, 1900°F, 100 Hours, Stress 500 Psi, 750X; Cross Section, Unetched.

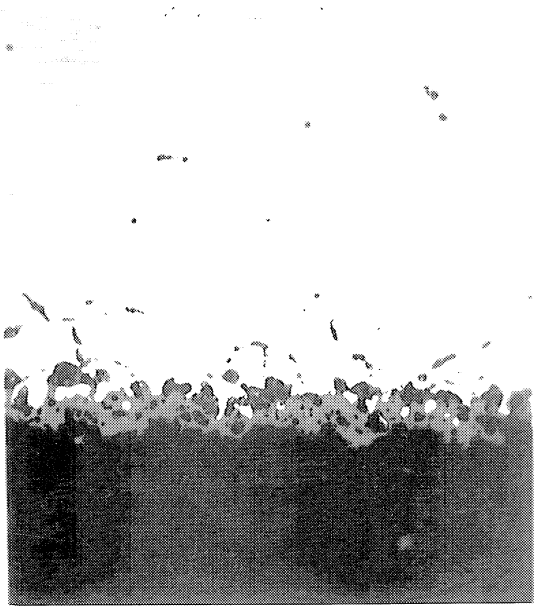

Fig. 17. Intergranular Penetrations; Chromel ARM Alloy, Heat A, 1900°F, 100 Hours, Stress 250 Psi, 750X; Cross Section, Unetched.

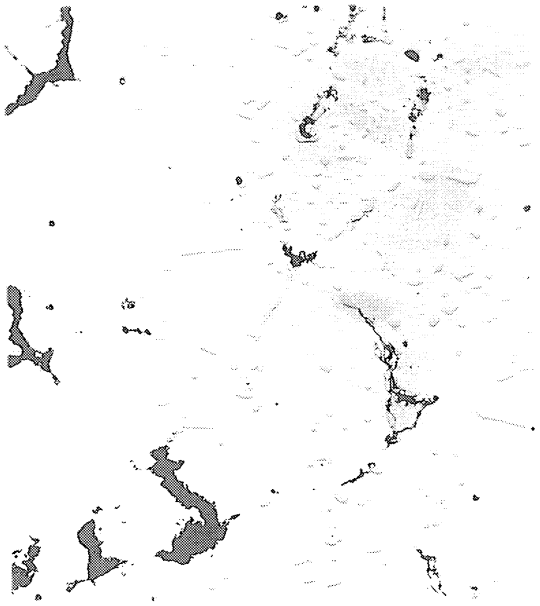

Fig. 18. Excess Constituent and Pre-rupture Fissures; Chromel Alloy ARM, Heat A, 1800°F, 100 Hours, Stress 2000 Psi, 750X; Cross Section, Unetched, Oblique Light.

Fig. 19. Intergranular Penetrations; Type 310 Alloy, Heat X27258, 1900°F, 100 Hours, Unstressed, 750X; Cross Section, Unetched.

Fig. 20. Intergranular Penetrations; Type 310 Alloy, Heat X27258, 1900°F, 500 Hours, Unstressed, 750X; Cross Section, Unetched.

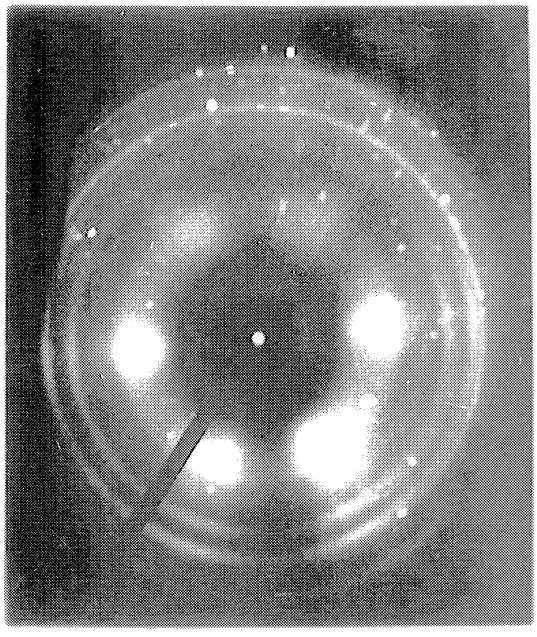

Fig. 21. X-ray Transmission Pattern; Type 310 Alloy, Heat 31372; Cold-Reduced 97% in Thickness.

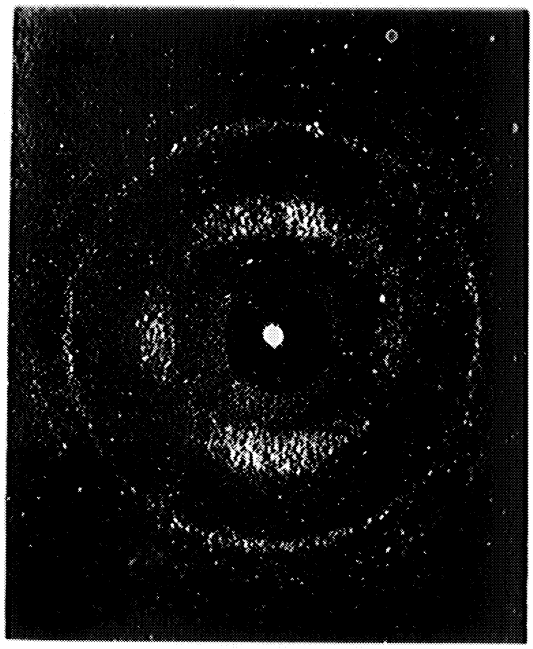

Fig. 22. X-ray Transmission Pattern; Type 310 Alloy, Heat 31372; Cold-Reduced 97% in Thickness and Annealed in Argon at 2000°F for 5-1/2 Hours.

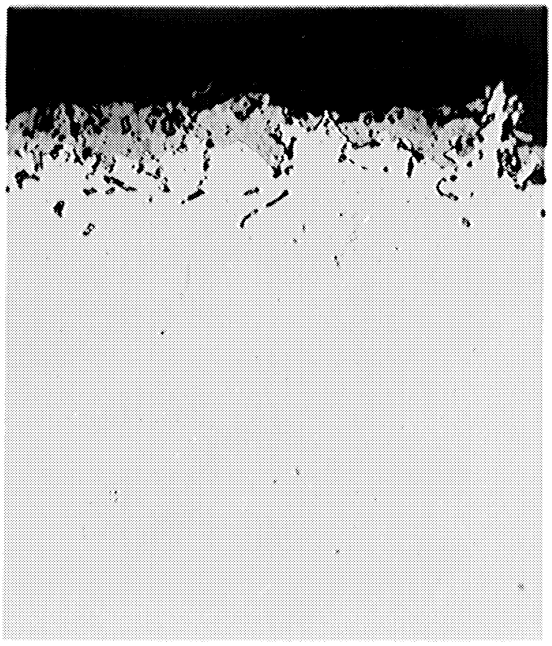

Fig. 23. Intergranular Penetrations; Type 310 Alloy, Heat 31372; Cold-Reduced 97% in Thickness and Annealed; Oxidized at 1900°F for 100 Hours; Unstressed, 750X; Cross Section, Unetched.

Fig. 24. Intergranular Penetrations; Type 310 Alloy, Heat 31372; Cold-Reduced 10% in Thickness and Oxidized at 1900°F for 100 Hours; Unstressed, 750X; Cross Section, Unetched.

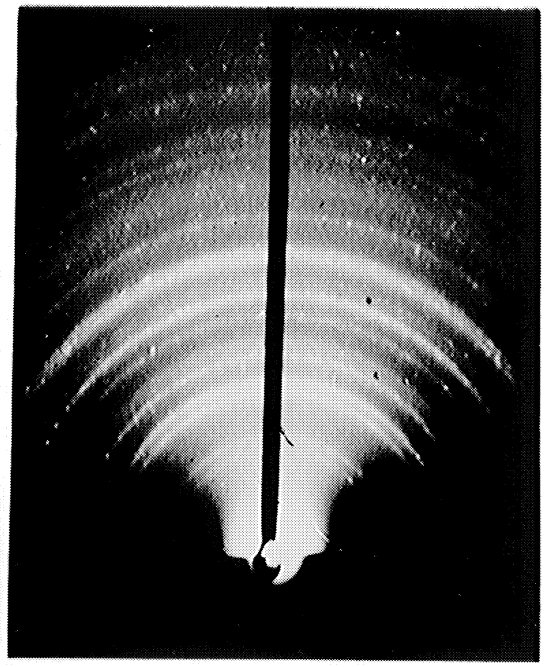

Fig. 25. Typical Electron Diffraction Pattern of Rhombohedral Phase.

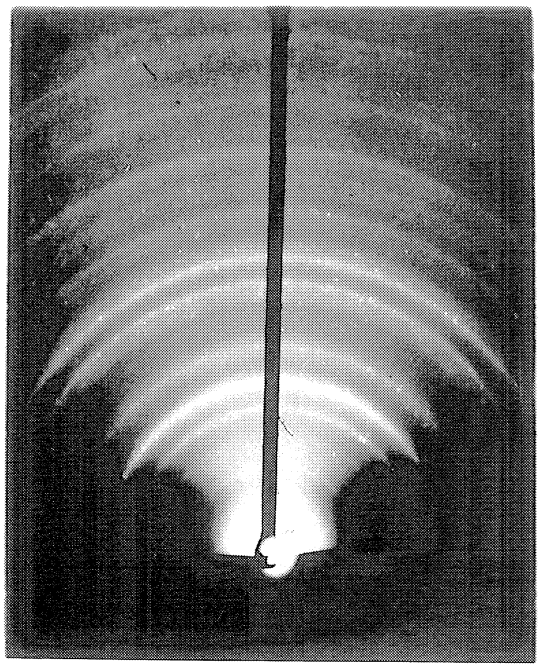

Fig. 26. Typical Electron Diffraction Pattern of Spinel Phase (Same Rhombohedral Phase Also Present).

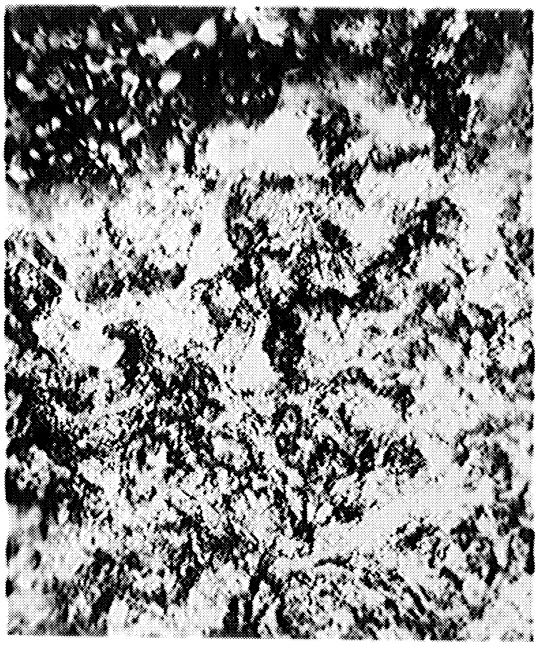

Fig. 27. Metallographic Appearance of Typical Oxidized Specimen Surface; Unetched, 250X; Oblique Light.

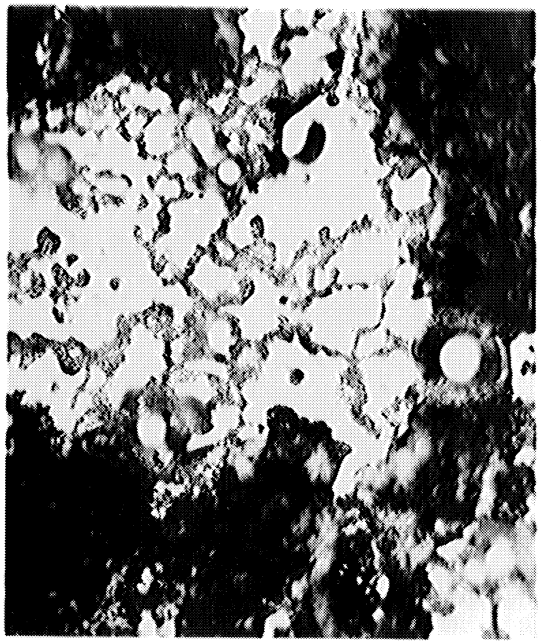

Fig. 28. Metallographic Appearance of Typical Oxidized Specimen Surface after 4 Minutes; Electrolytically Etched in 90% Glacial Acetic Acid and 10% Perchloric Acid; Removed 0.0004 Inch, 250X; Oblique Light.

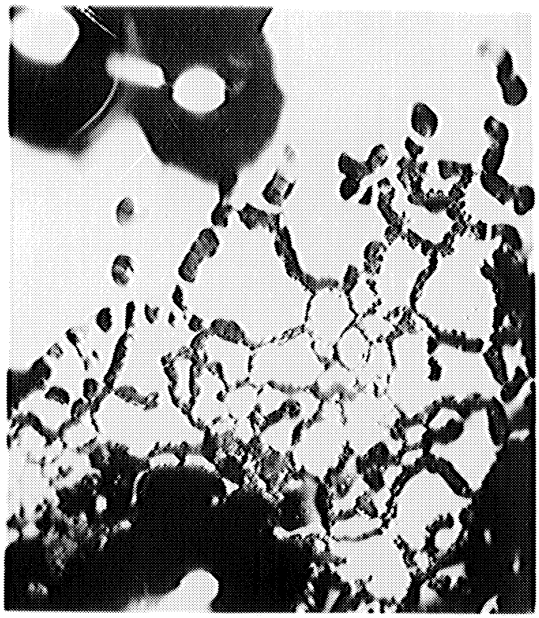

Fig. 29. Metallographic Appearance of Typical Oxidized Specimen Surface after 10 Minutes; Electrolytically Etched in 90% Glacial Acetic Acid and 10% Perchloric Acid; Removed 0.0004 Inch, 250X; Oblique Light.

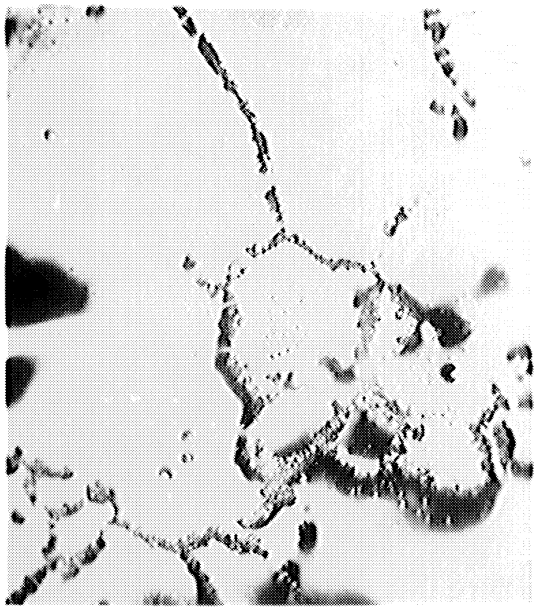

Fig. 30. Metallographic Appearance of Typical Oxidized Specimen Surface after 12 Minutes; Electrolytically Etched in 90% Glacial Acetic Acid and 10% Perchloric Acid; Removed 0.0011 Inch, 250X; Oblique Light.

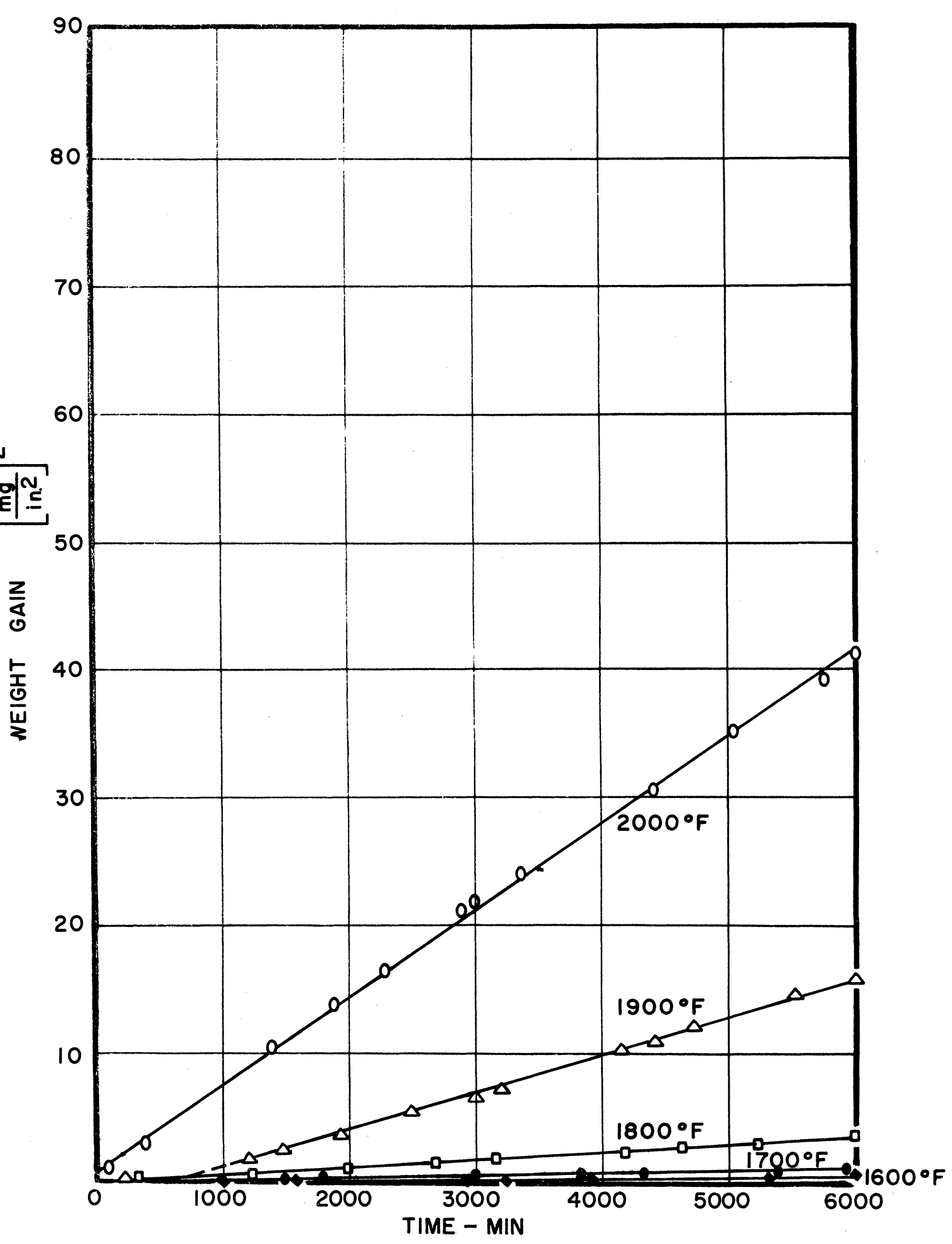

Fig. 31. Application of Parabolic Relationship to Weight-Gain Data; Type 310 Alloy, Heat J10.

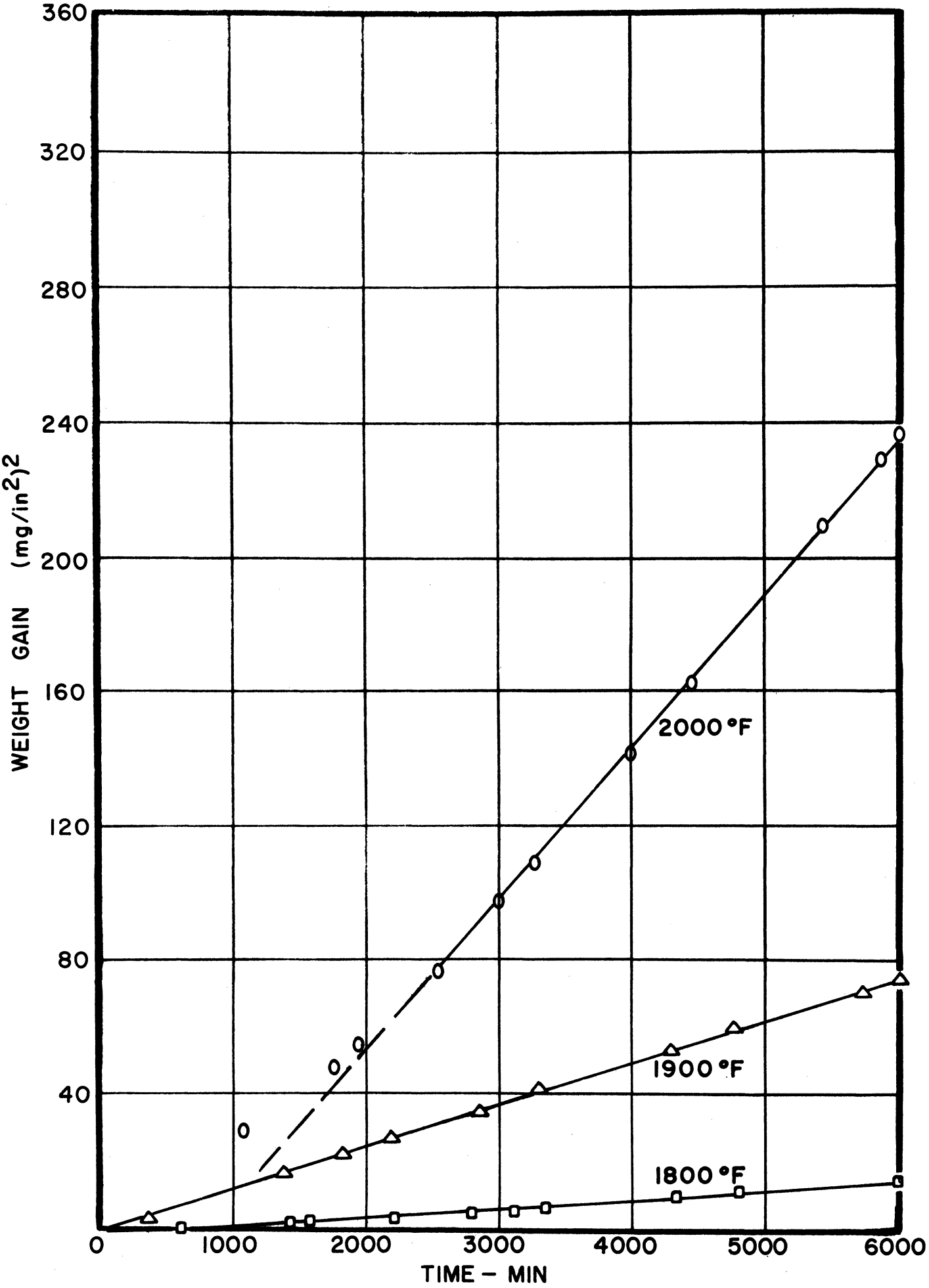

Fig. 32. Application of Parabolic Relationship to Weight-Gain Data; Chromel ARM Alloy, Heat A.

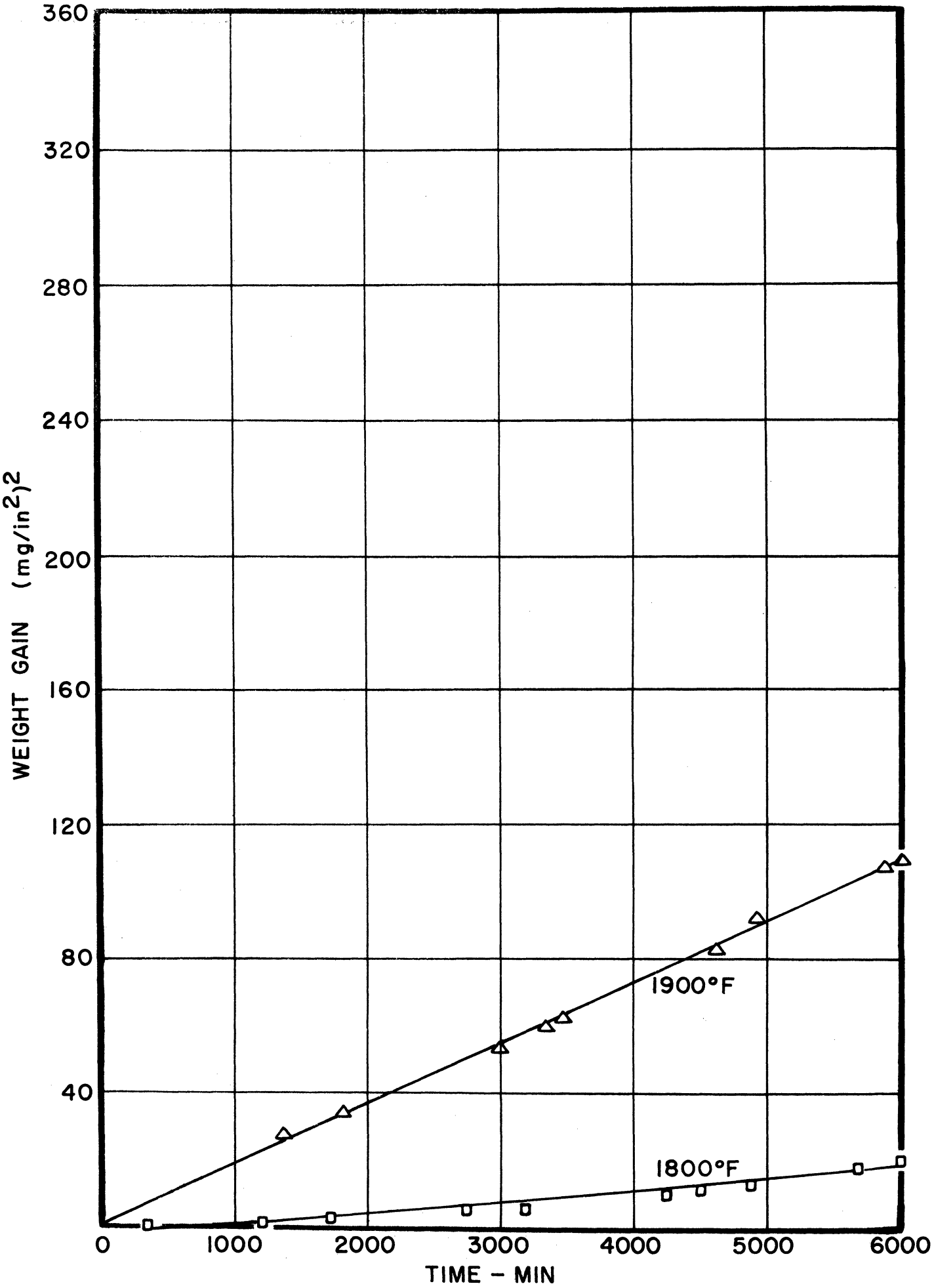

Fig. 33. Application of Parabolic Relationship to Weight-Gain Data; Type 310 Alloy, Heat Vt-7.

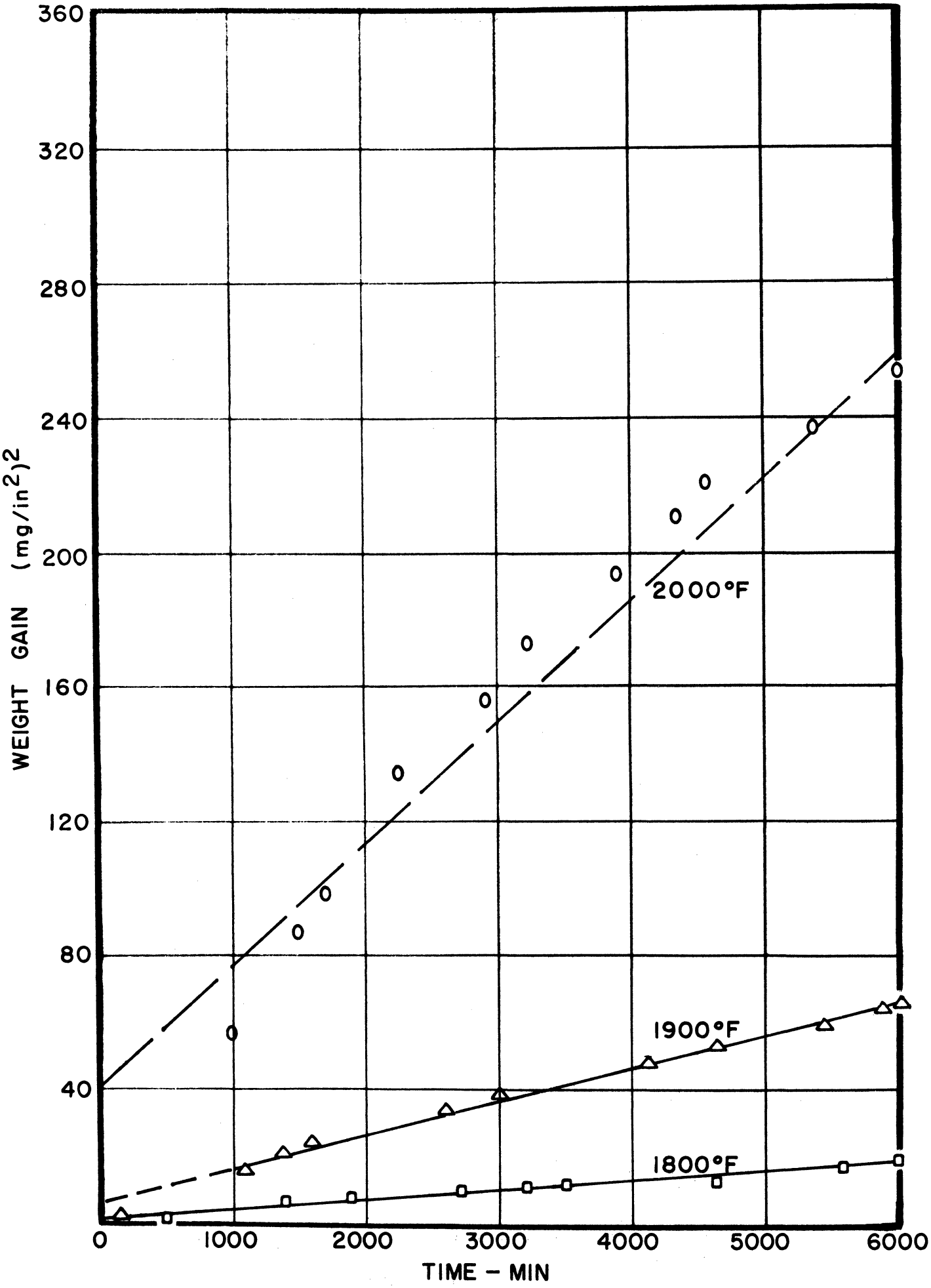

Fig. 34. Application of Parabolic Relationship to Weight-Gain Data; Chromel ASM Alloy.

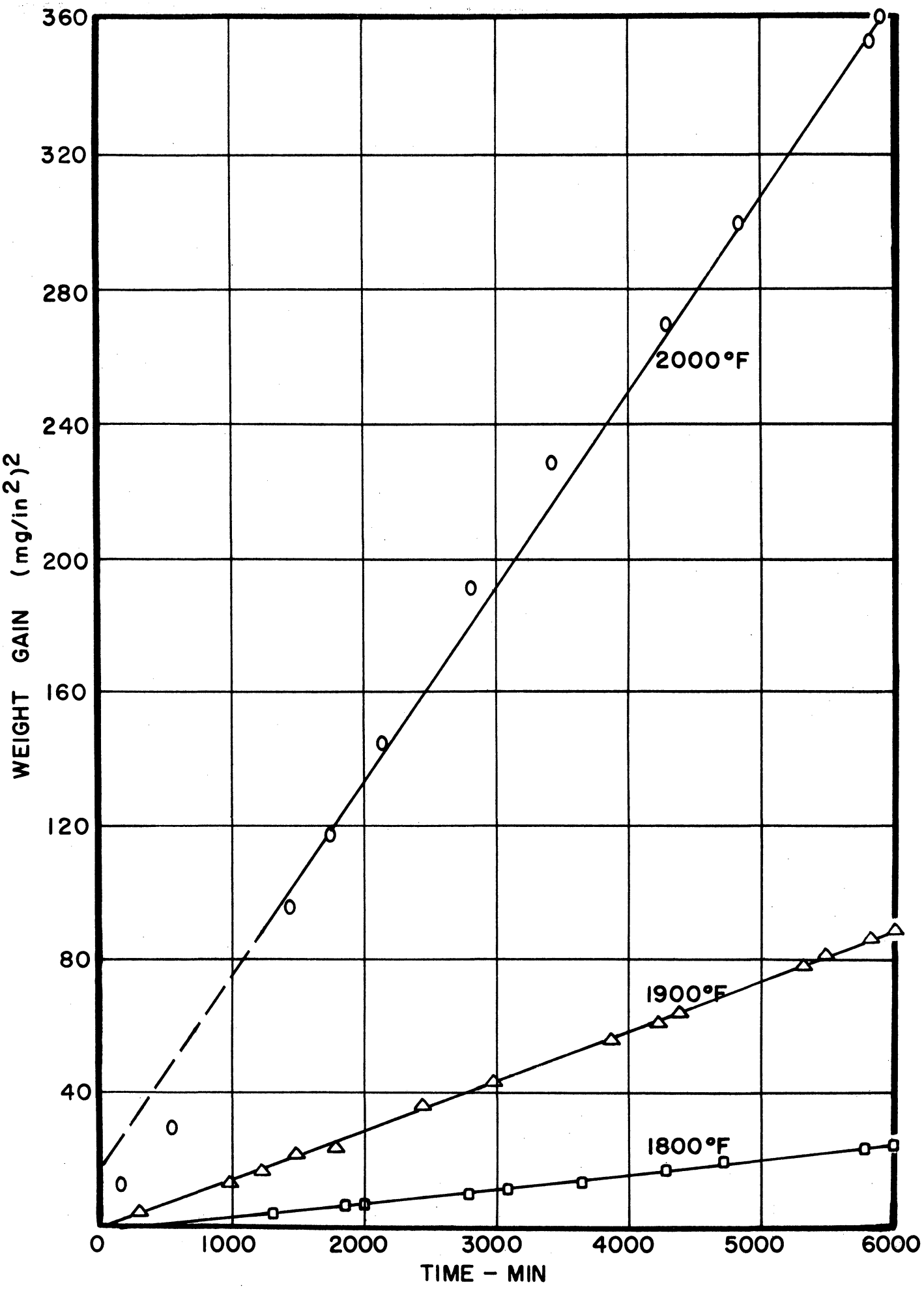

Fig. 35. Application of Parabolic Relationship to Weight-Gain Data; Type 310 Alloy, Heat Vt-5.

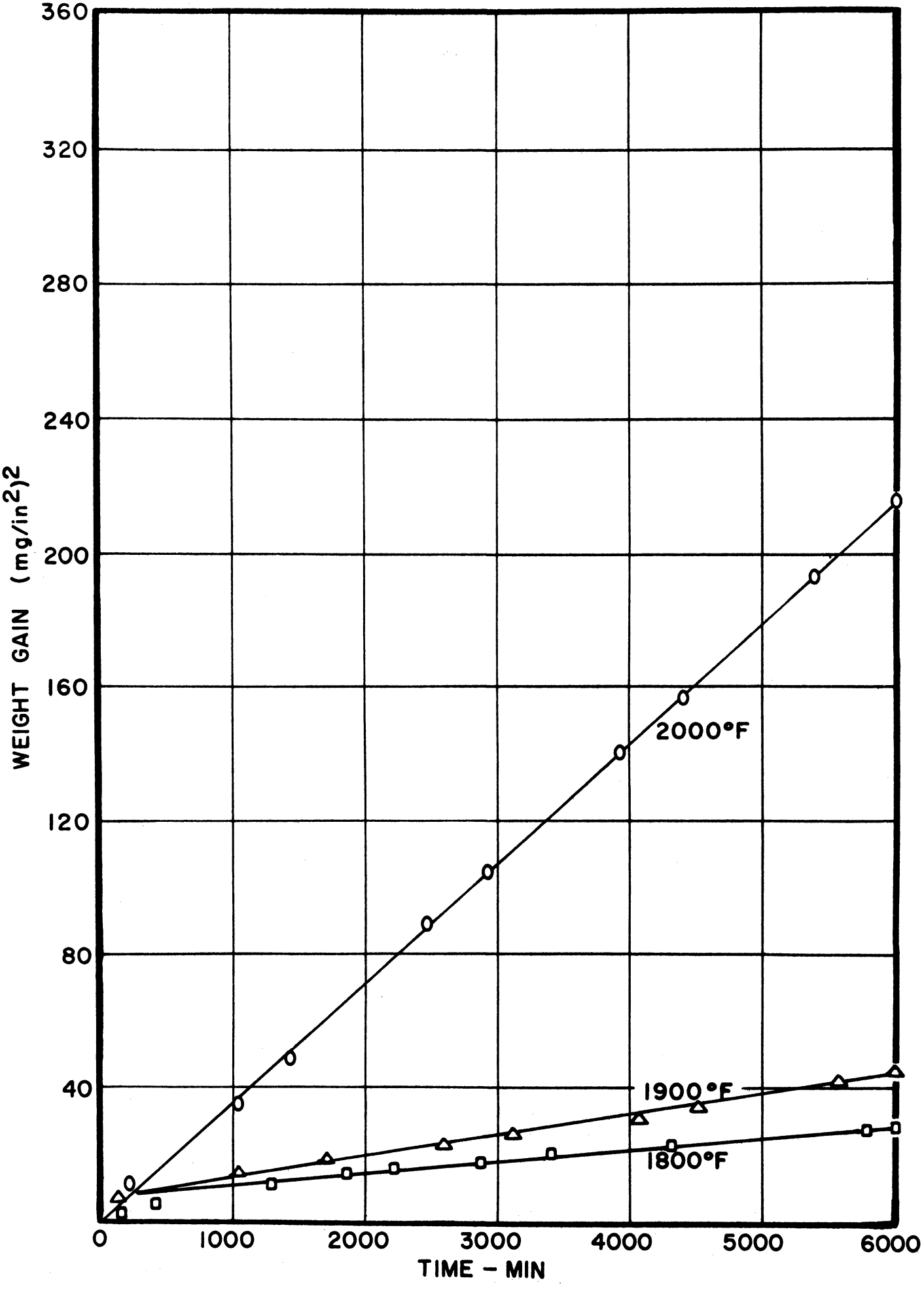

Fig. 36. Application of Parabolic Relationship to Weight-Gain Data; Chromel D Alloy.

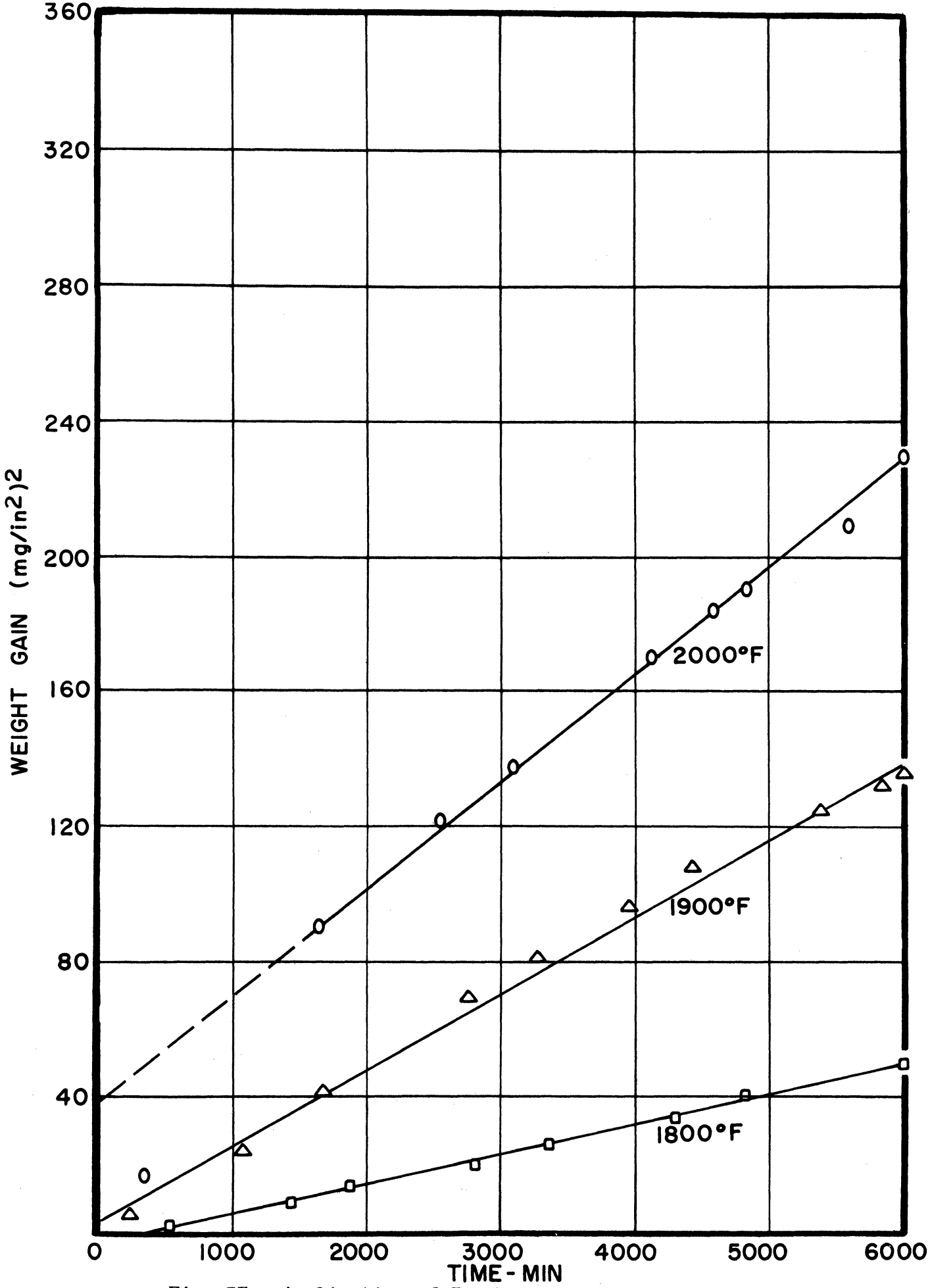

Fig. 37. Application of Parabolic Relationship to Weight-Gain Data; Type 310 Alloy, Heat X46572.

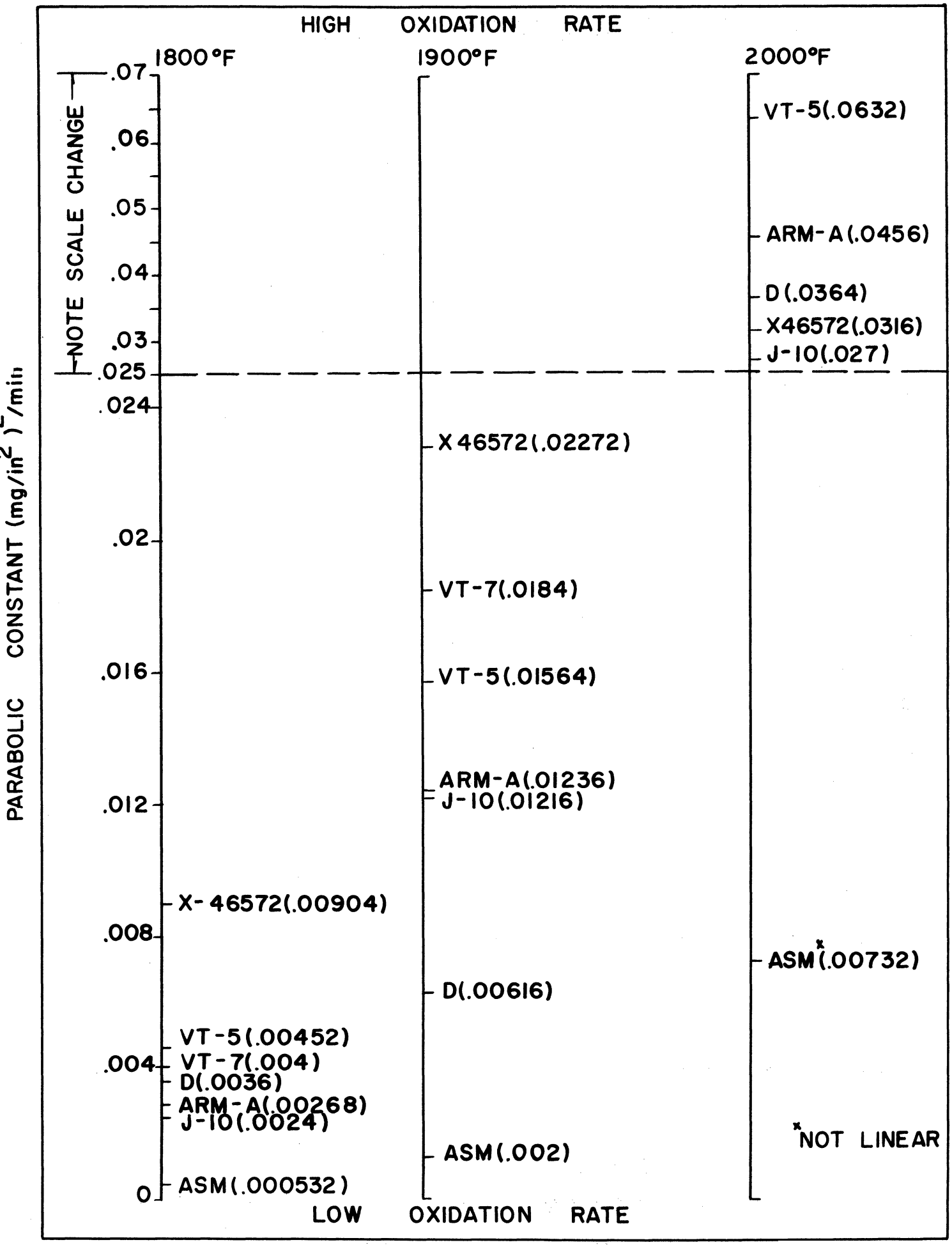

Fig. 38. Ratings of Alloys Tested on the Basis of Parabolic Rate Constant.

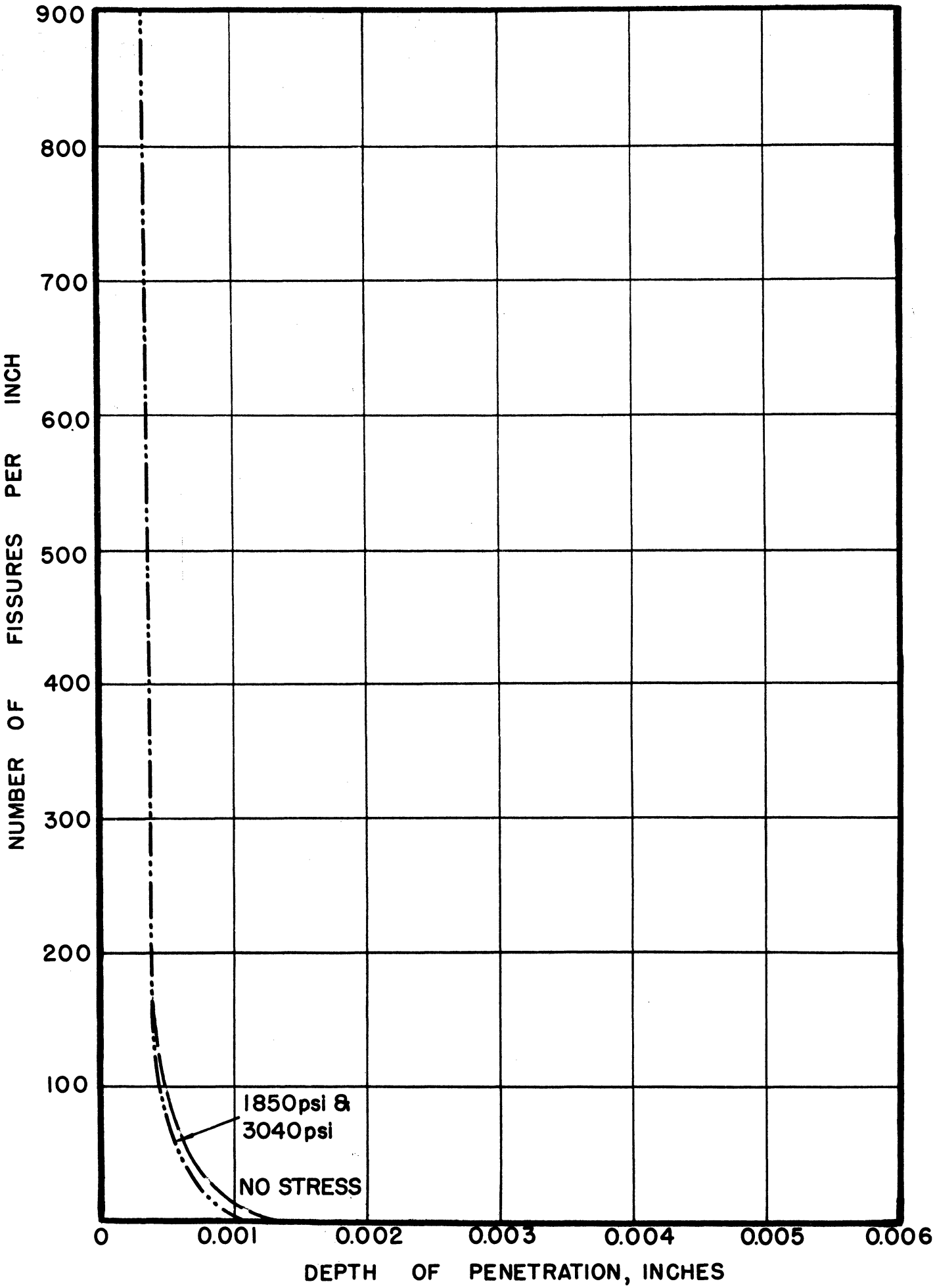

Fig. 39. Penetration vs. Depth Below Surface; Type 310 Alloy, Heat X27258, 1600°F, 100 Hours.

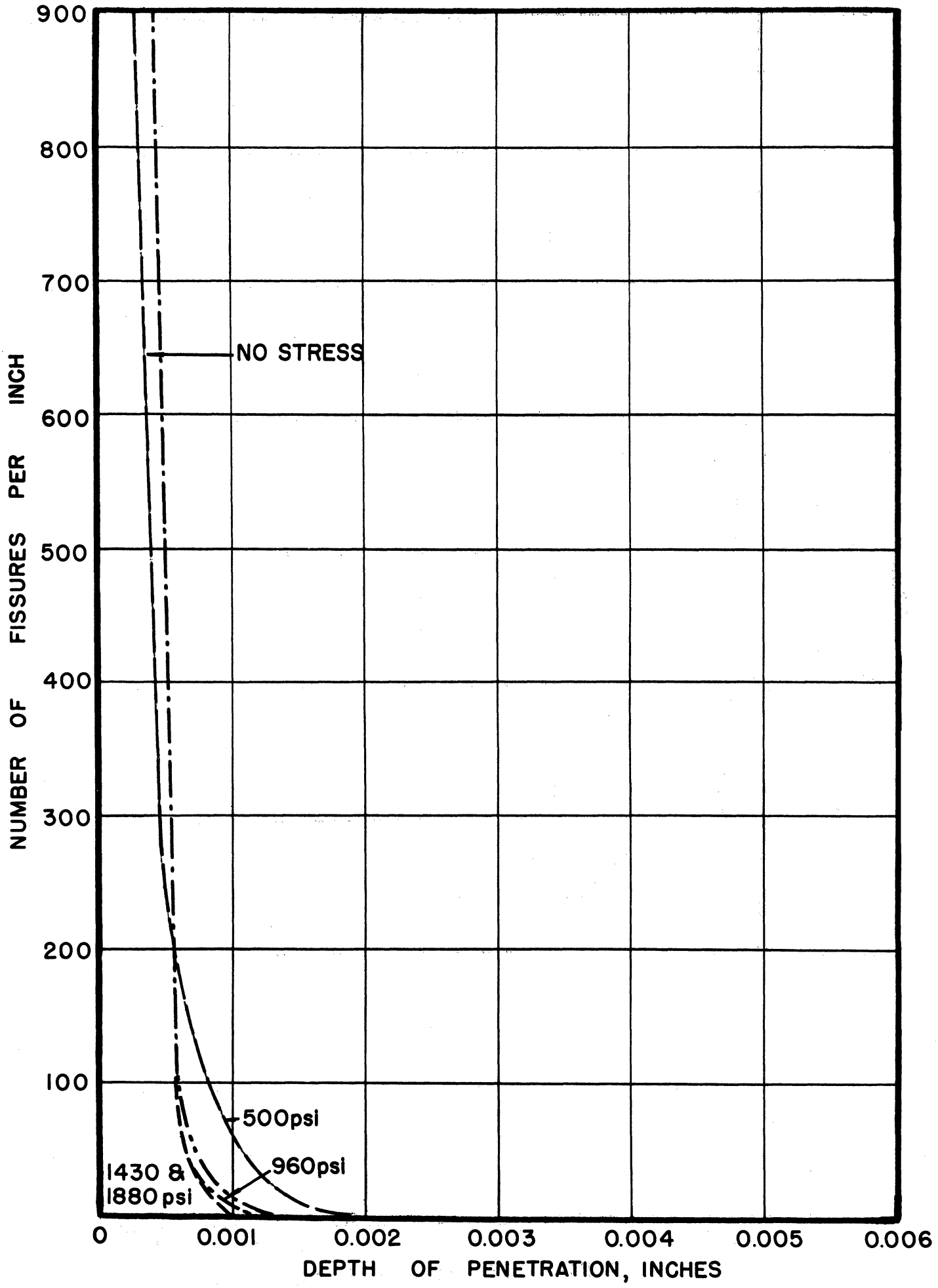

Fig. 40. Penetration vs. Depth Below Surface; Type 310 Alloy, Heat X27258, 1700°F, 100 Hours.

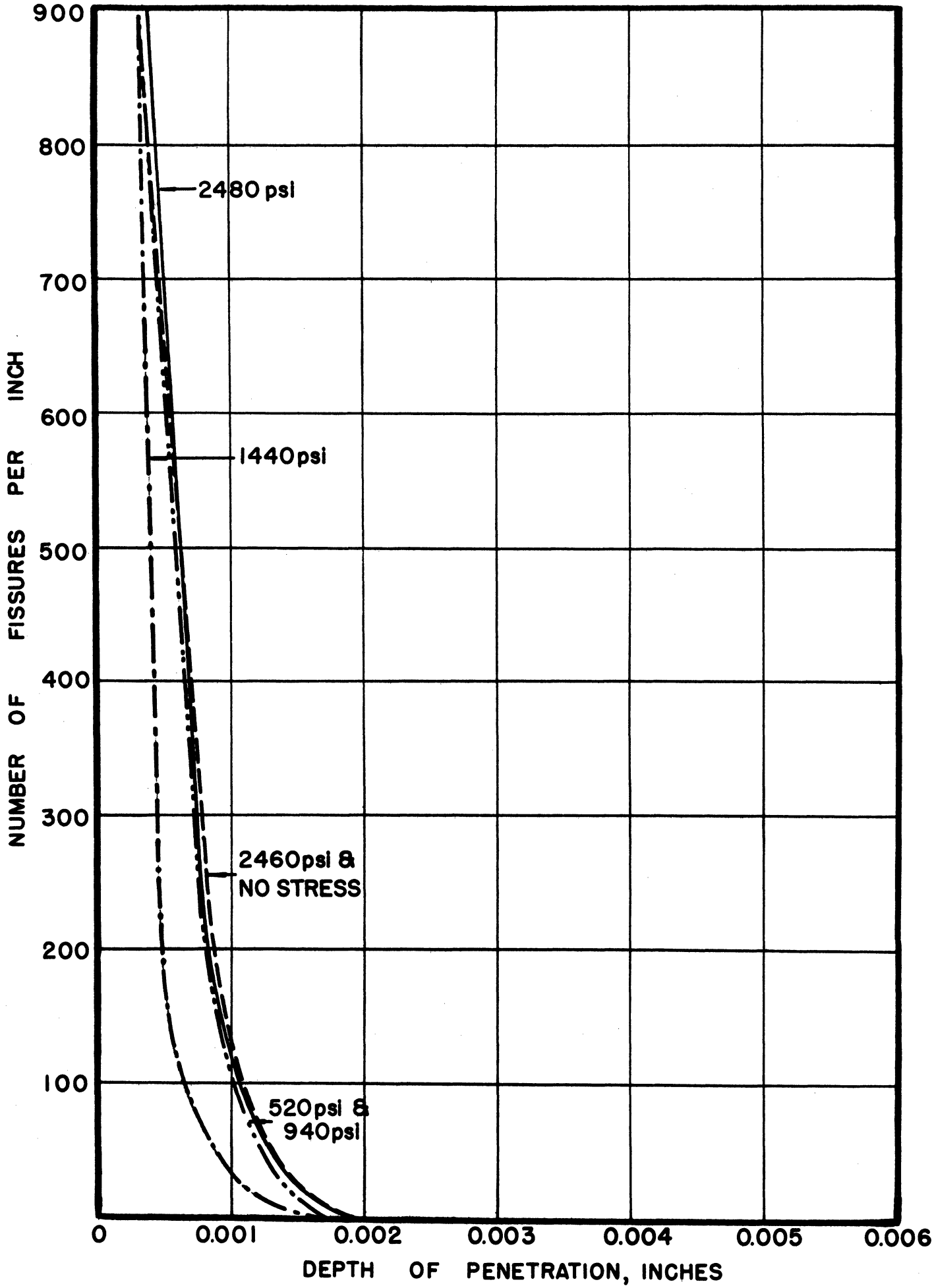

Fig. 41. Penetration vs. Depth Below Surface; Type 310 Alloy, Heat X27258, 1800°F, 100 Hours.

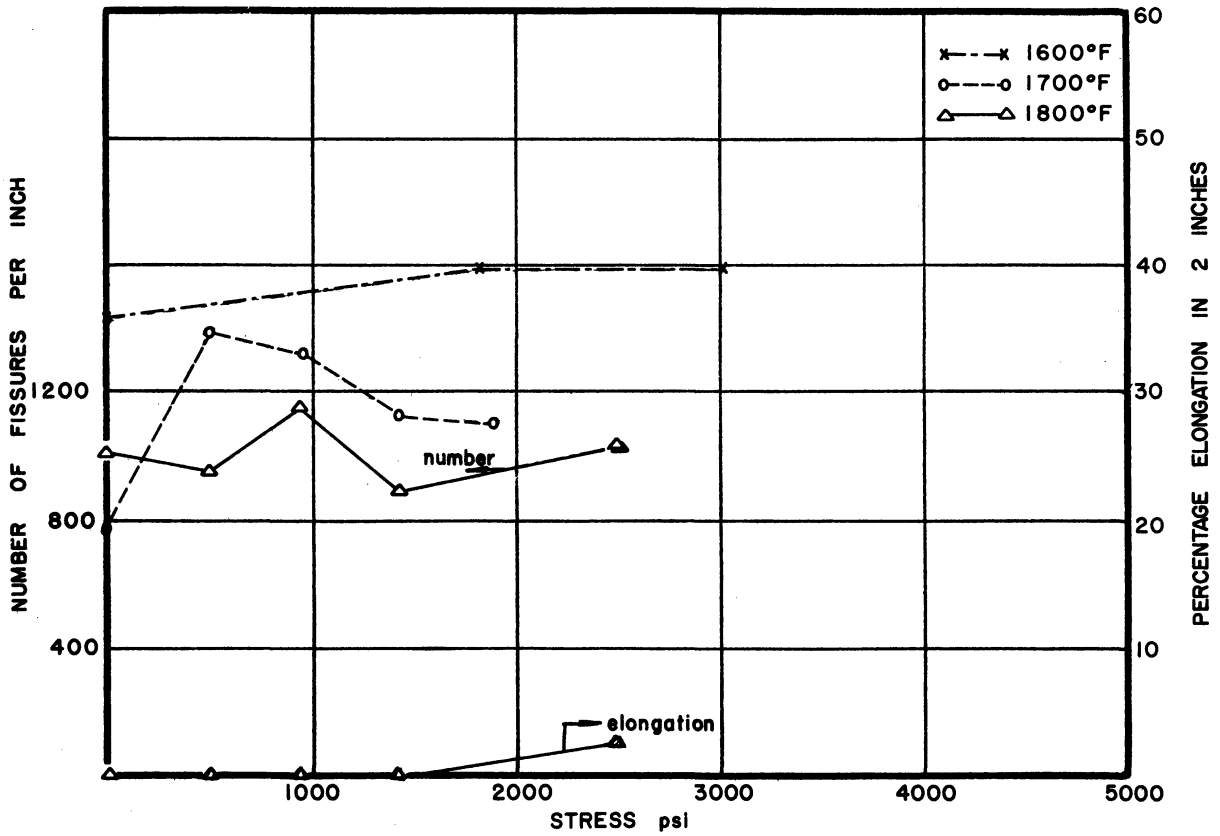

Fig. 42. Summary Penetration-Frequency Curves; Type 310 Alloy, Heat X27258, 1600°, 1700°, and 1800°F, 100 Hours.

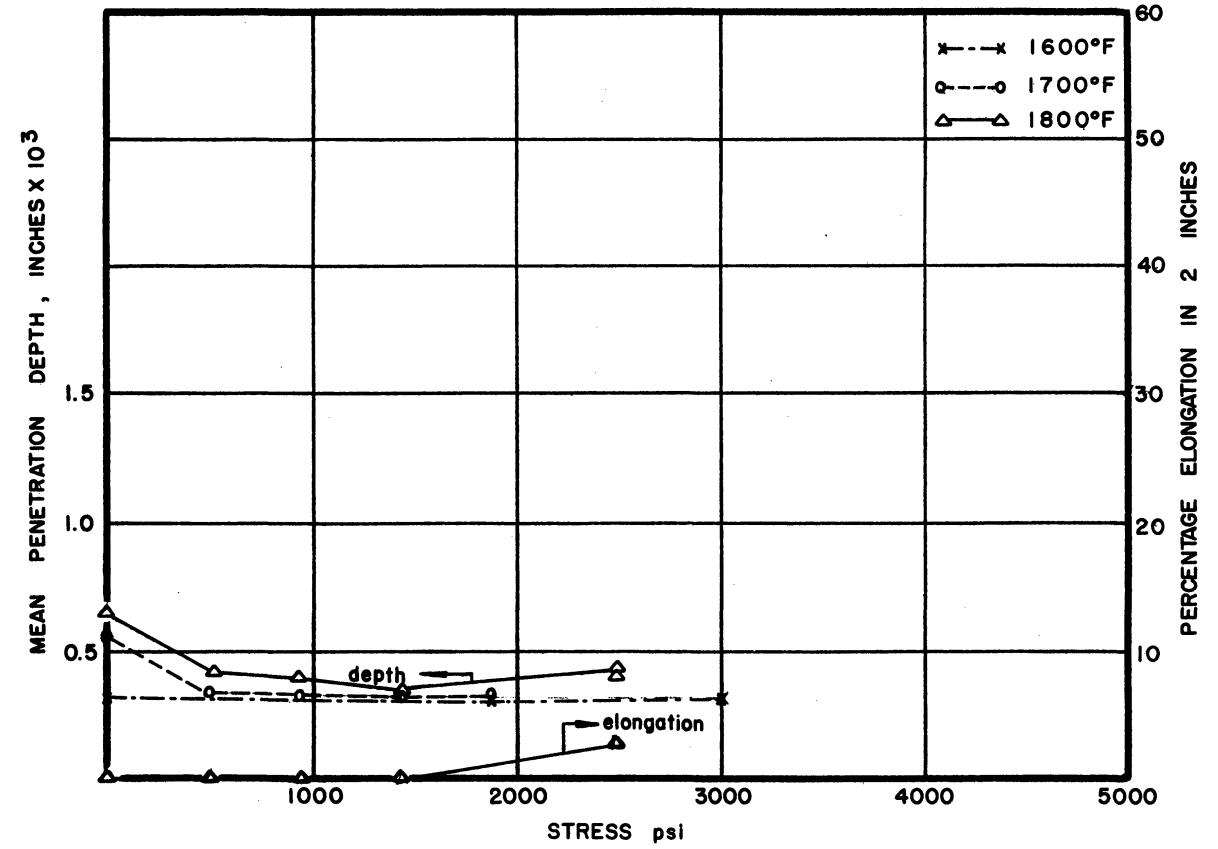

Fig. 43. Summary Penetration Depth Curves; Type 310 Alloy, Heat X27258, 1600°, 1700°, and 1800°F, 100 Hours.

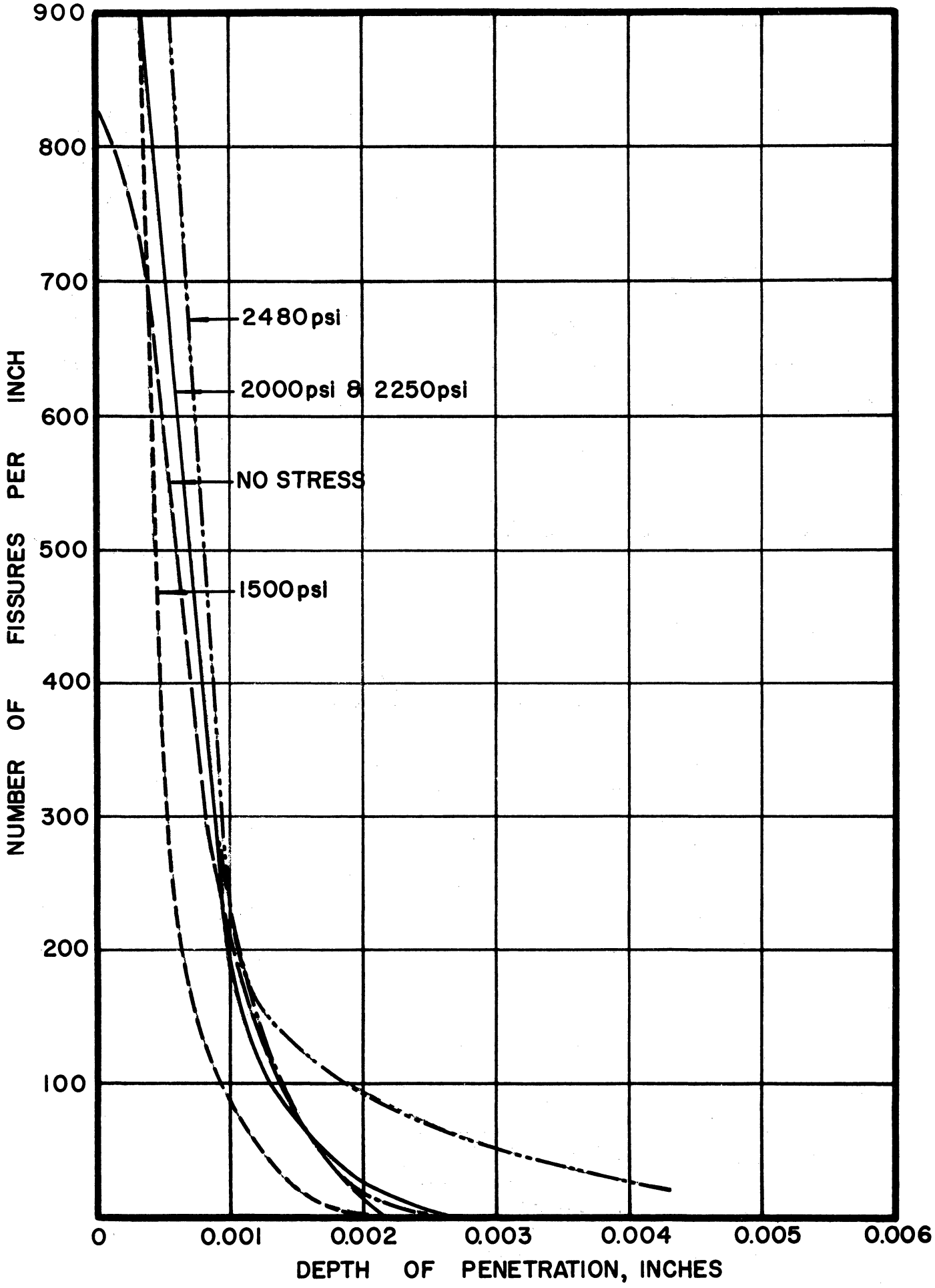

Fig. 44. Penetration vs. Depth Below Surface; Type 310 Alloy, Heat X46572, 1800°F, 100 Hours.

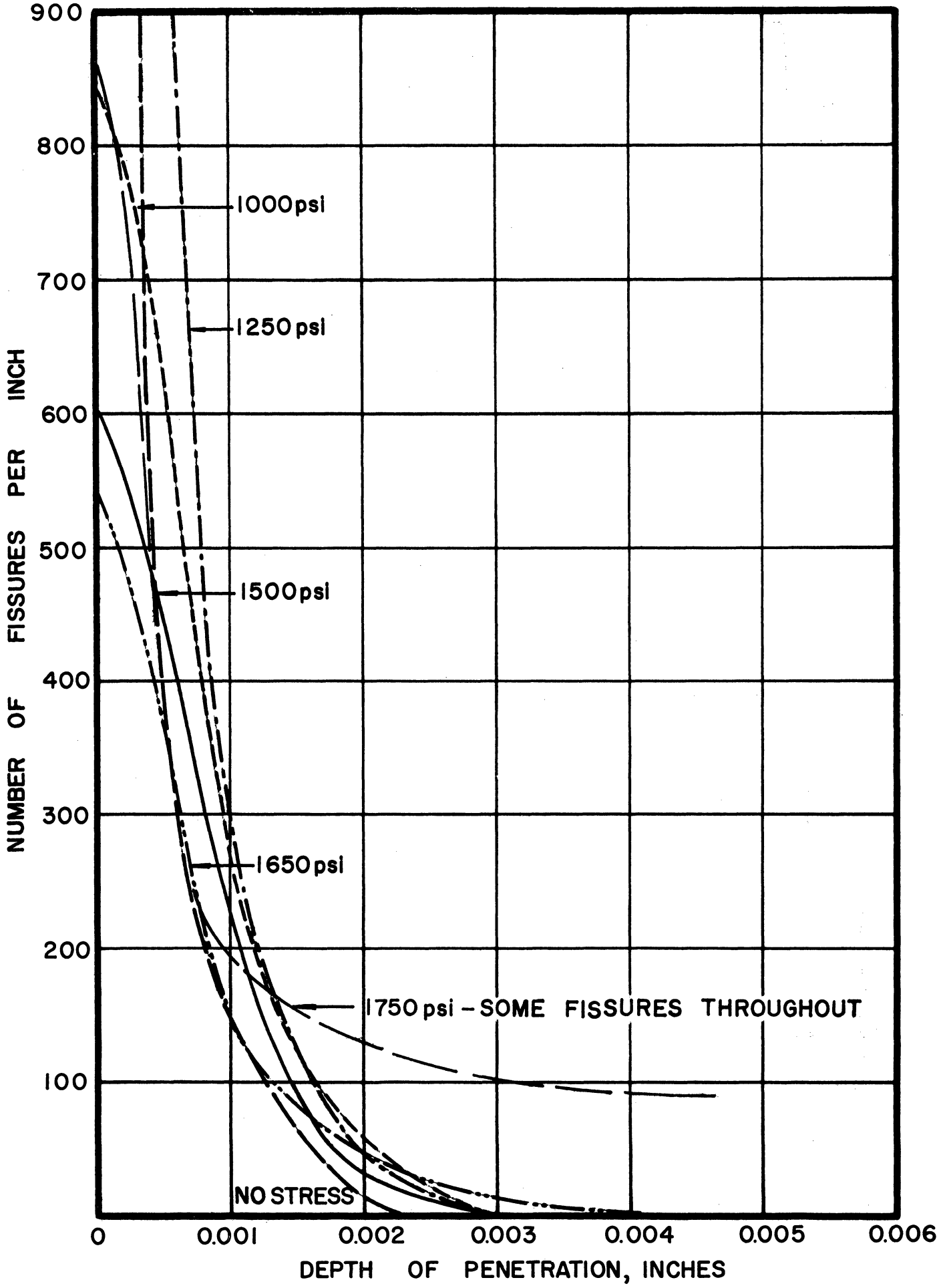

Fig. 45. Penetration vs. Depth Below Surface; Type 310 Alloy, Heat X46572, 1900°F, 100 Hours.

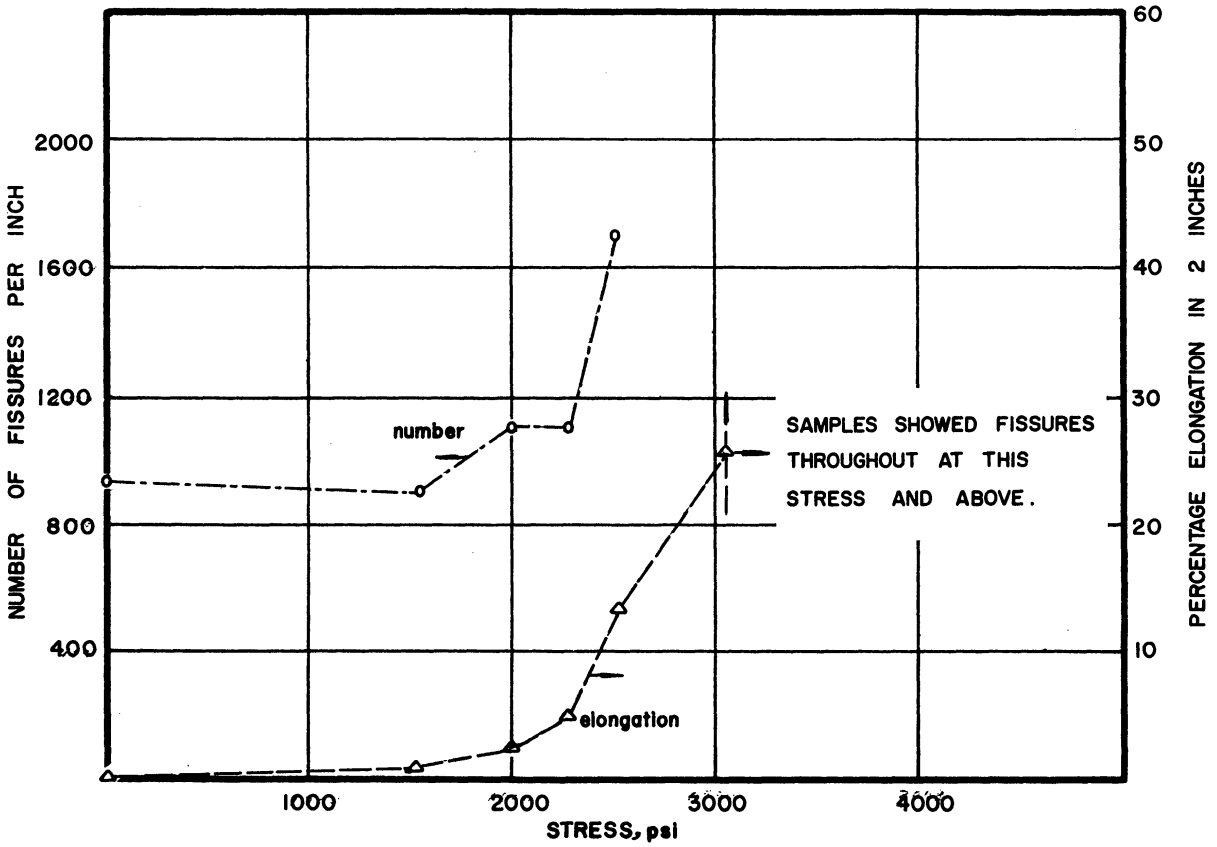

Fig. 46. Summary Penetration-Frequency Curves; Type 310 Alloy, Heat X46572, 1800°F, 100 Hours.

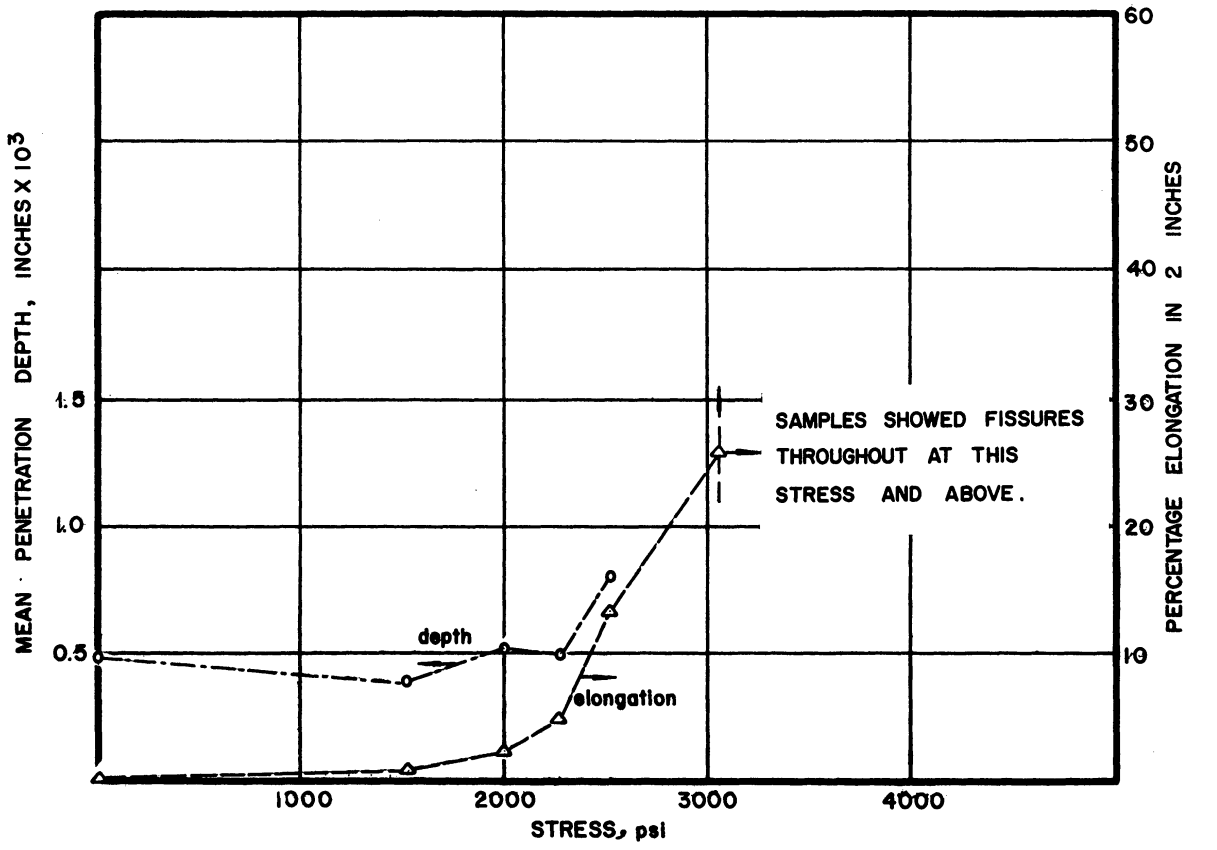

Fig. 47. Summary Penetration Depth Curves; Type 310 Alloy, Heat X46572, 1800°F, 100 Hours.

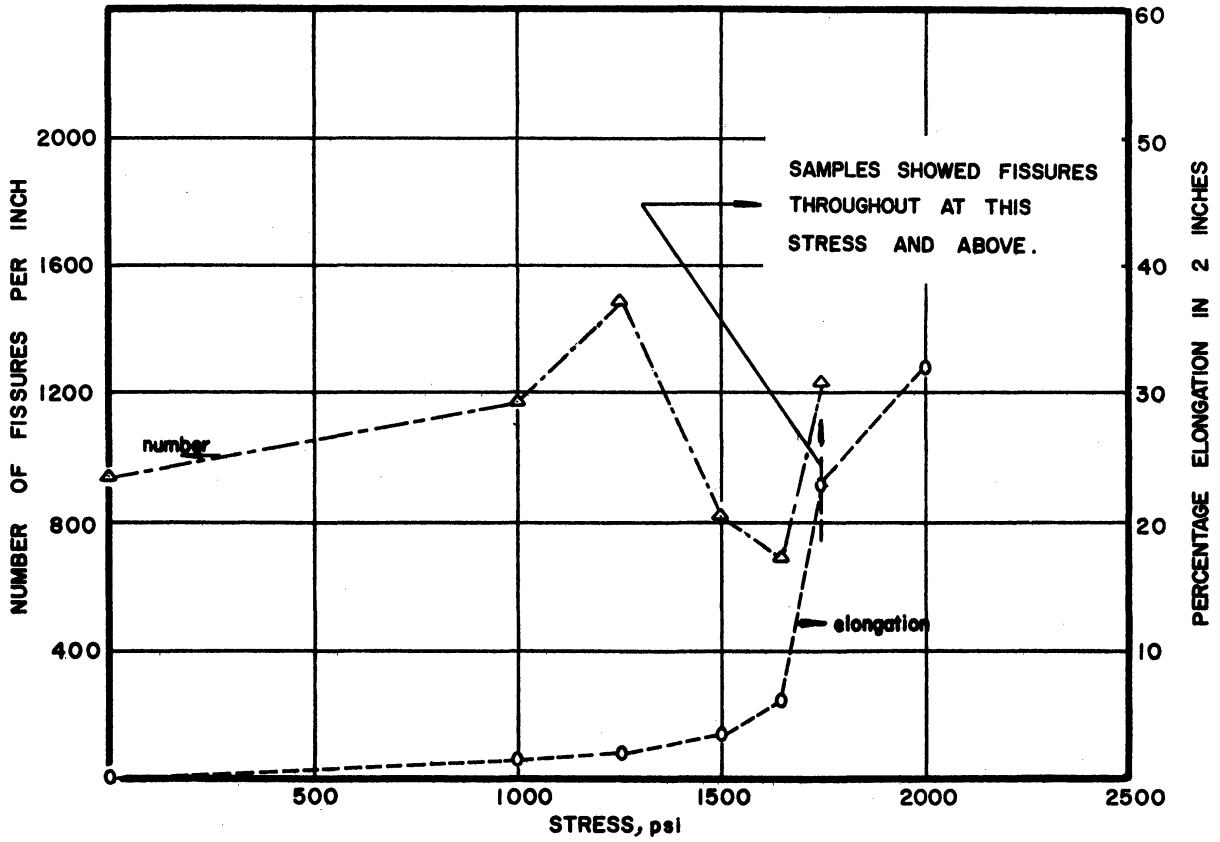

Fig. 48. Summary Penetration-Frequency Curves; Type 310 Alloy, Heat X46572, 1900°F, 100 Hours.

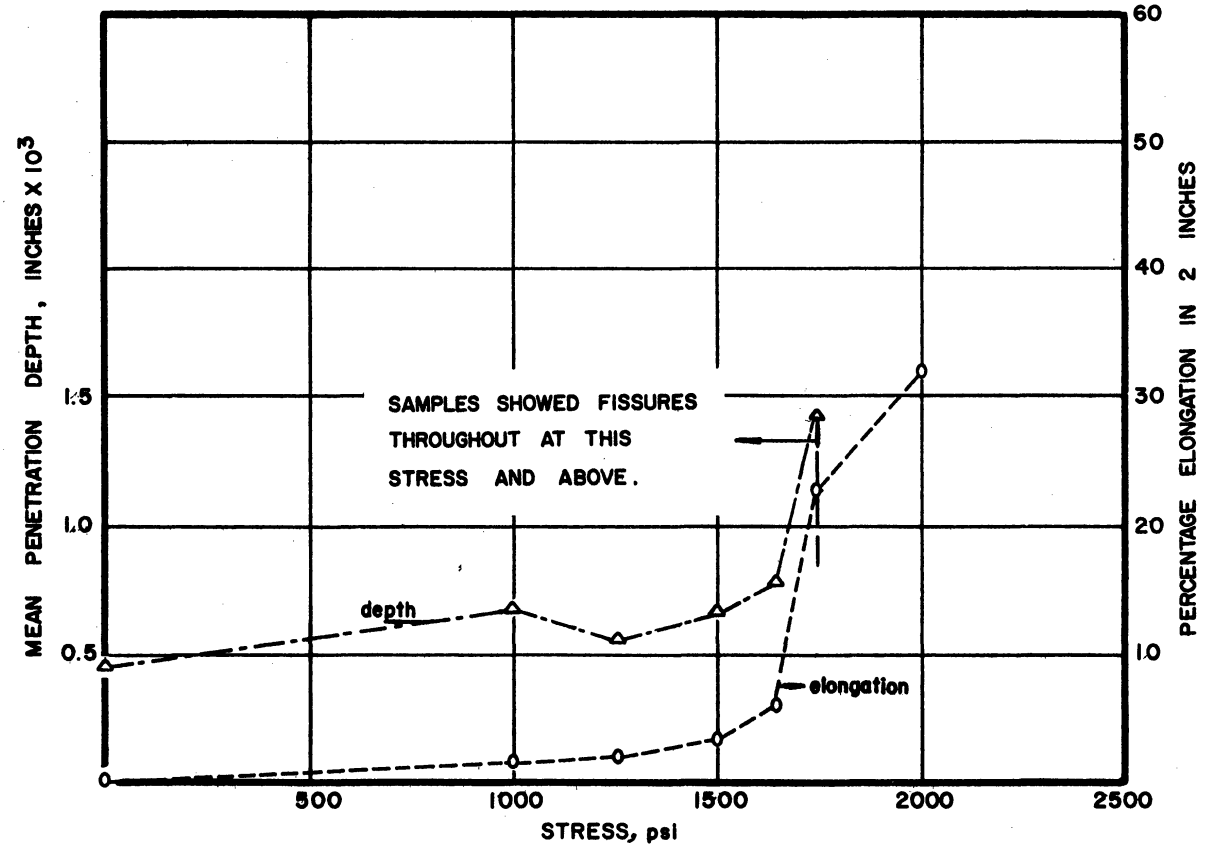

Fig. 49. Summary Penetration Depth Curves; Type 310 Alloy, Heat X46572, 1900°F, 100 Hours.

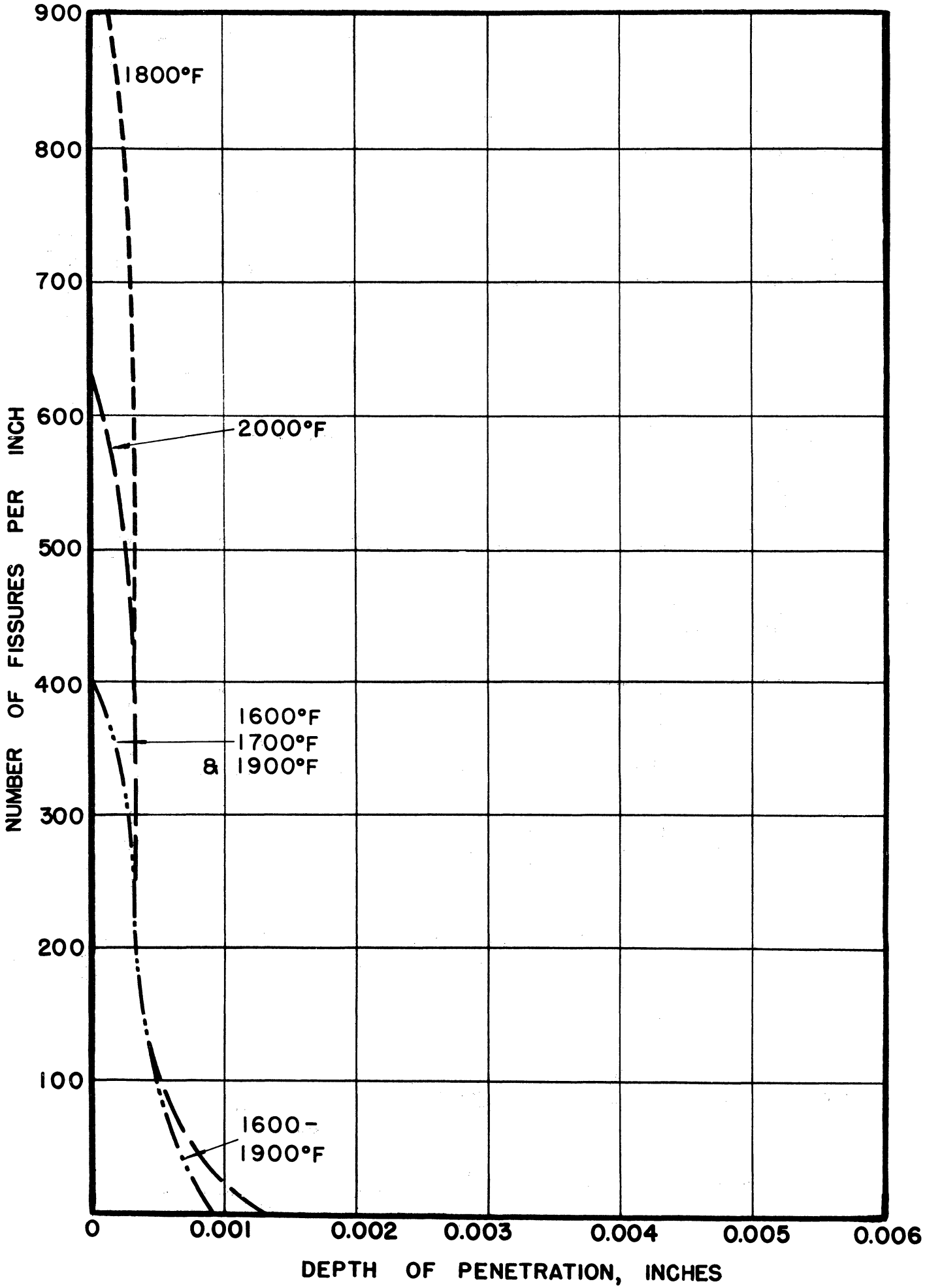

Fig. 50. Penetration vs. Depth Below Surface;
Type 310 Alloy, Heat J10, Unstressed.

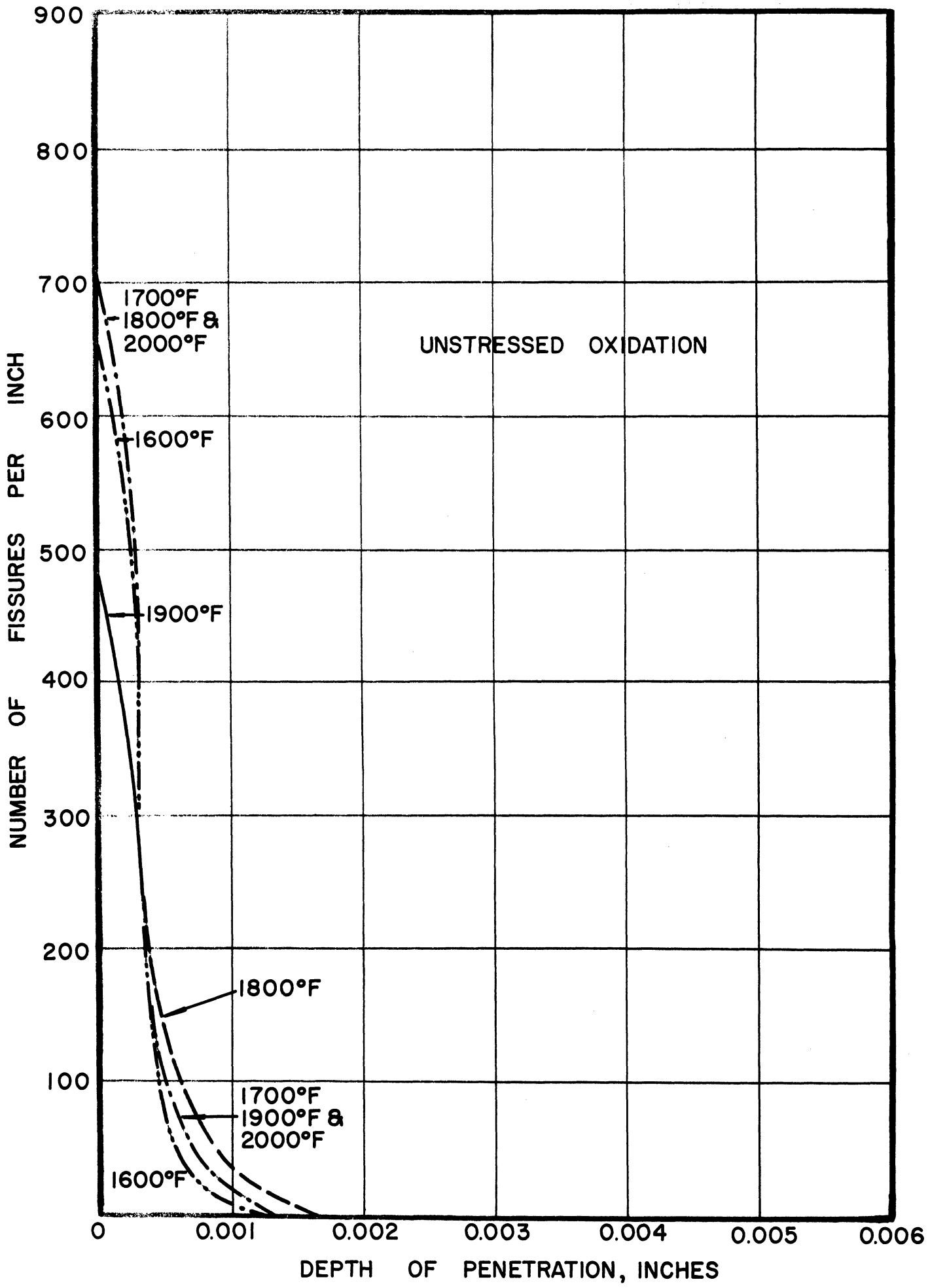

Fig. 51. Penetration vs. Depth Below Surface; Type 310 Alloy, Heat Vt-5, 100 Hours, Unstressed.

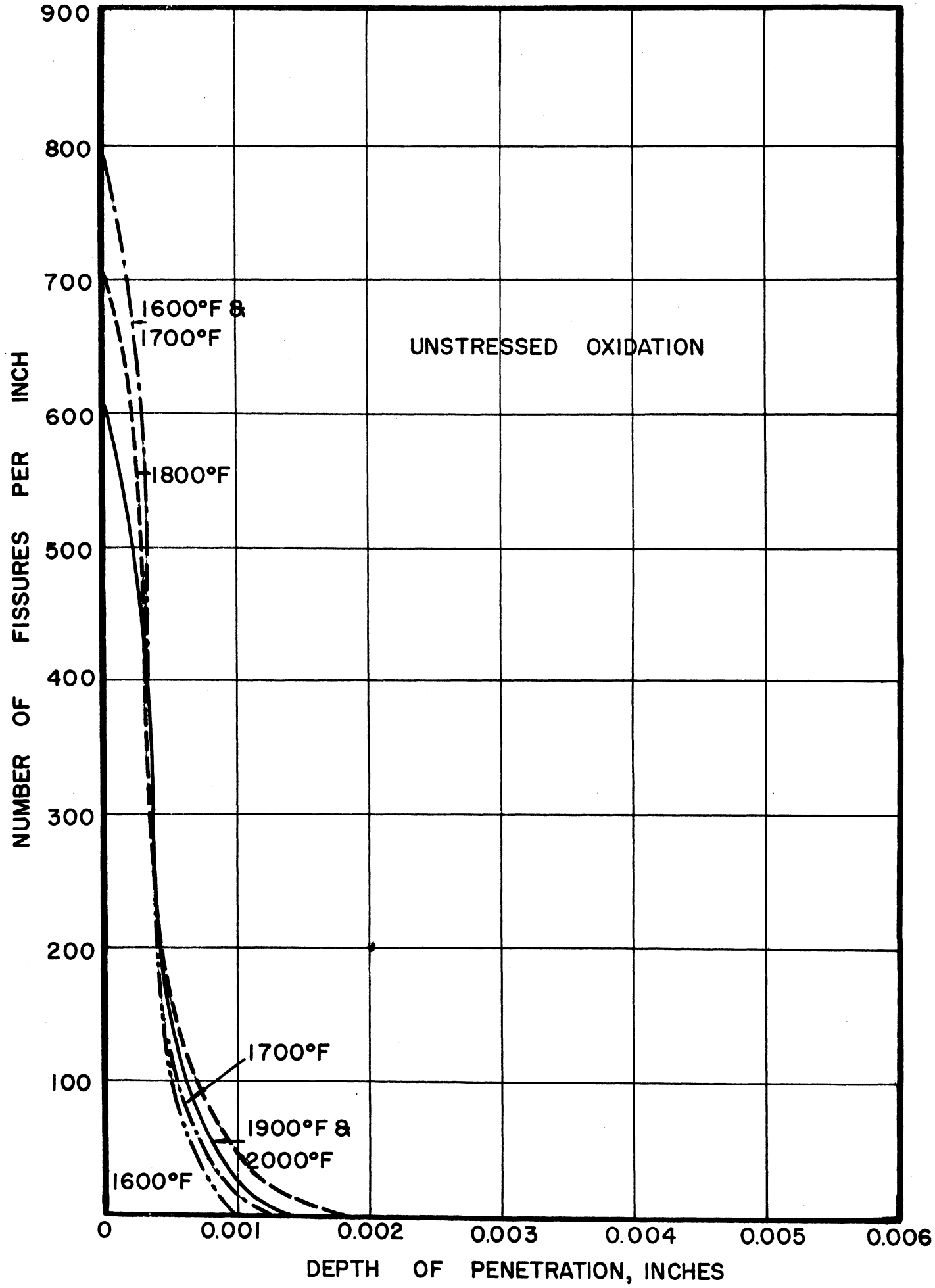

Fig. 52. Penetration vs. Depth Below Surface;
Type 310 Alloy, Heat Vt-7, 100 Hours.

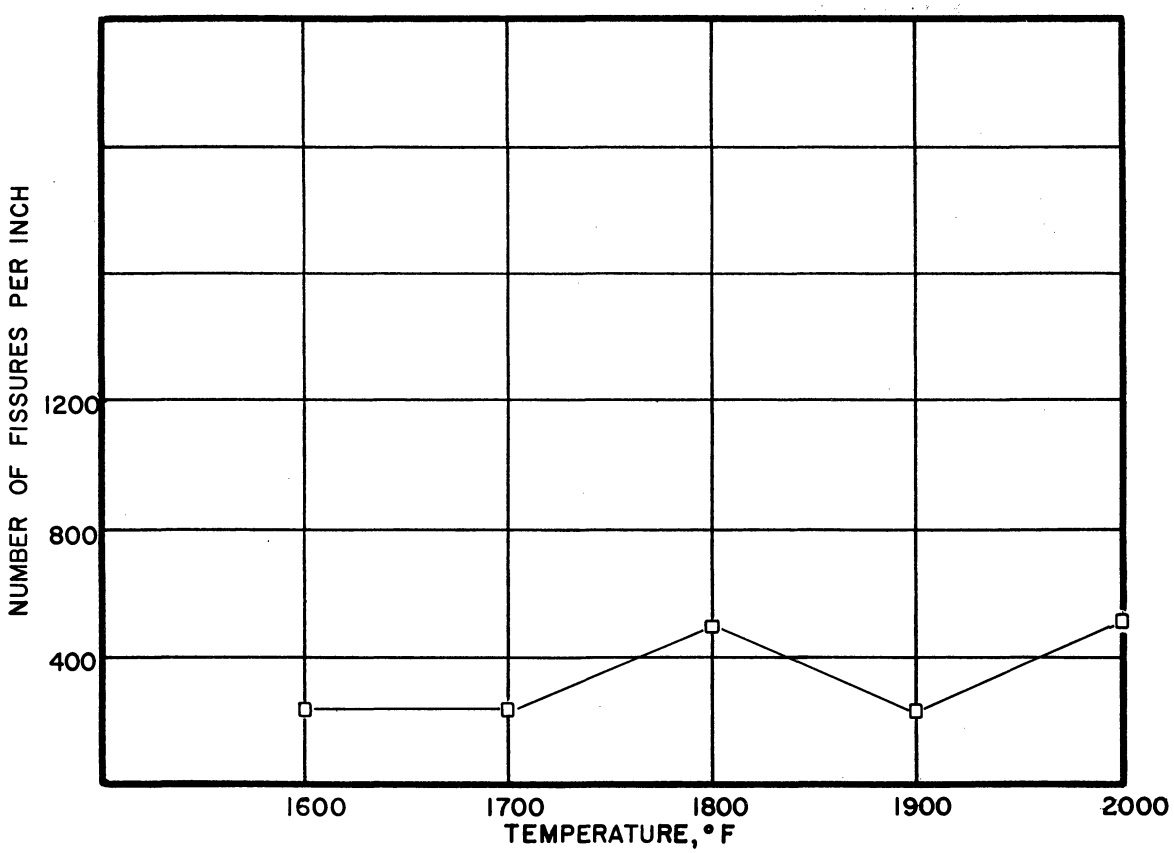

Fig. 53. Summary Penetration-Frequency Curve;
Type 310 Alloy, Heat J10.

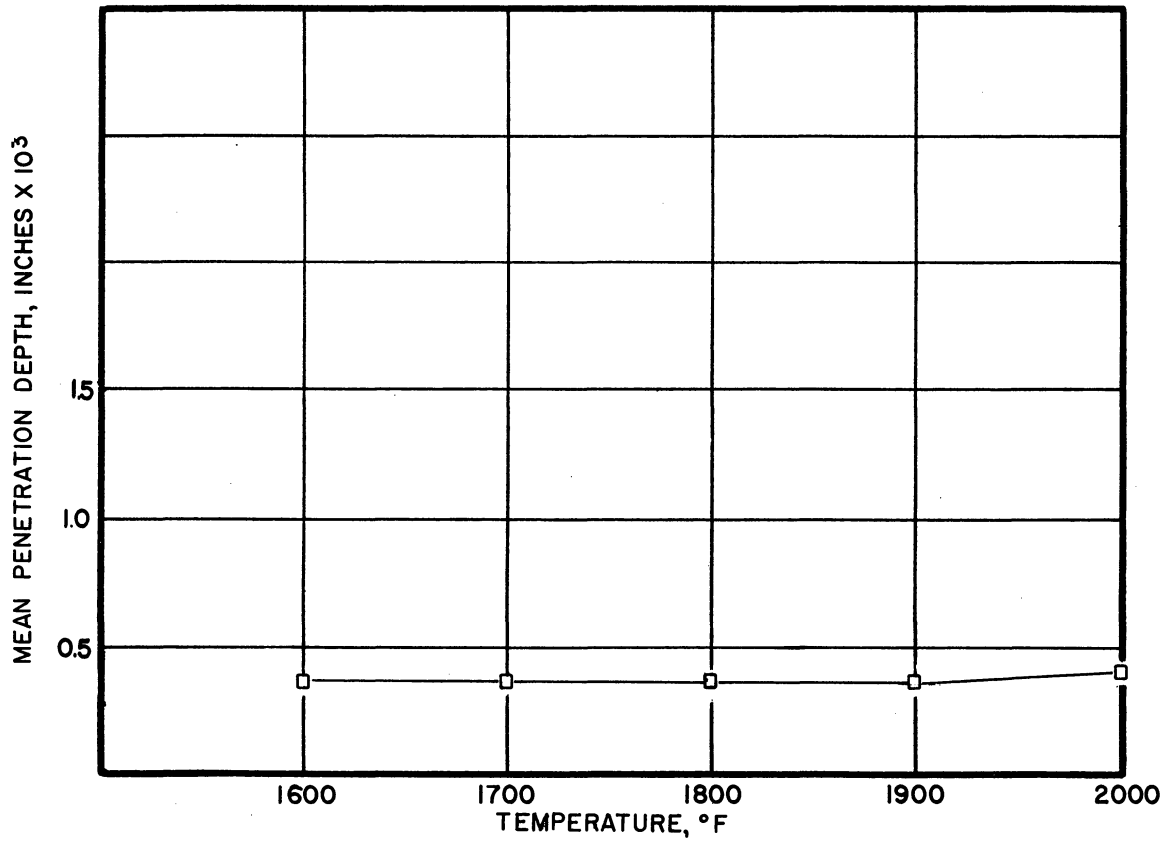

Fig. 54. Summary Penetration Depth Curve;
Type 310 Alloy, Heat J10.

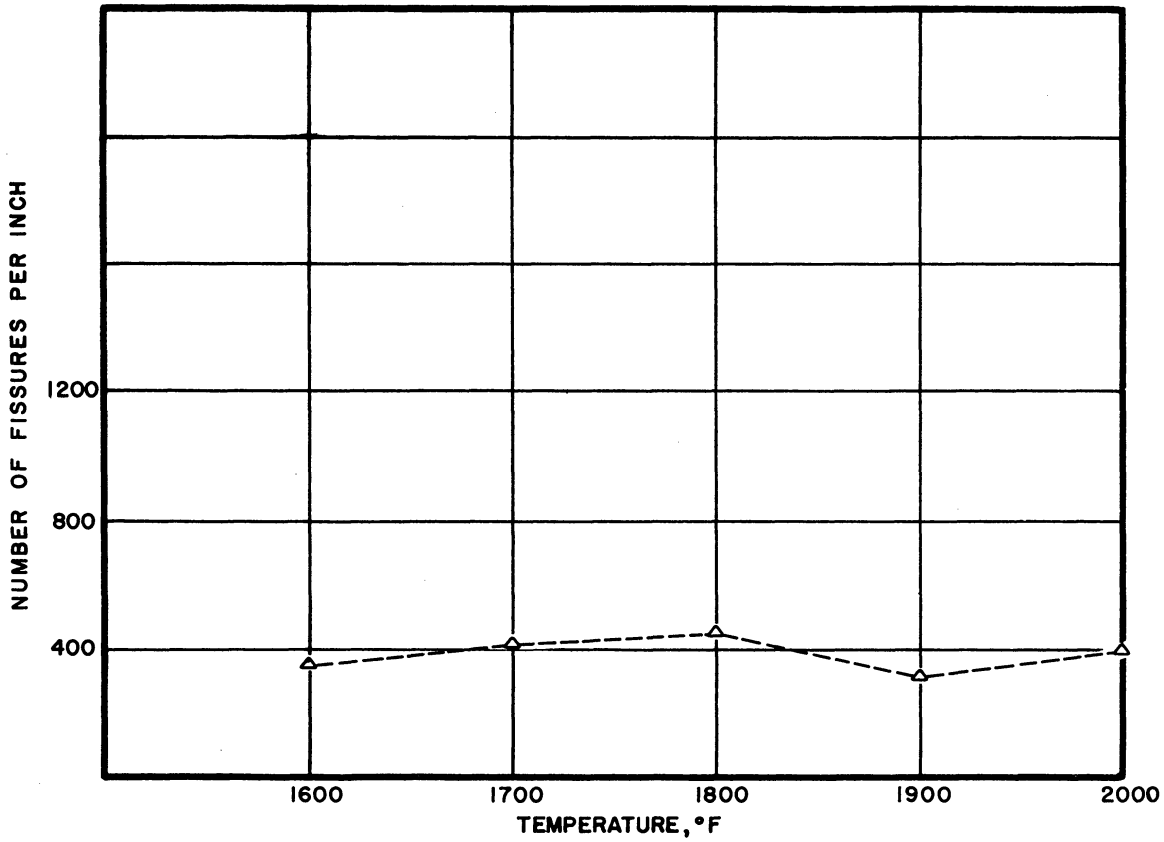

Fig. 55. Summary Penetration-Frequency Curve;
Type 310 Alloy, Heat Vt-5, 100 Hours.

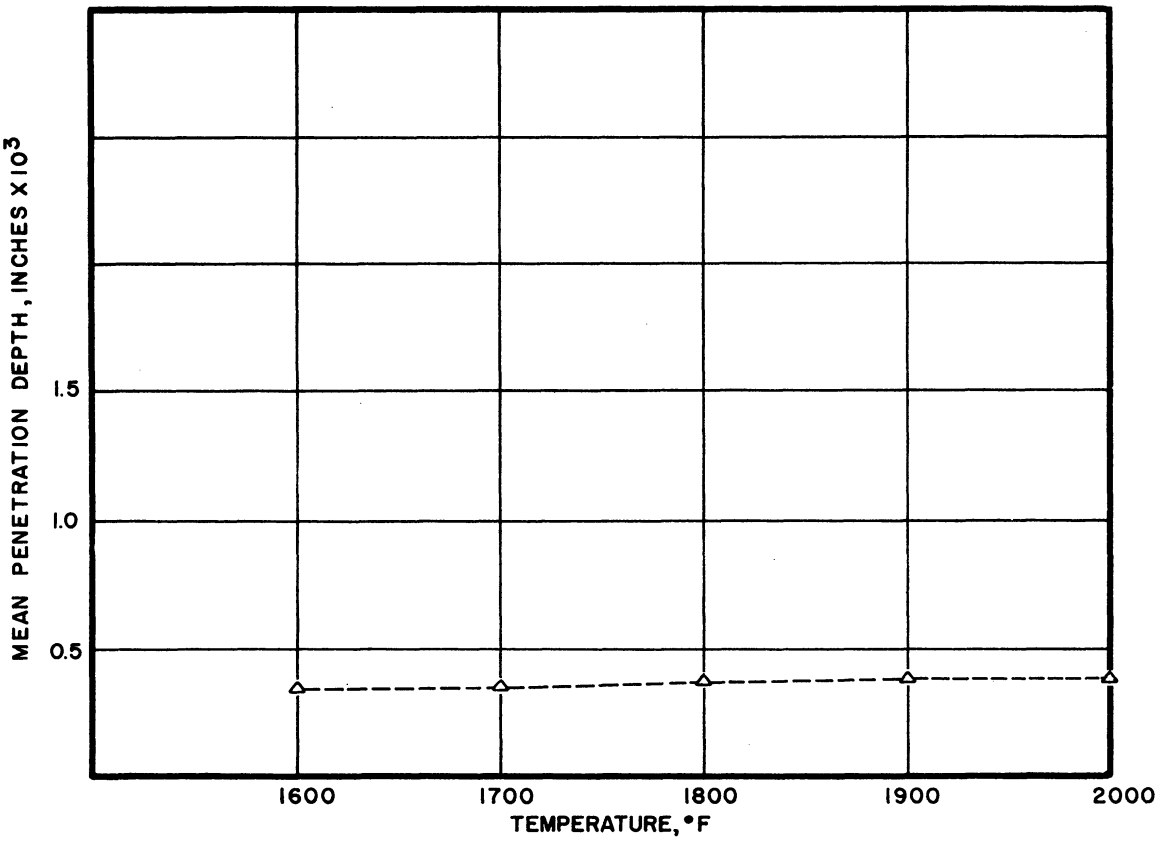

Fig. 56. Summary Penetration Depth Curve;
Type 310 Alloy, Heat Vt-5, 100 Hours.

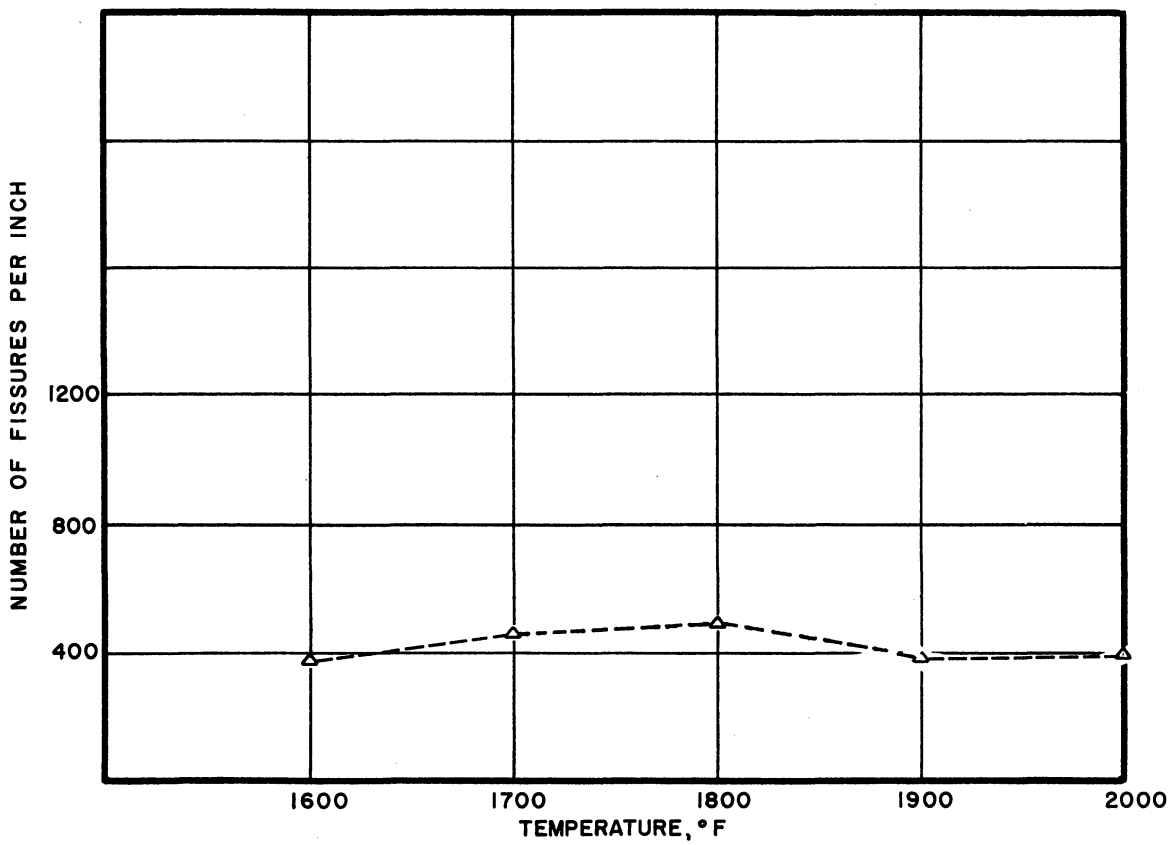

Fig. 57. Summary Penetration-Frequency Curve;
Type 310 Alloy, Heat Vt-7, 100 Hours.

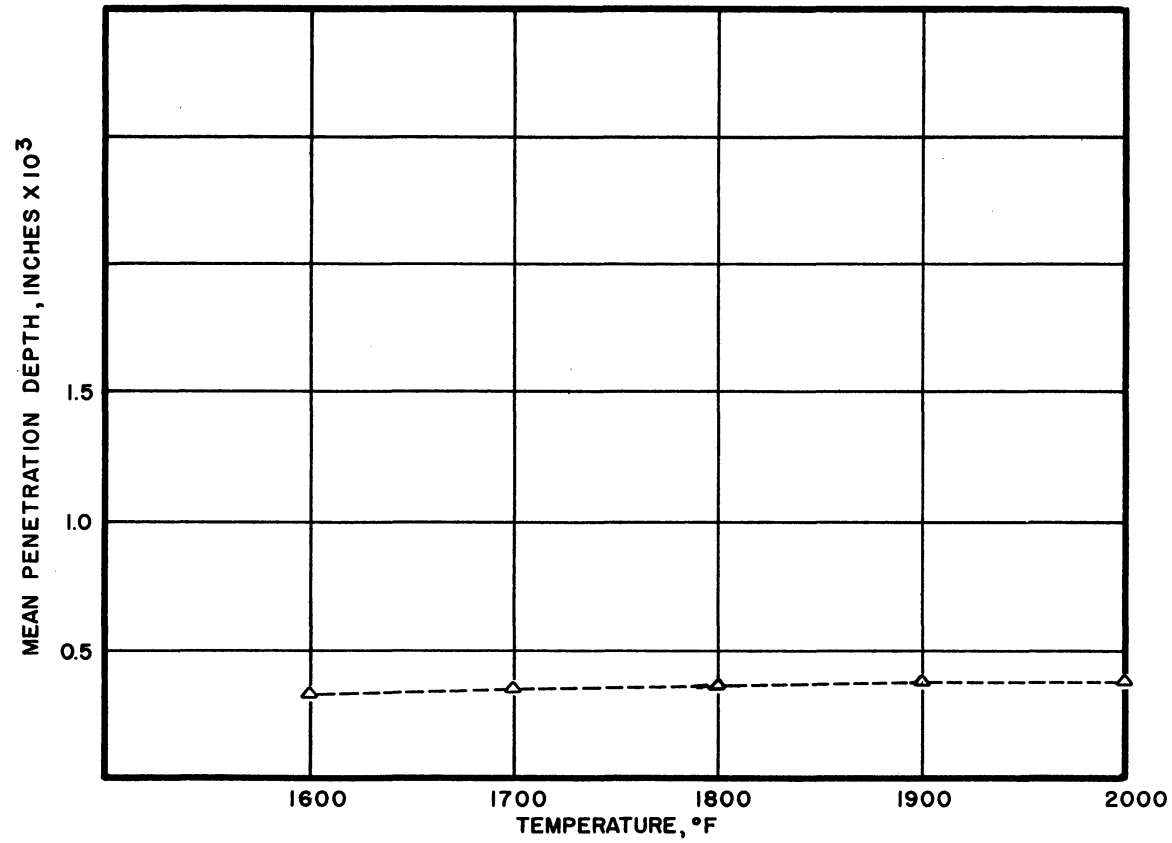

Fig. 58. Summary Penetration Depth Curve;
Type 310 Alloy, Heat Vt-7, 100 Hours.

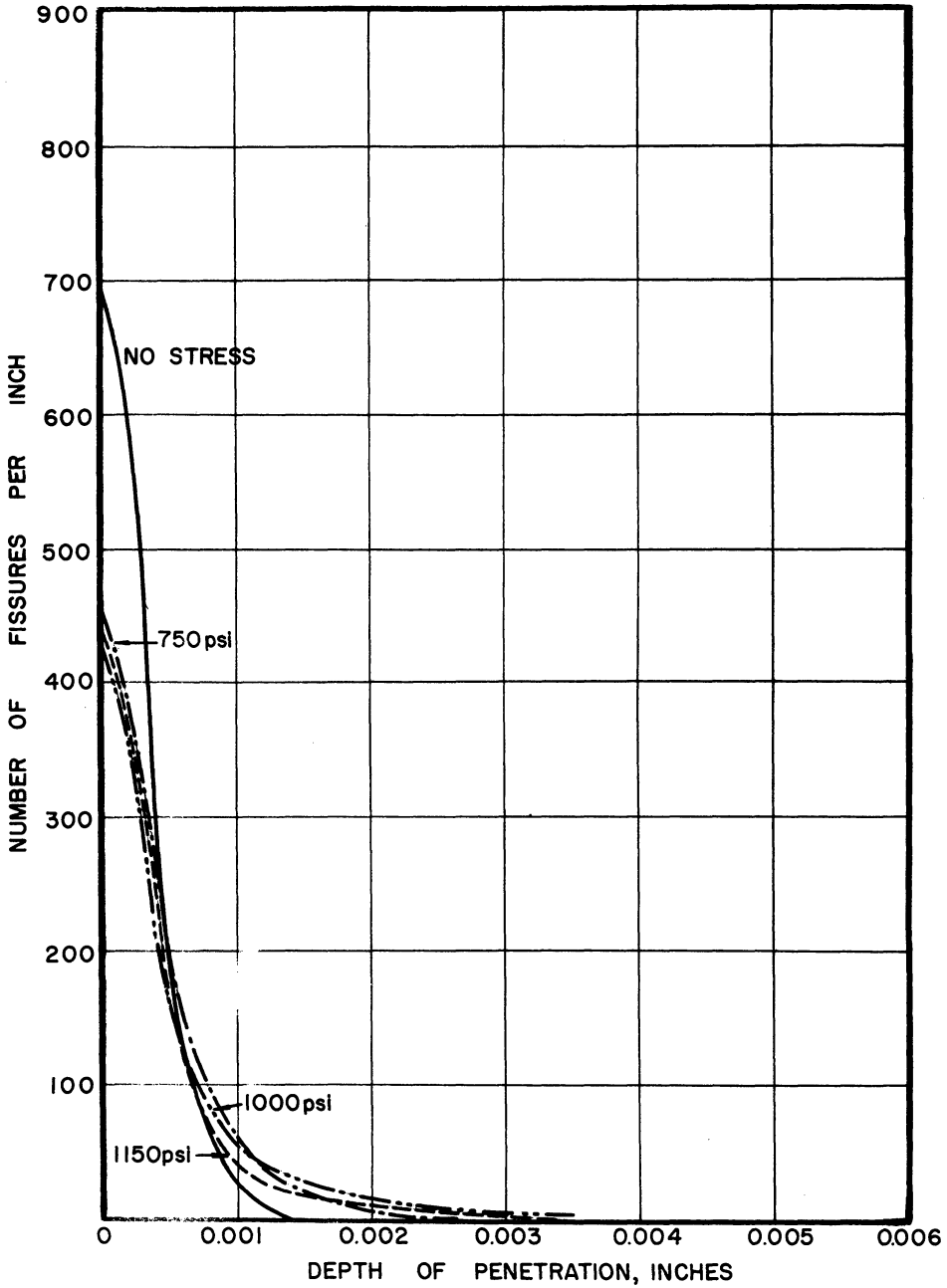

Fig. 59. Penetration vs. Depth Below Surface; Type 310 Alloy, Heat Vt-5, 1800°F, 100 Hours.

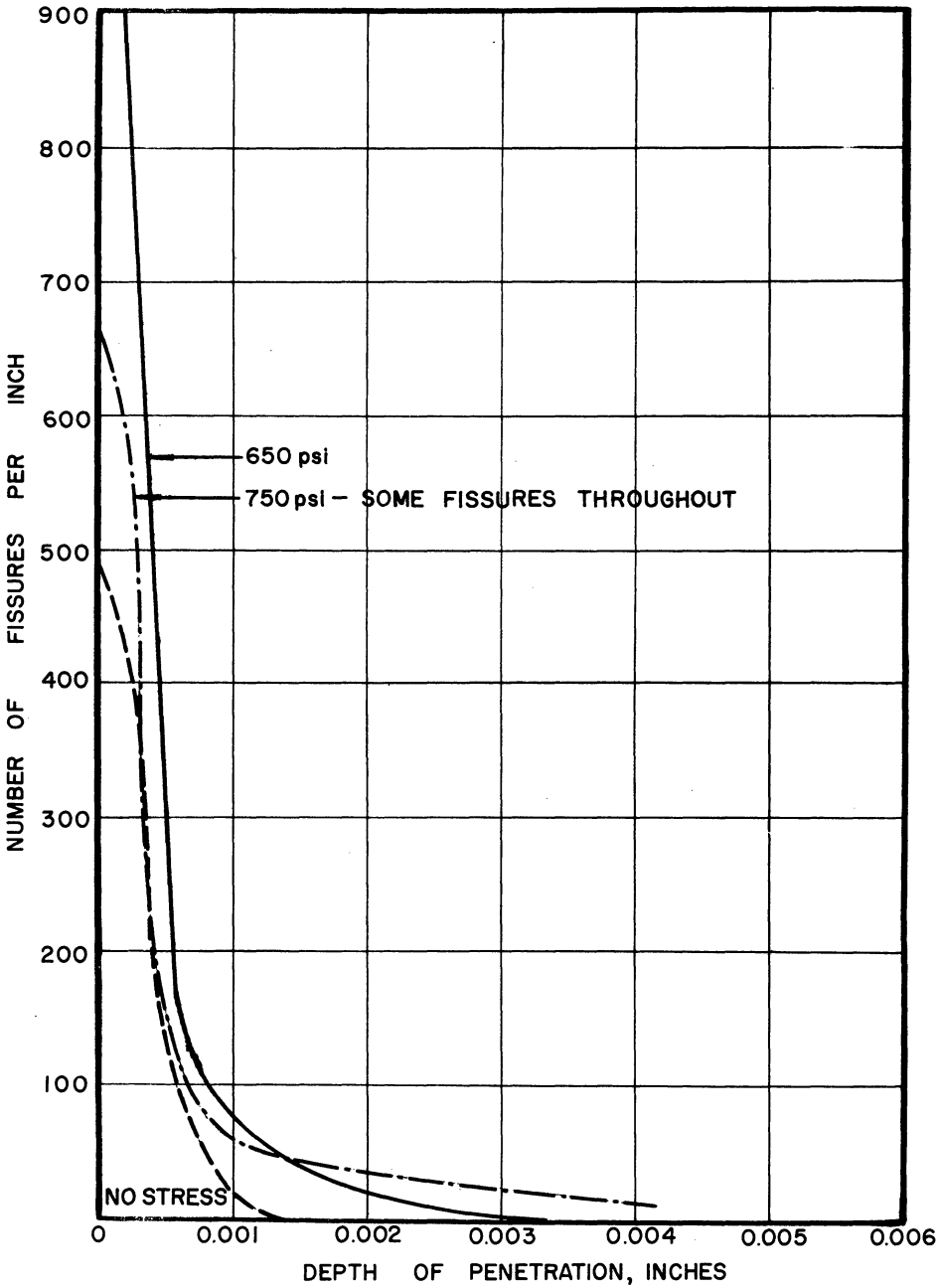

Fig. 60. Penetration vs. Depth Below Surface; Type 310 Alloy, Heat Vt-5, 1900°F, 100 Hours.

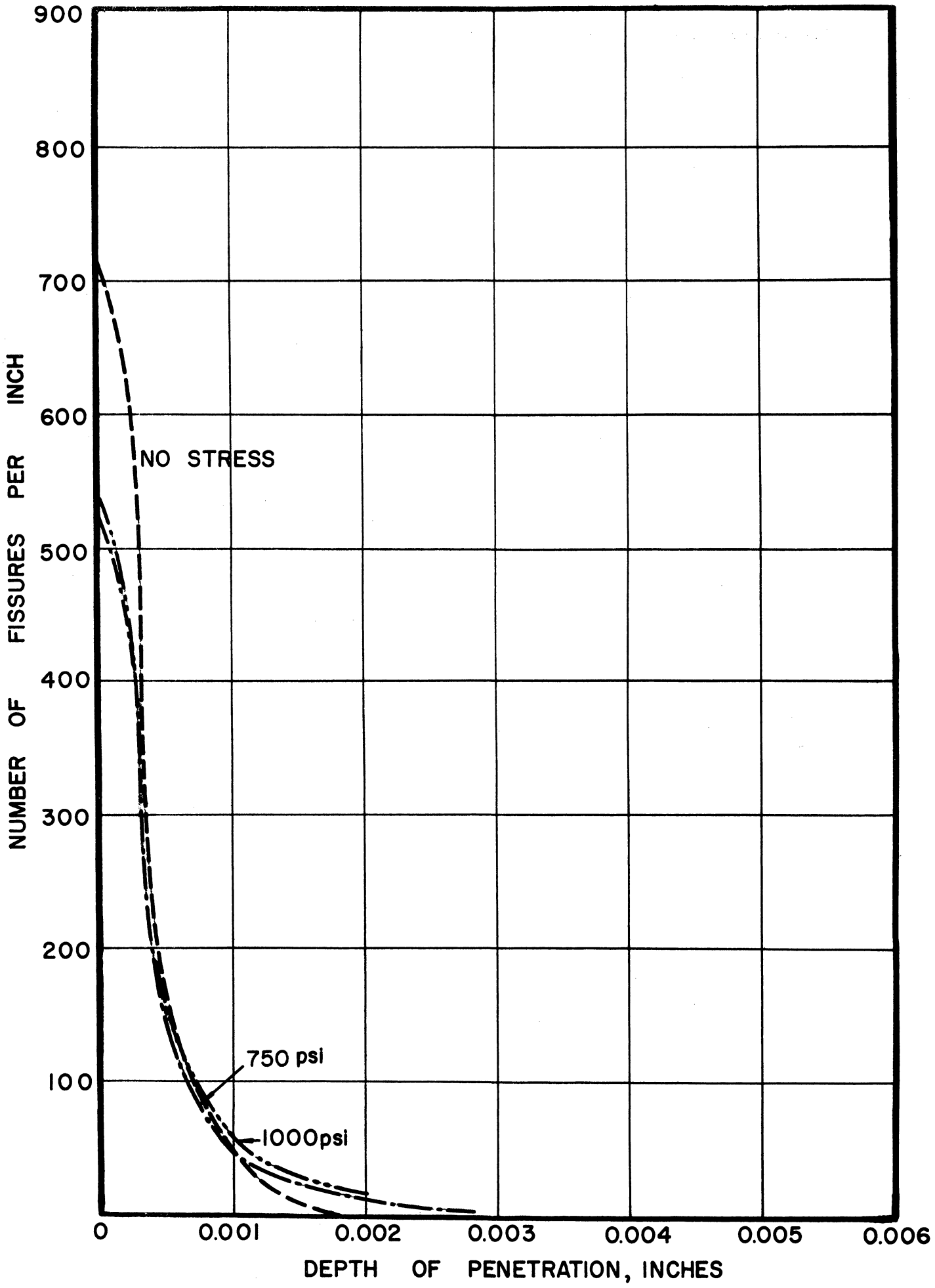

Fig. 61. Penetration vs. Depth Below Surface;
Type 310 Alloy, Heat Vt-7, 1800°F, 100 Hours.

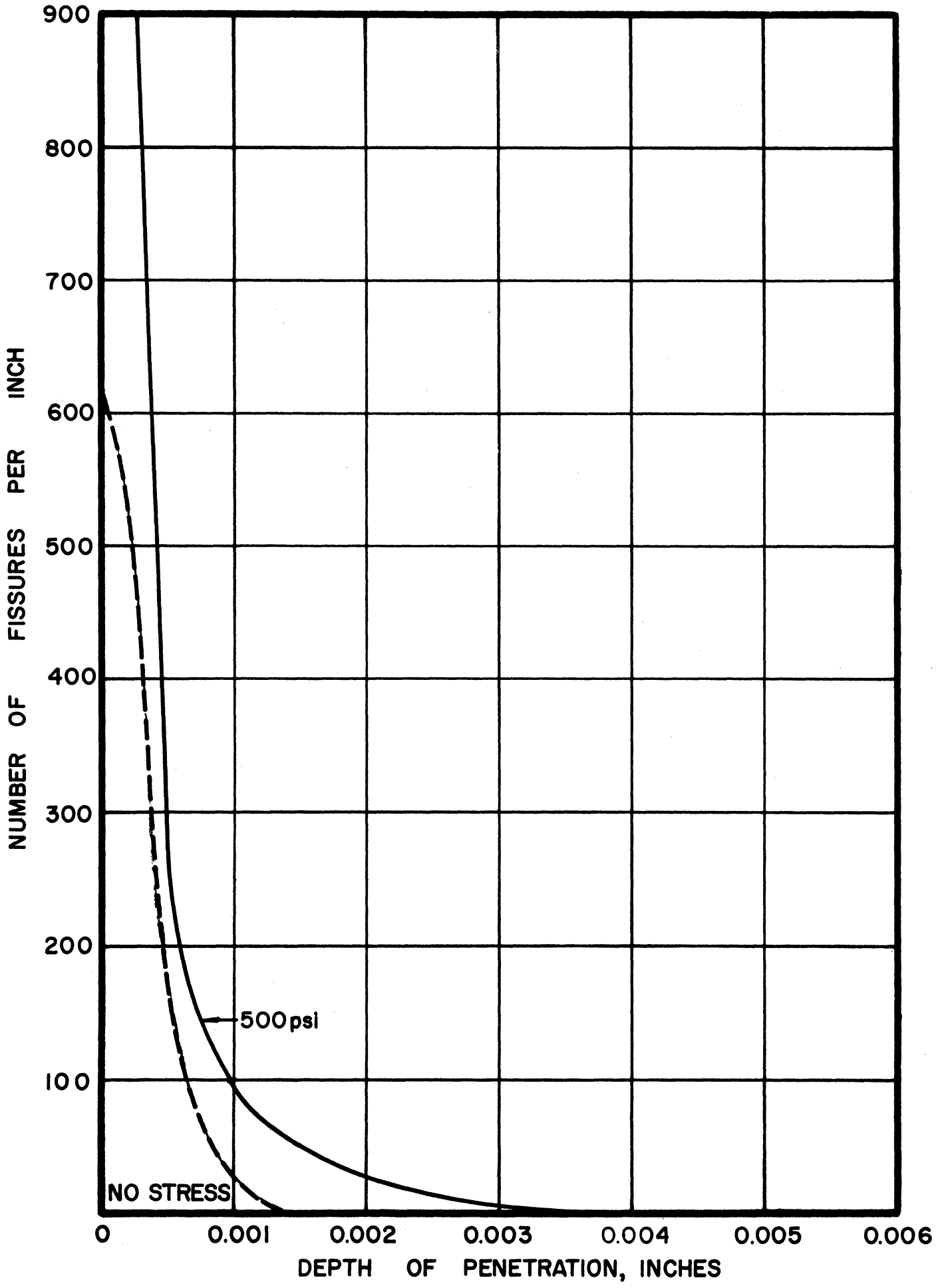

Fig. 62. Penetration vs. Depth Below Surface;
Type 310 Alloy, Heat Vt-7, 1900°F, 100 Hours.

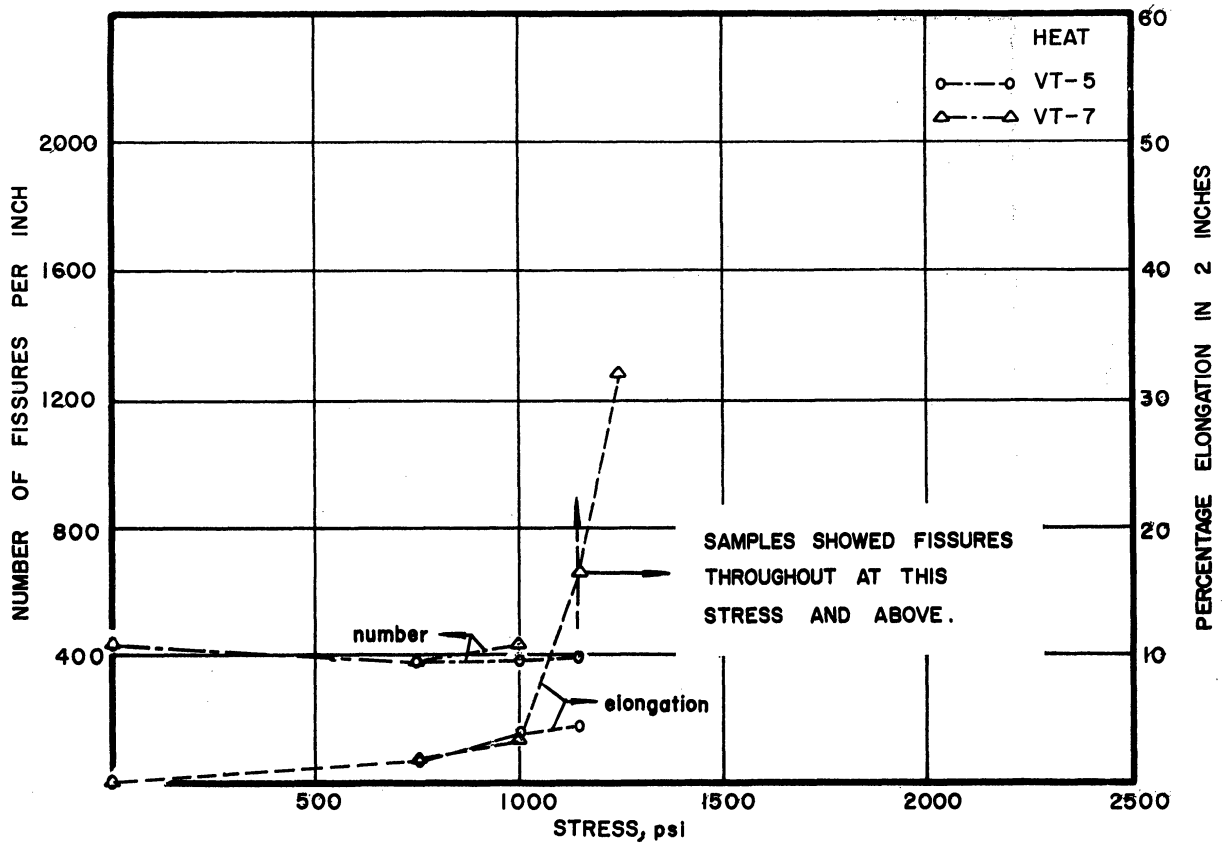

Fig. 63. Summary Penetration-Frequency Curves; Type 310 Alloys, Heats Vt-5 and Vt-7, 1800°F, 100 Hours.

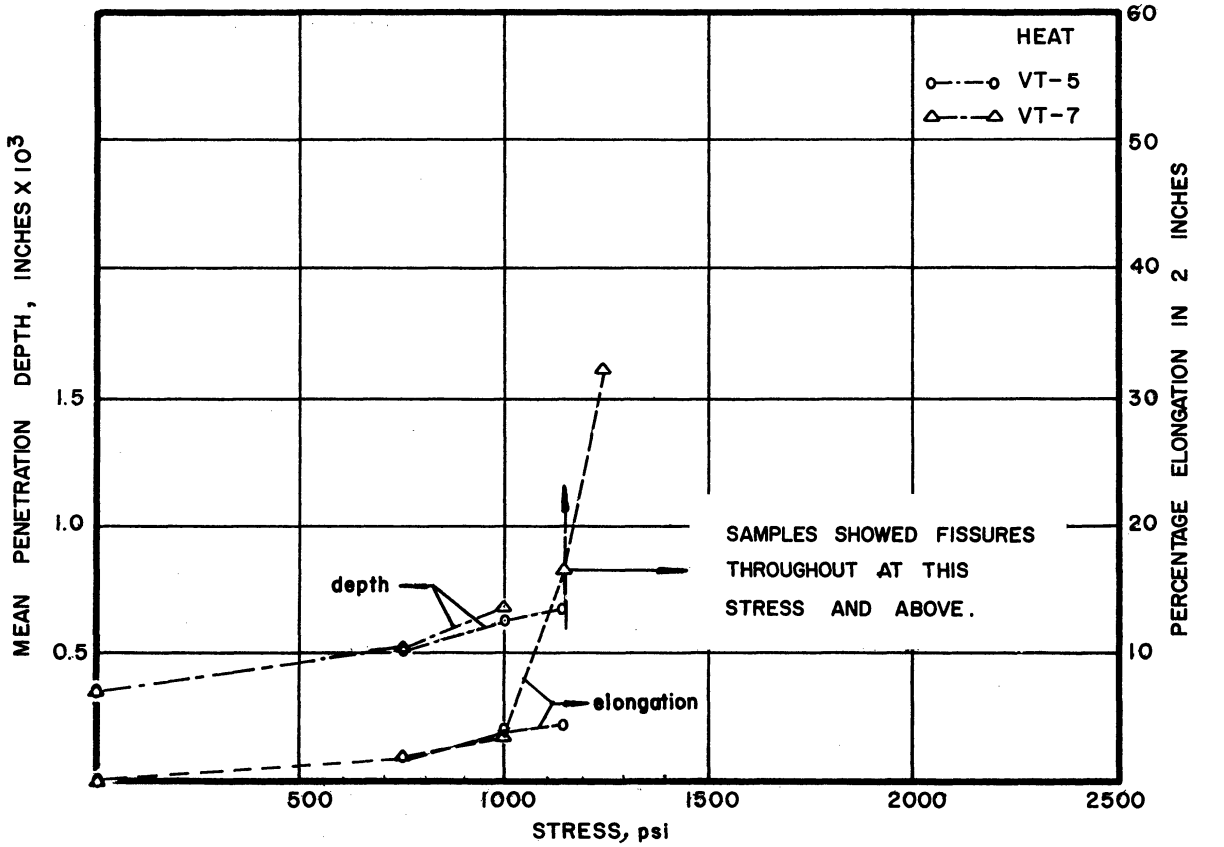

Fig. 64. Summary Penetration Depth Curves; Type 310 Alloys, Heats Vt-5 and Vt-7, 1800°F, 100 Hours.

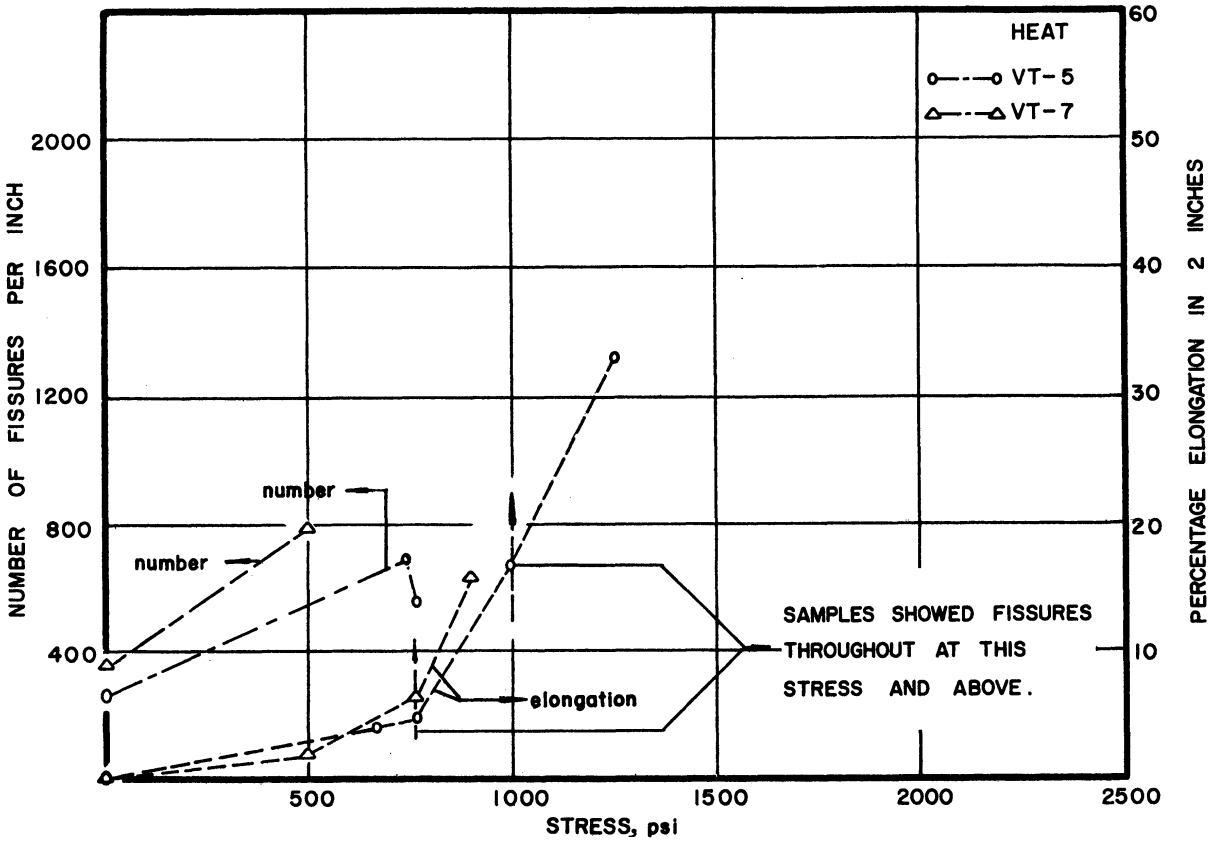

Fig. 65. Summary Penetration-Frequency Curves; Type 310 Alloys, Heats Vt-5 and Vt-7, 1900°F, 100 Hours.

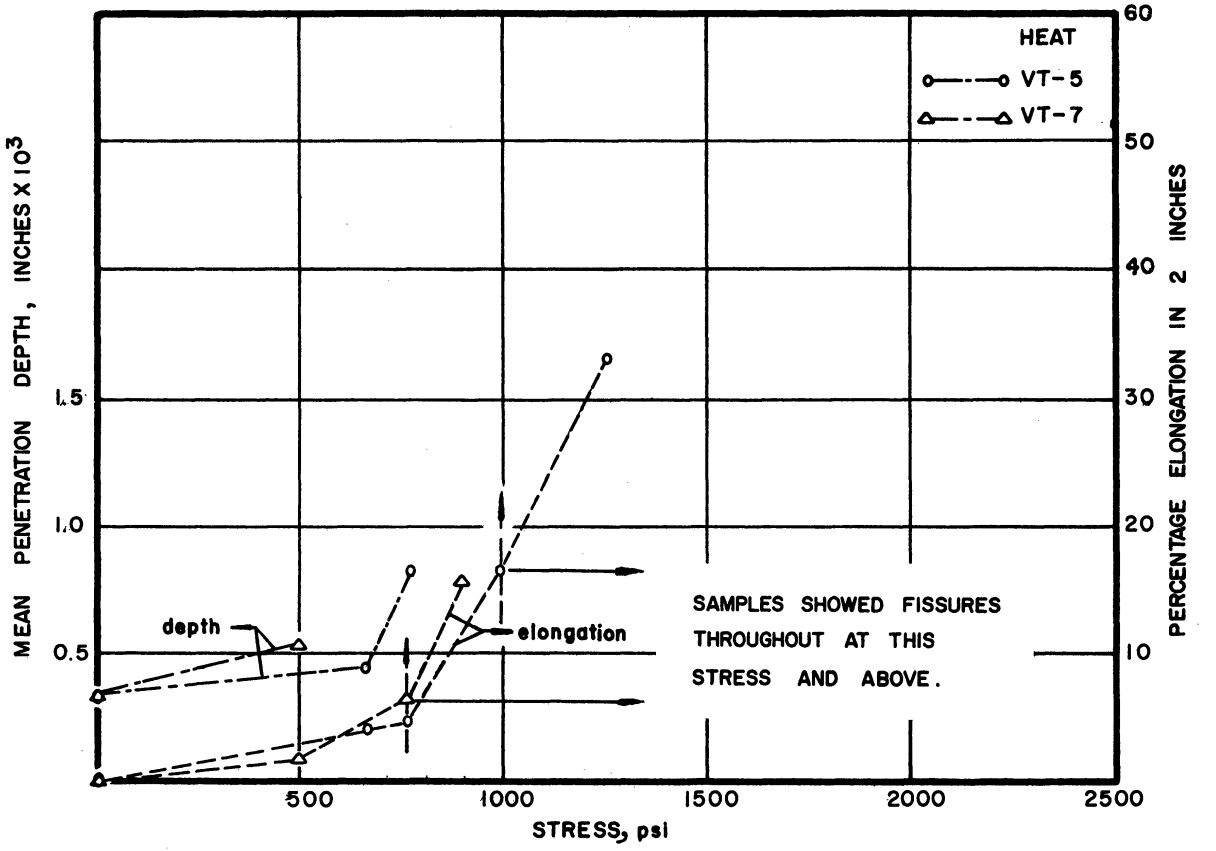

Fig. 66. Summary Penetration Depth Curves; Type 310 Alloys, Heats Vt-5 and Vt-7, 1900°F, 100 Hours.

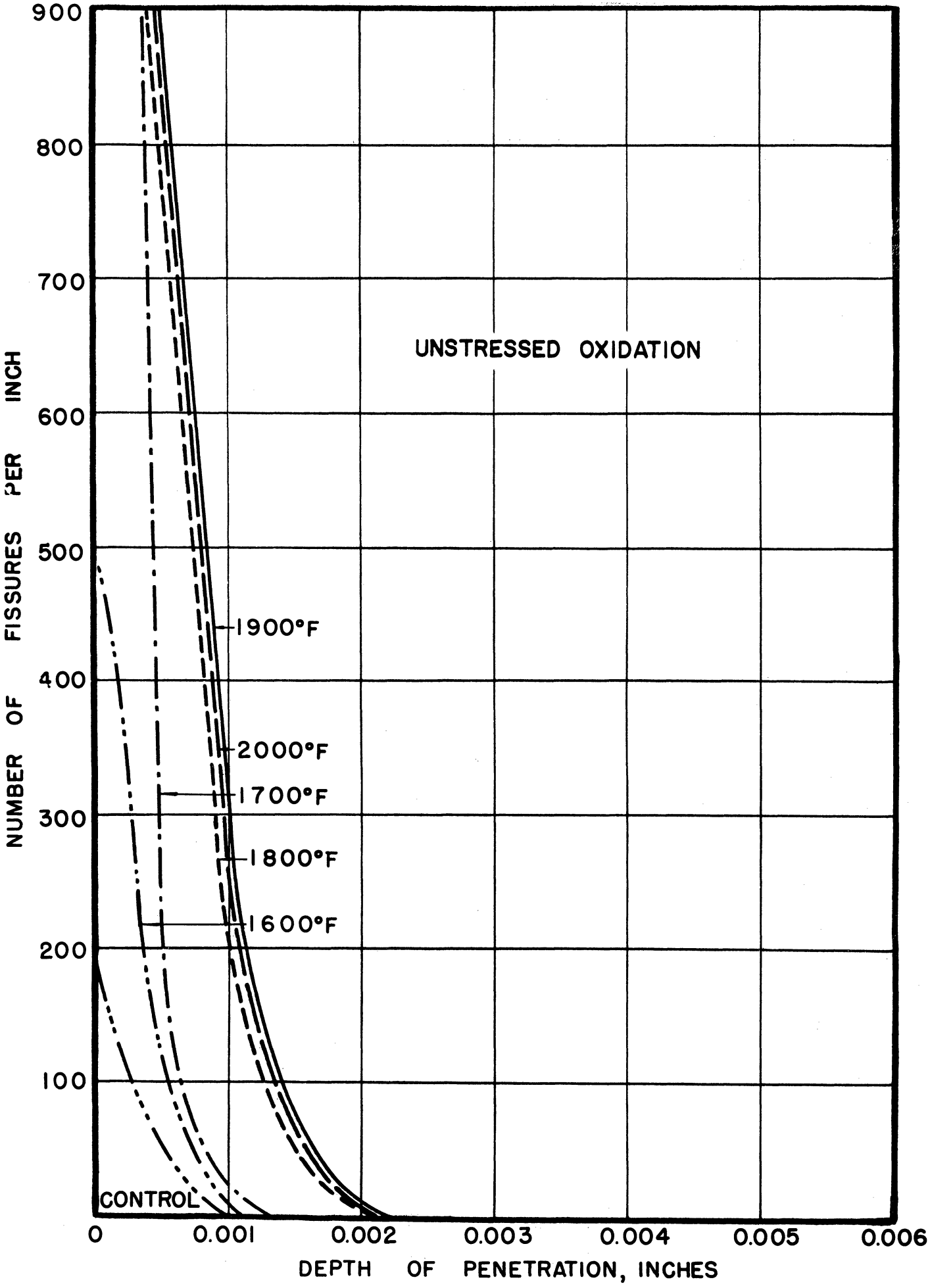

Fig. 67. Penetration vs. Depth Below Surface; Chromel ARM Alloy, Heat A, 100 Hours.

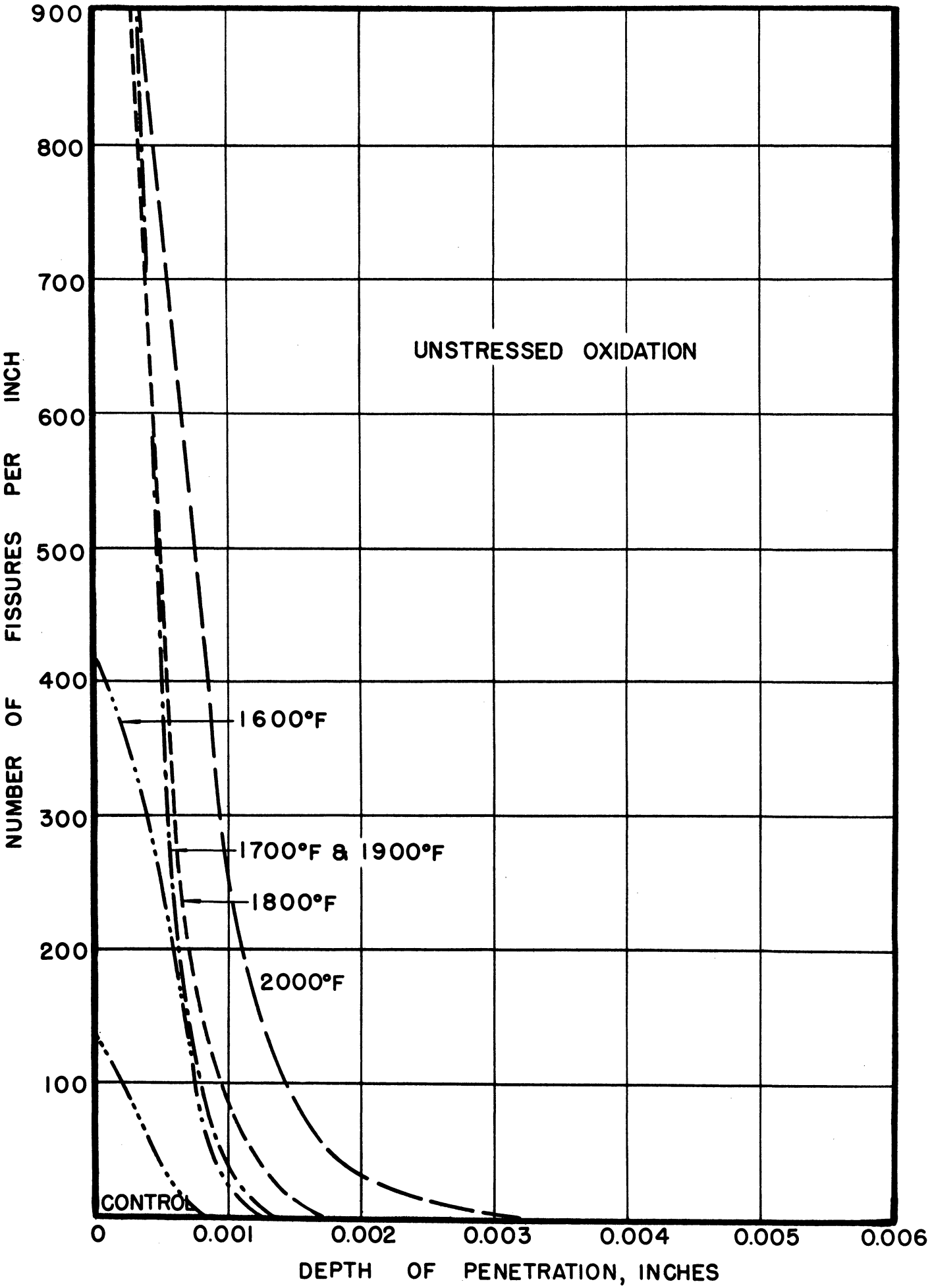

Fig. 68. Penetration vs. Depth Below Surface; Chromel ARM Alloy, Heat B, Runs 34 and 34'; 100 Hours.

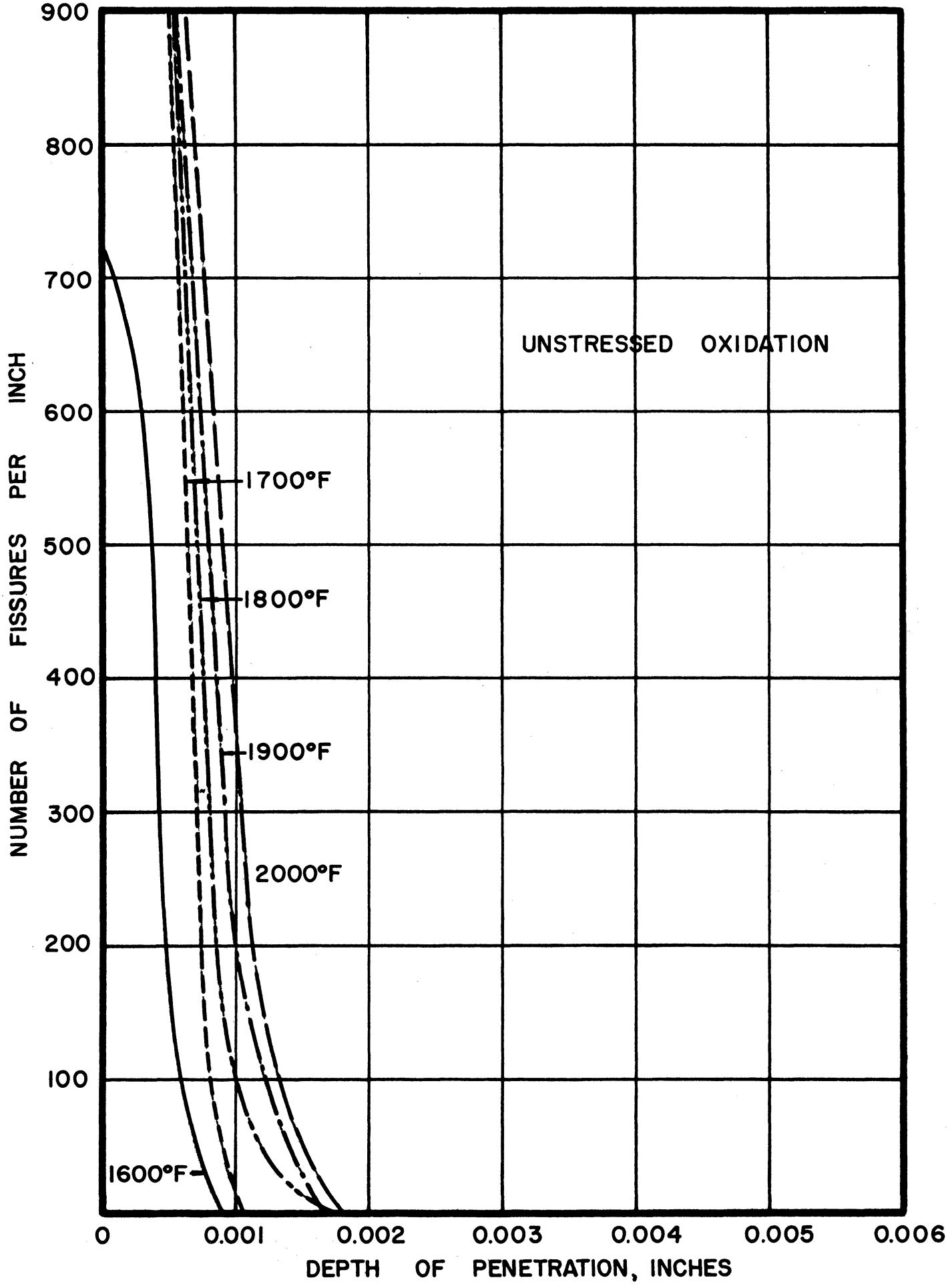

Fig. 69. Penetration vs. Depth Below Surface; Chromel ASM Alloy, 100 Hours.

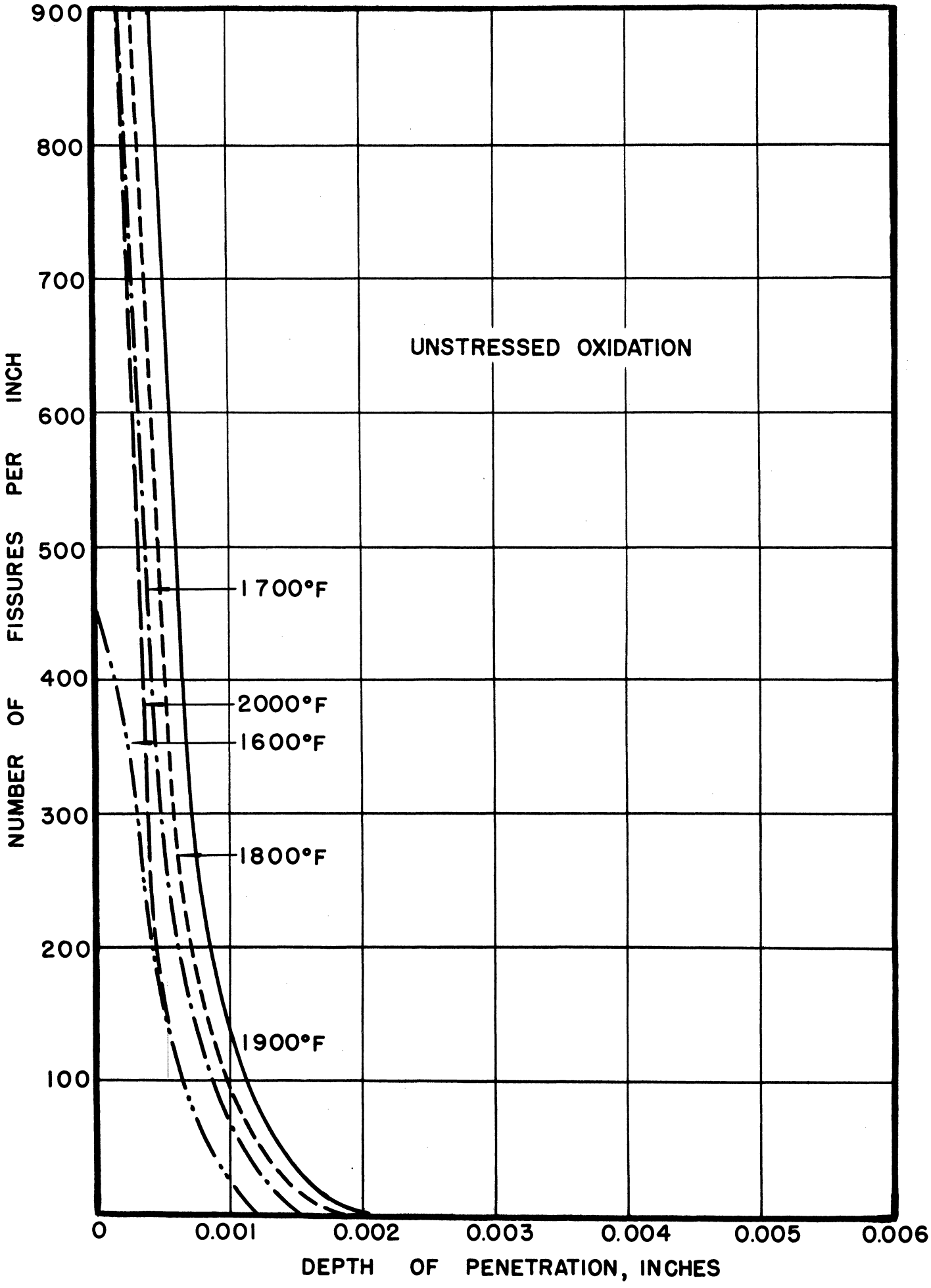

Fig. 70. Penetration vs. Depth Below Surface; Chromel D Alloy, 100 Hours.

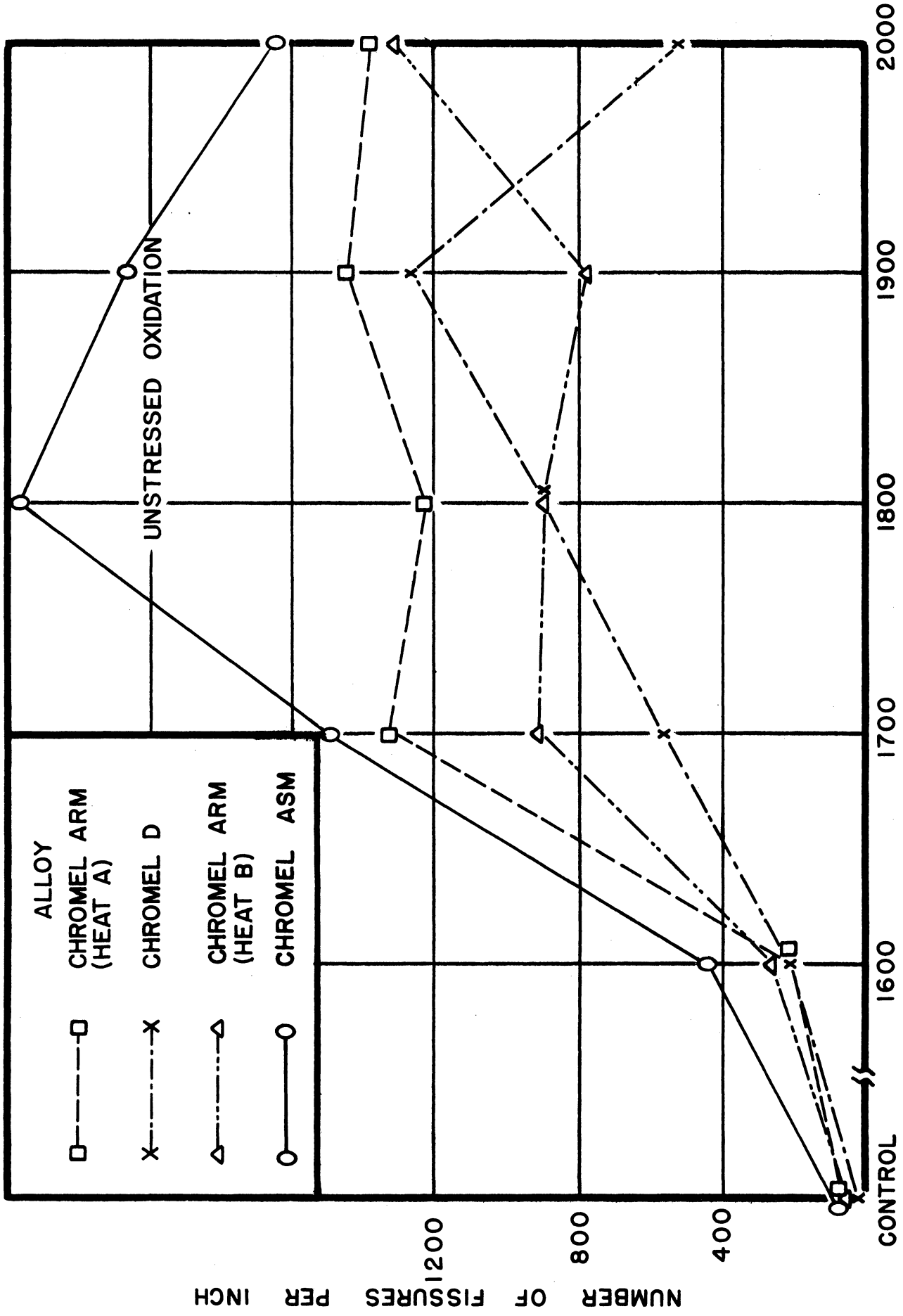

Fig. 71. Summary Penetration-Frequency Curves; Chromel Alloys, 100 Hours.

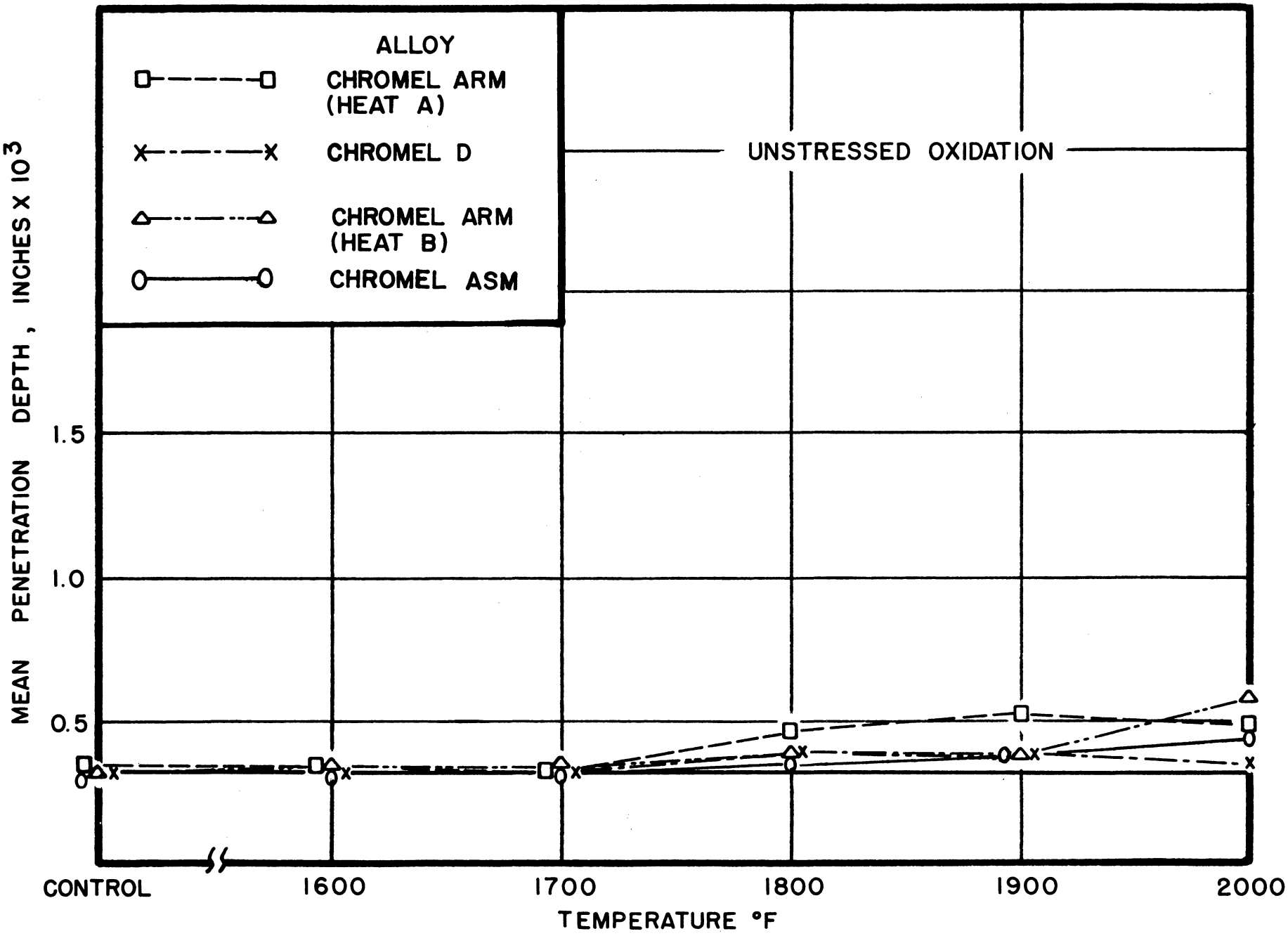

Fig. 72. Summary Penetration Depth Curves; Chromel Alloys, 100 Hours.

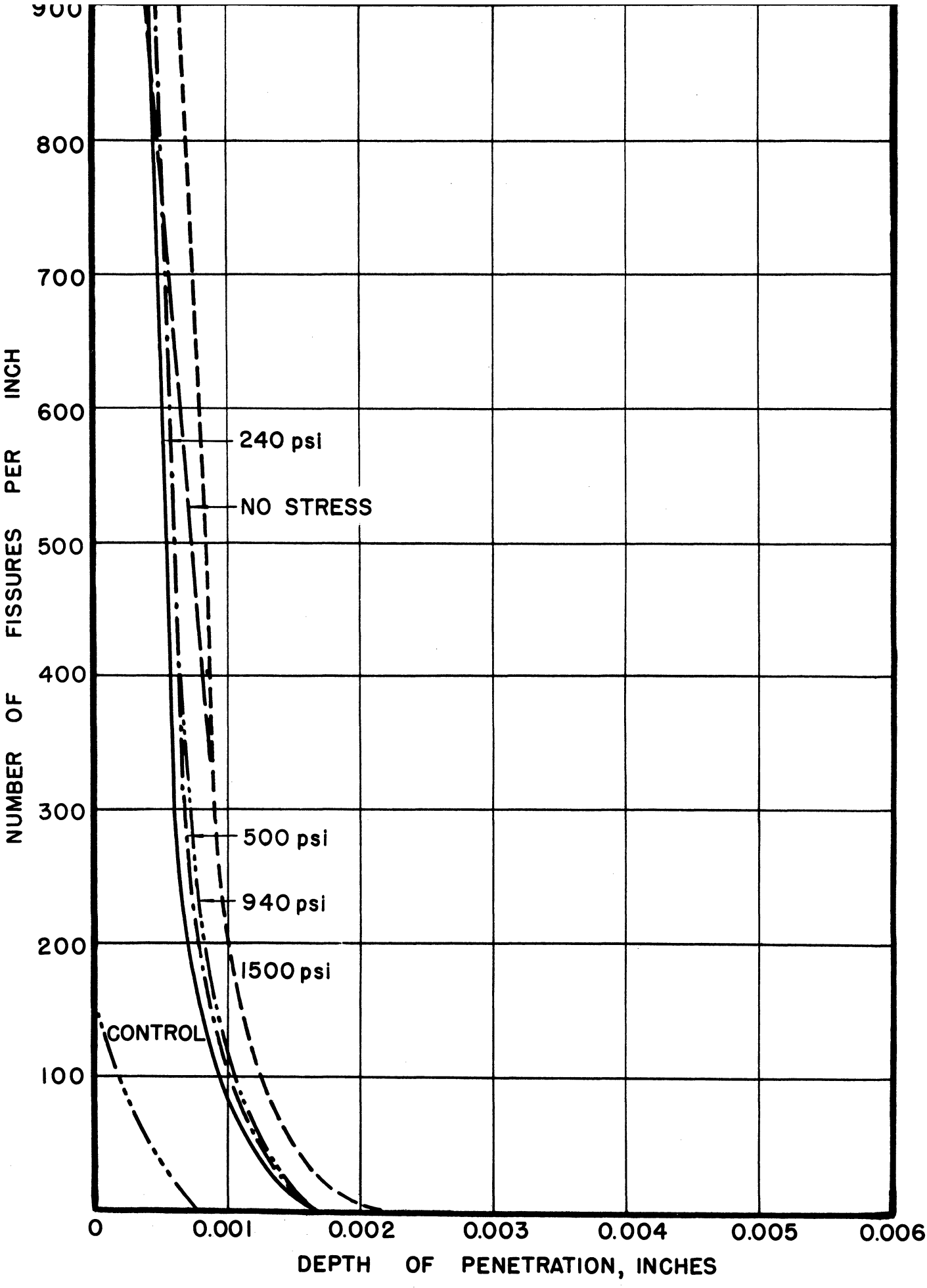

Fig. 73. Penetration vs. Depth Below Surface; Chromel ARM Alloy, Heat A, 1800°F, 100 Hours.

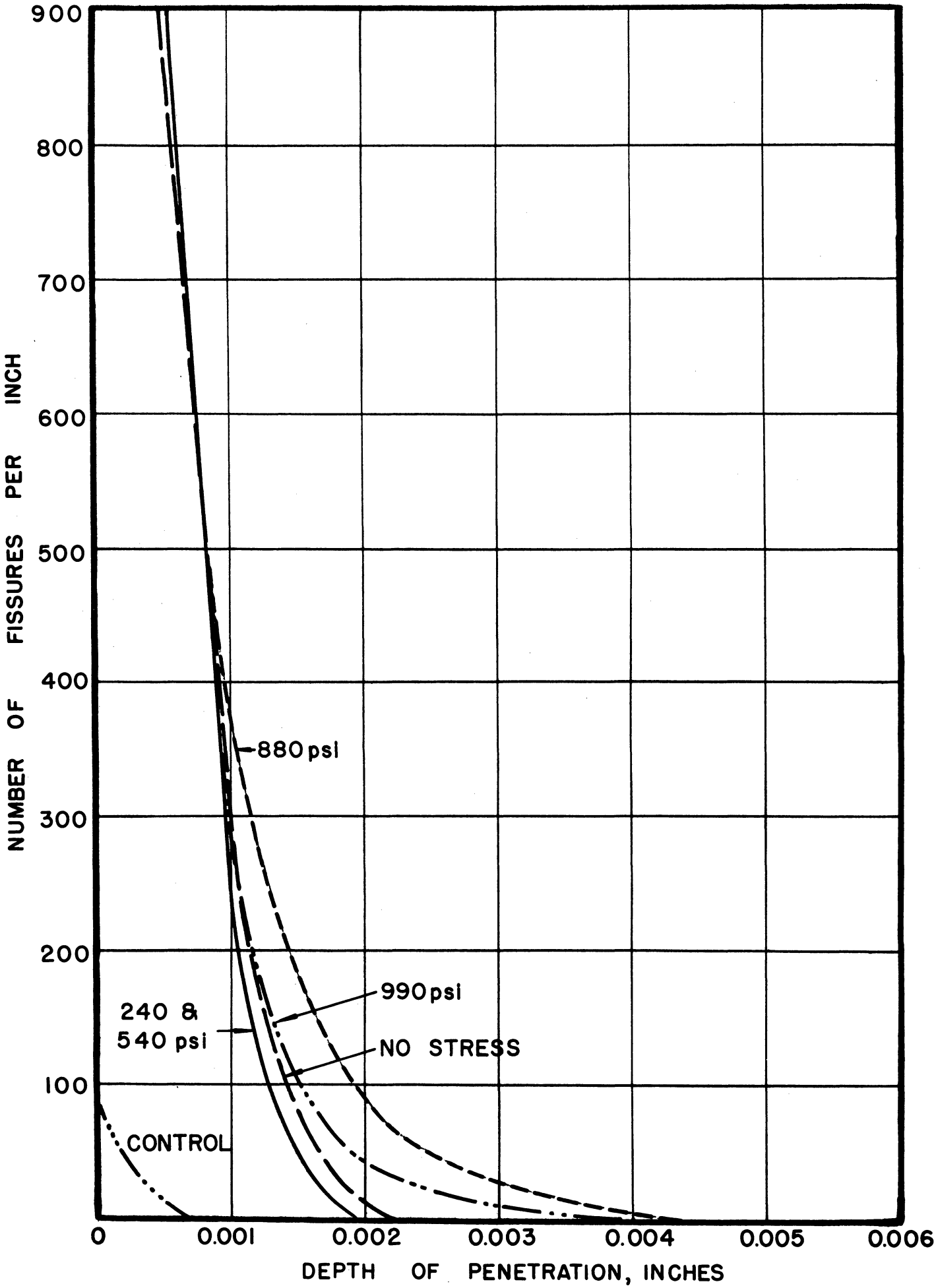

Fig. 74. Penetration vs. Depth Below Surface; Chromel ARM Alloy, Heat A, 1900°F, 100 Hours.

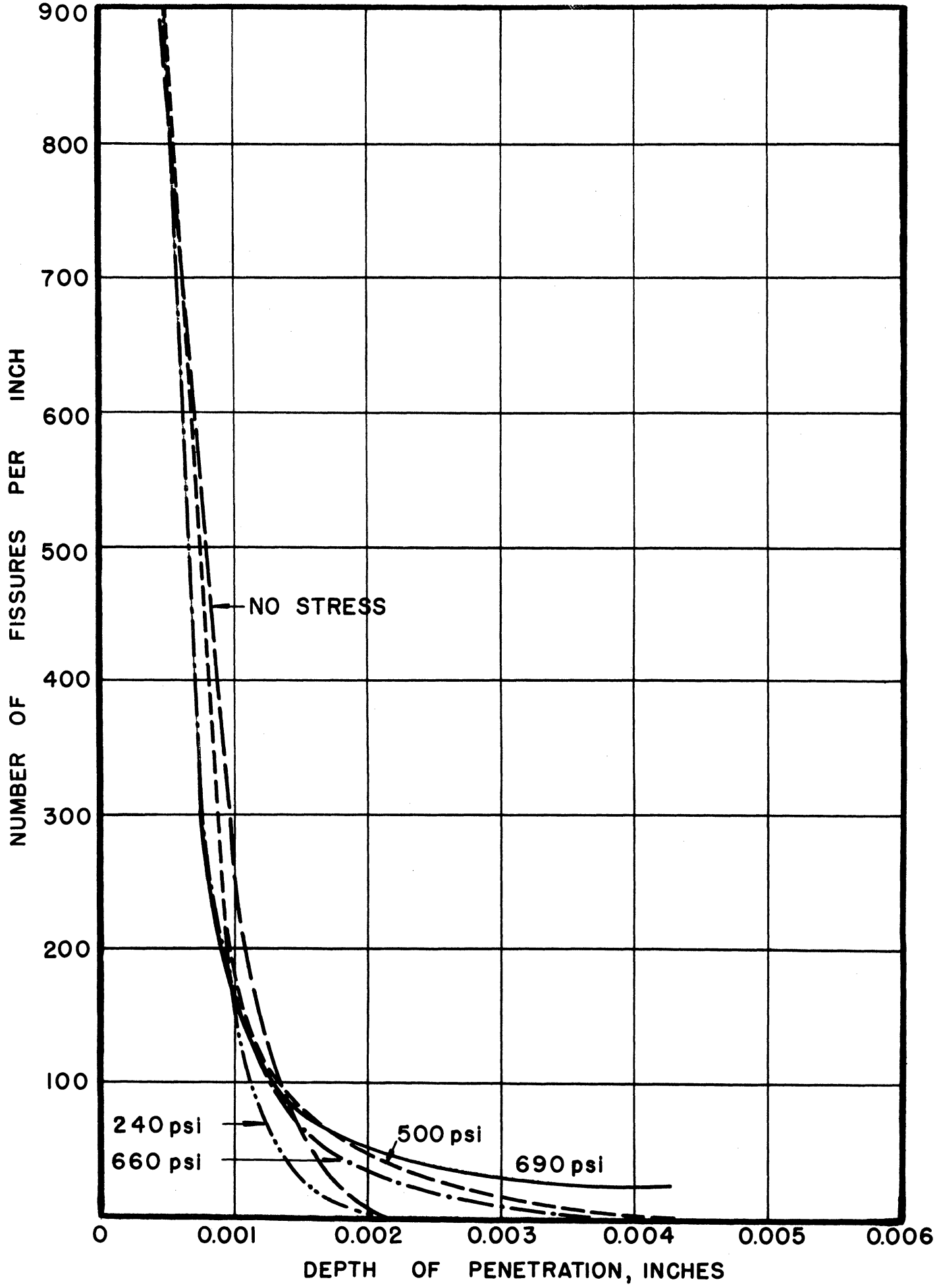

Fig. 75. Penetration vs. Depth Below Surface; Chromel ARM Alloy, Heat A, 2000°F, 100 Hours.

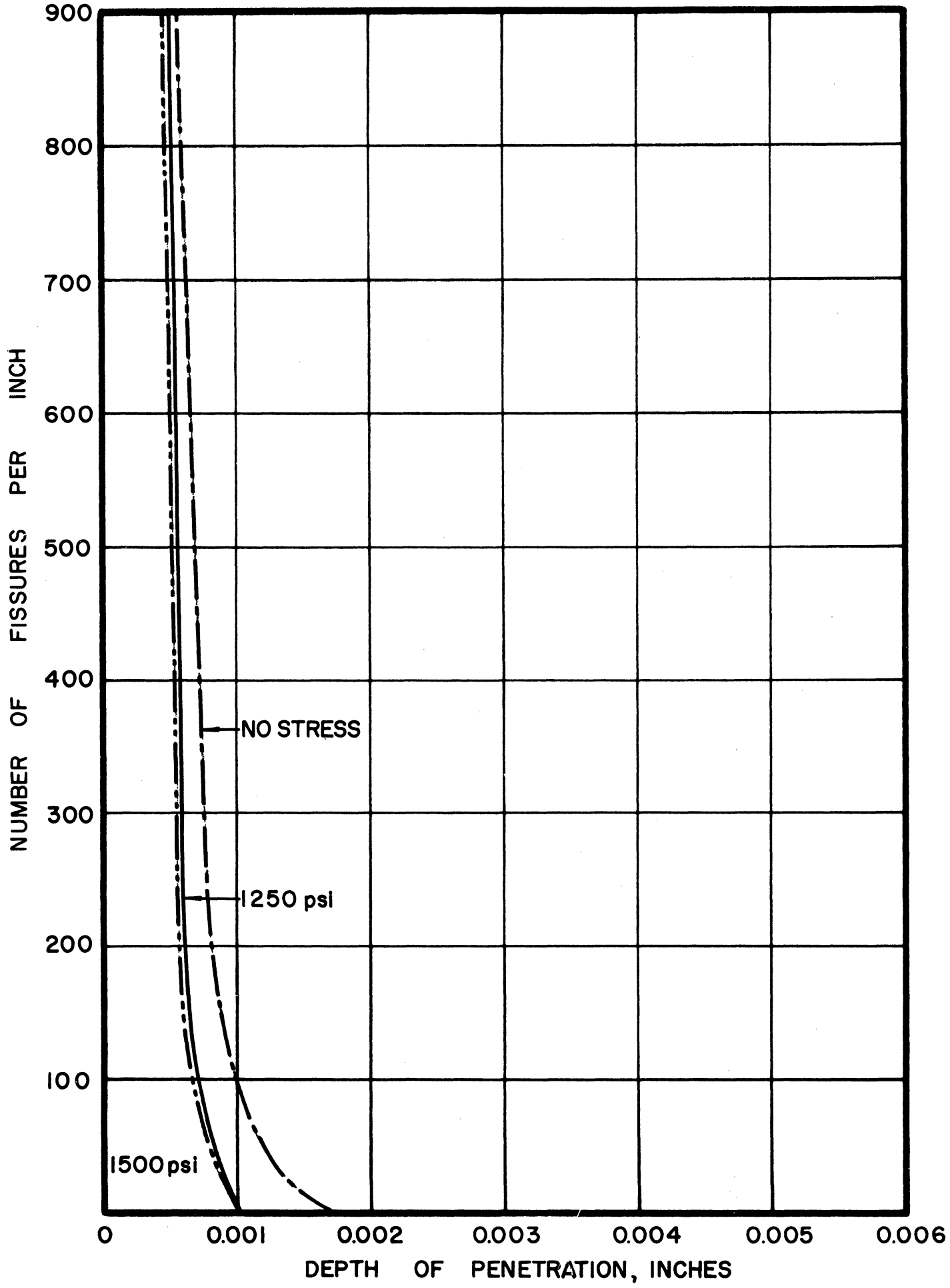

Fig. 76. Penetration vs. Depth Below Surface; Chromel ASM Alloy, 1800°F, 100 Hours.

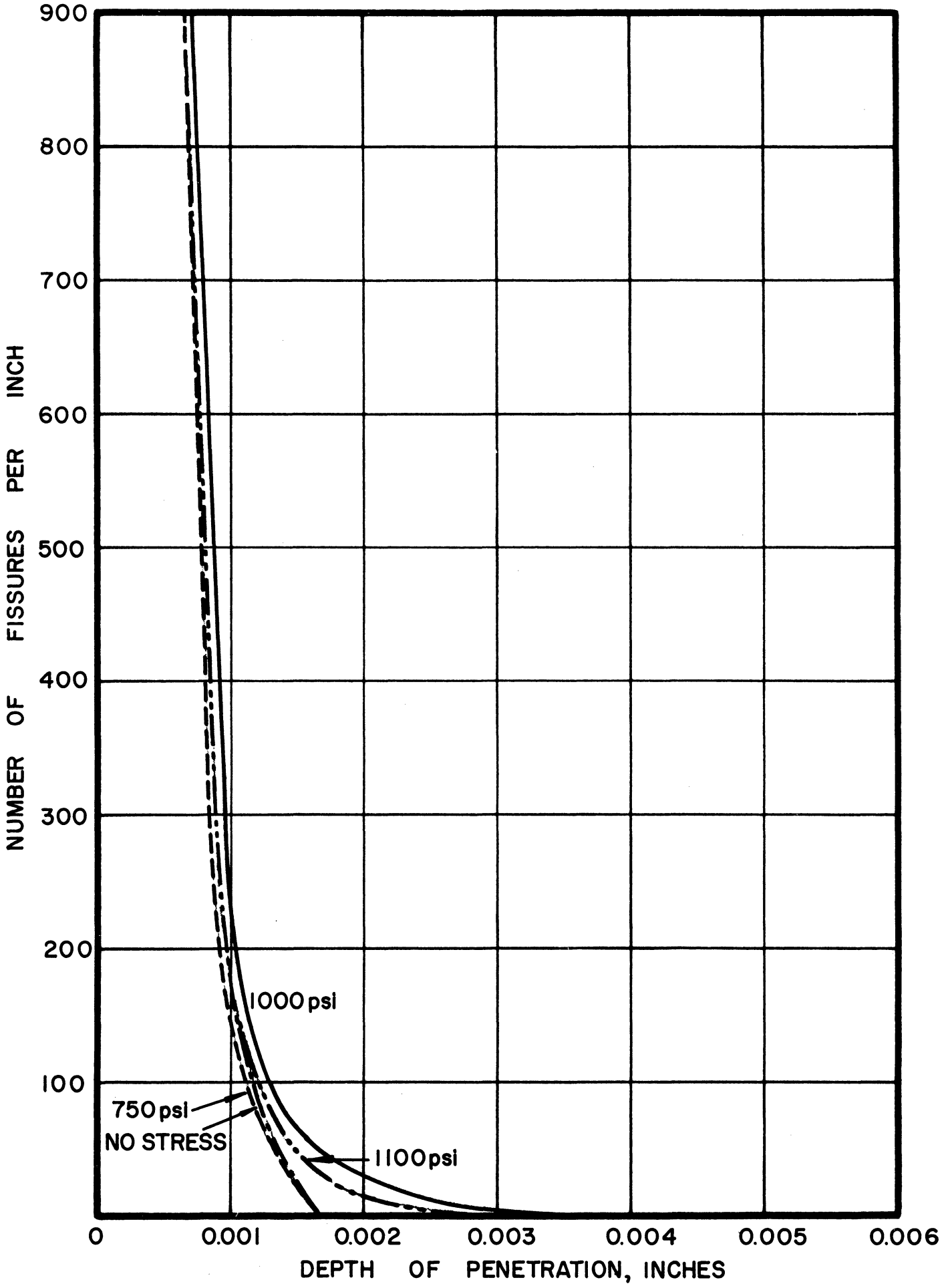

Fig. 77. Penetration vs. Depth Below Surface;
Chromel ASM Alloy, 1900°F, 100 Hours.

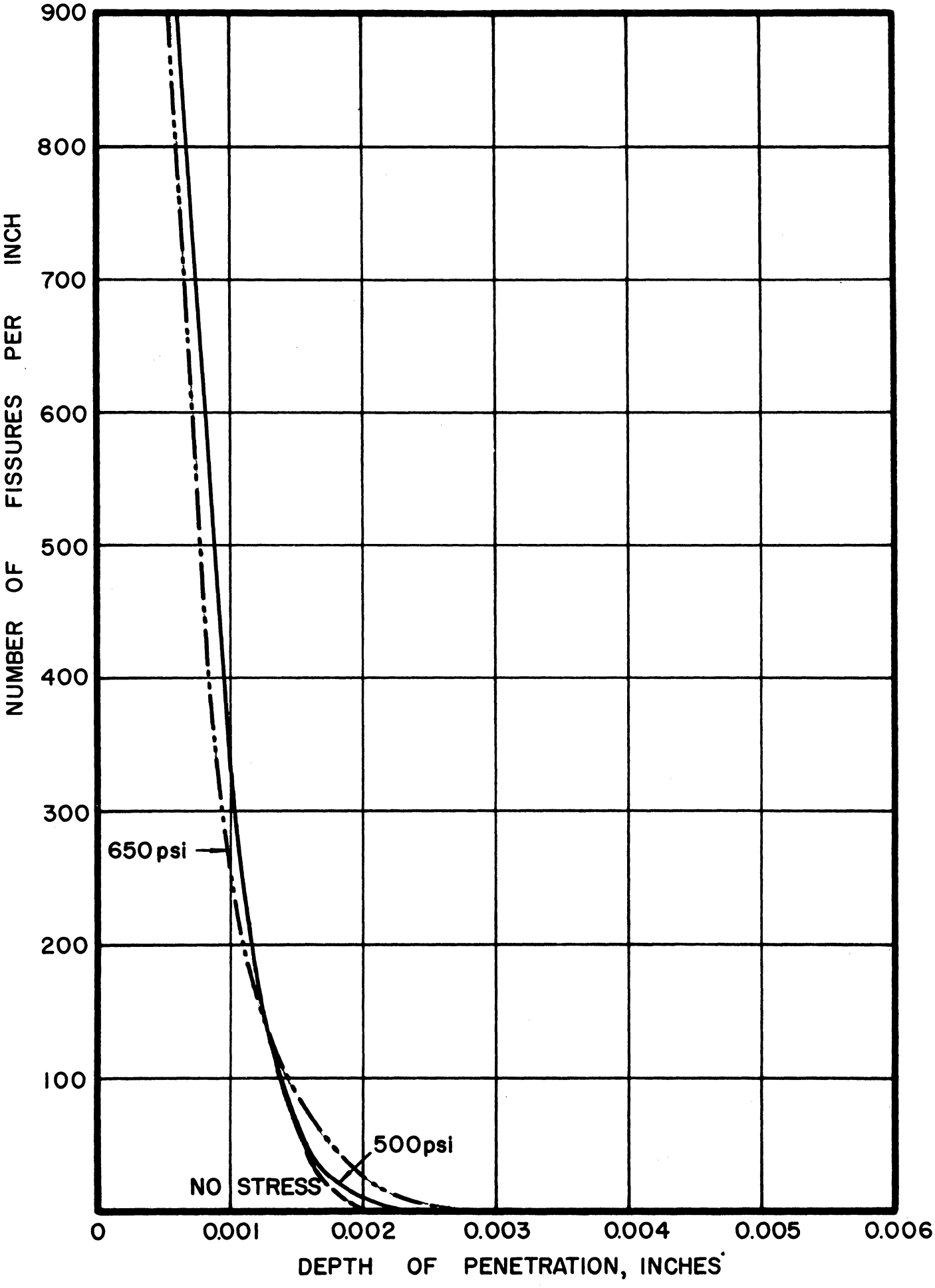

Fig. 78. Penetration vs. Depth Below Surface; Chromel ASM Alloy, 2000°F, 100 Hours.

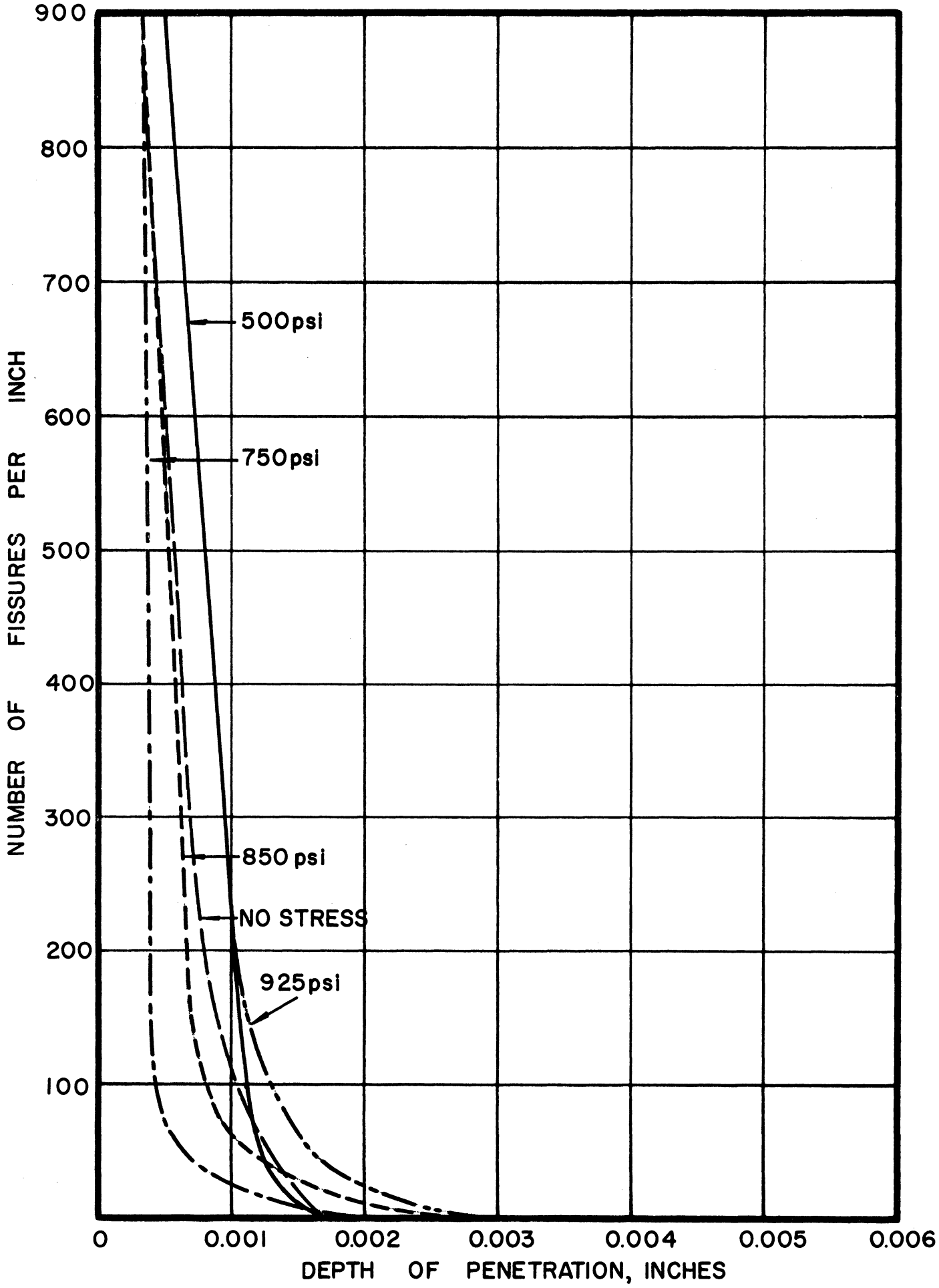

Fig. 79. Penetration vs. Depth Below Surface; Chromel D Alloy, 1800°F, 100 Hours.

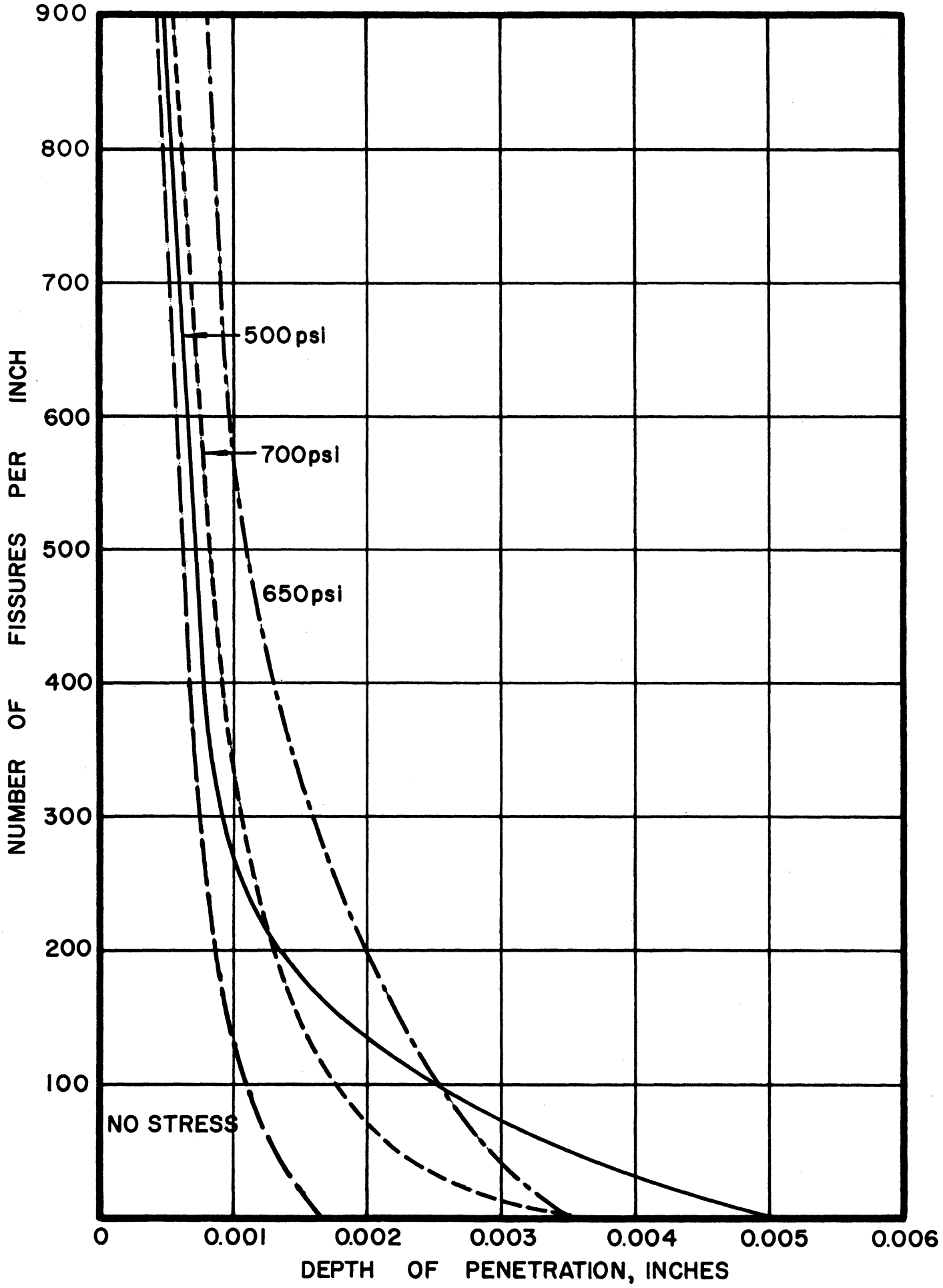

Fig. 80. Penetration vs. Depth Below Surface; Chromel D Alloy, 1900°F, 100 Hours.

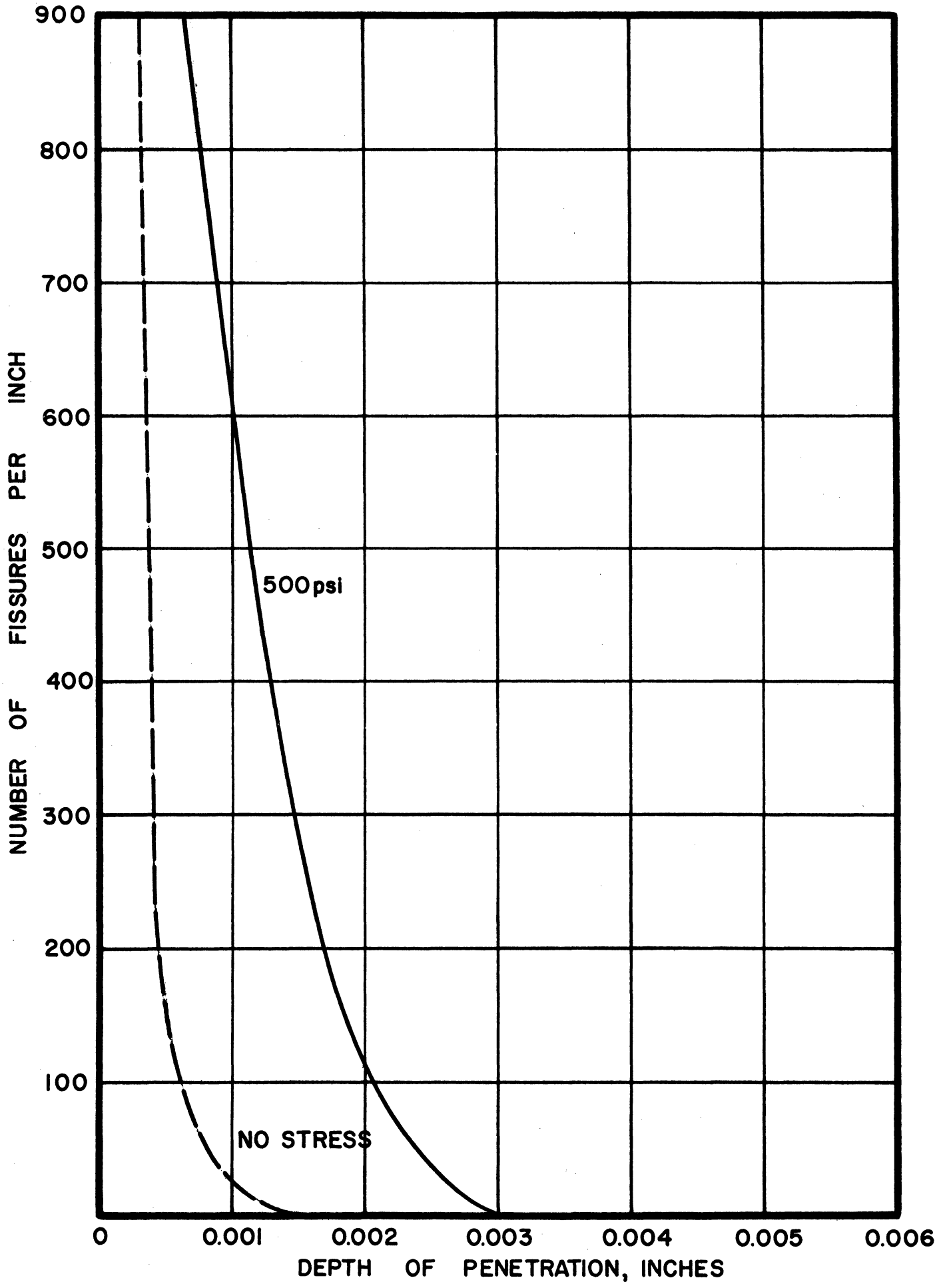

Fig. 81. Penetration vs. Depth Below Surface; Chromel D Alloy, 2000°F, 100 Hours.

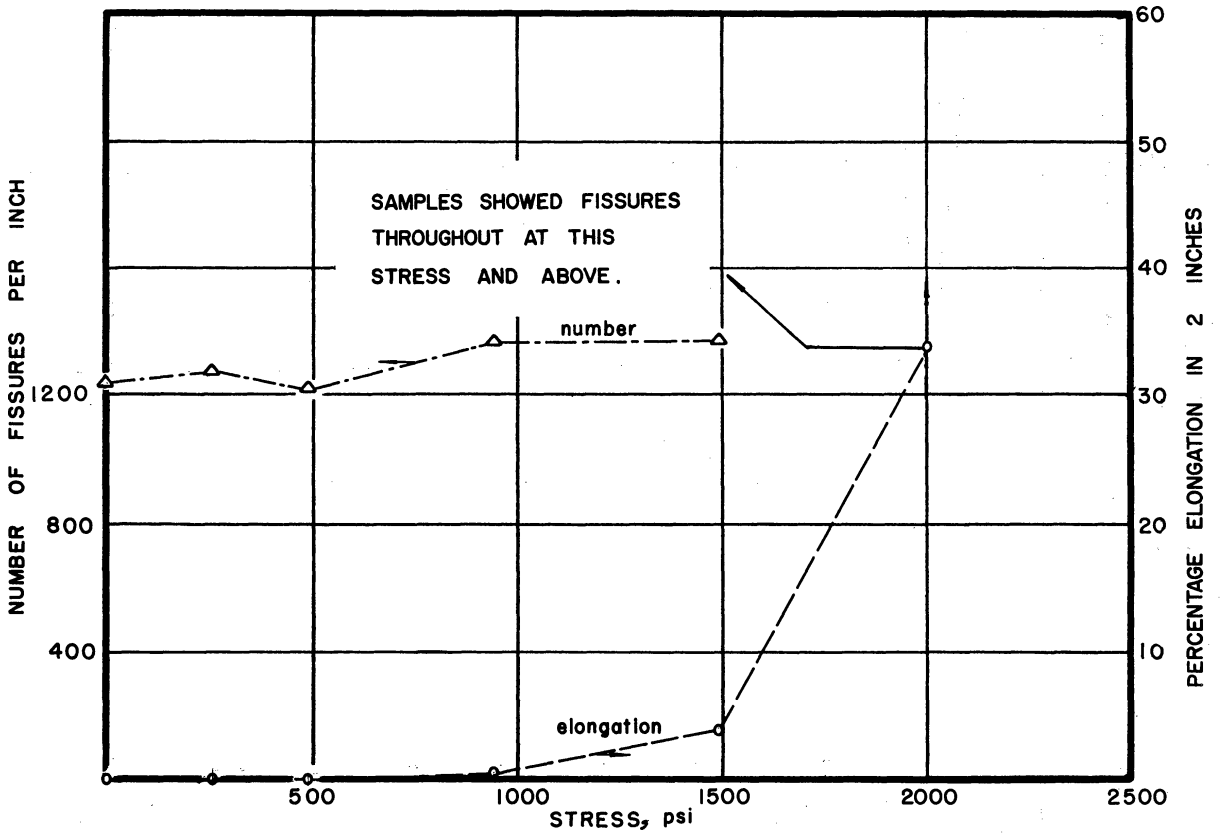

Fig. 82. Summary Penetration-Frequency Curves; Chromel ARM Alloy, Heat, 1800°F, 100 Hours.

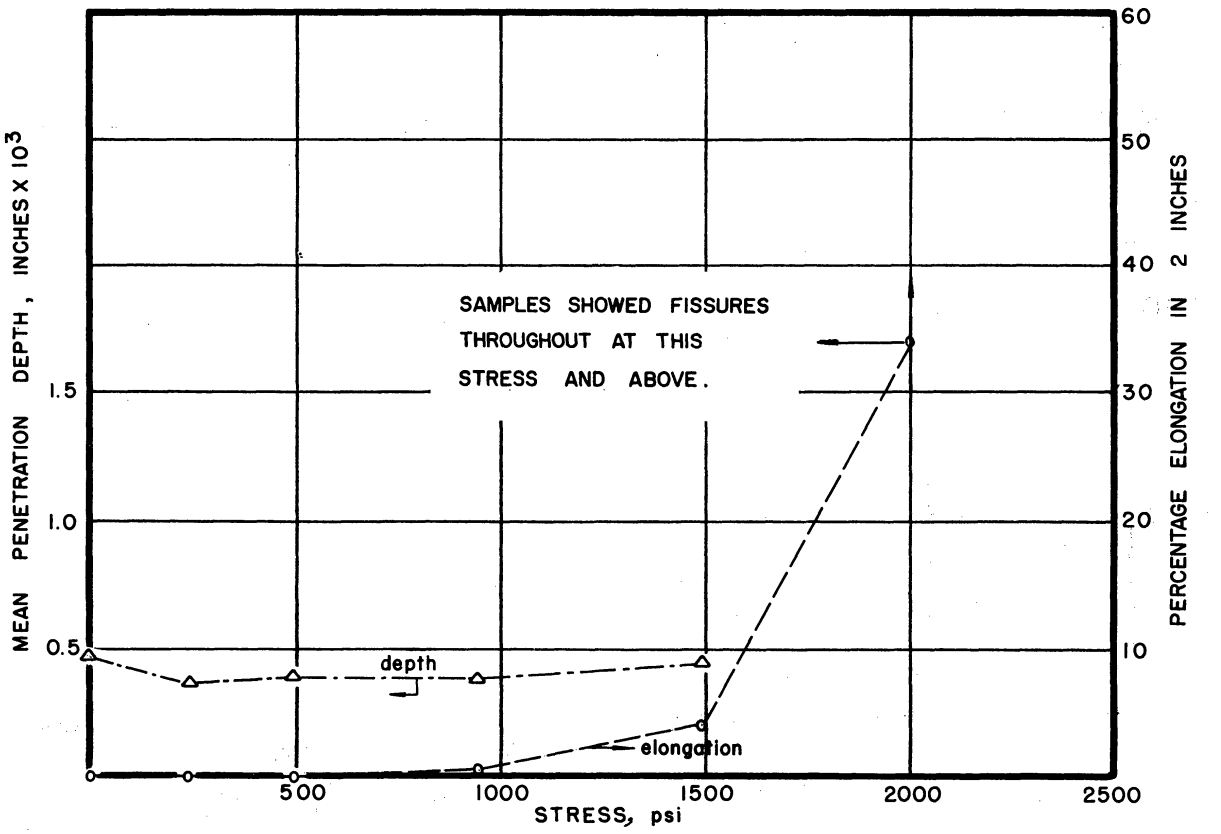

Fig. 83. Summary Penetration Depth Curves; Chromel ARM Alloy, Heat A, 1800°F, 100 Hours.

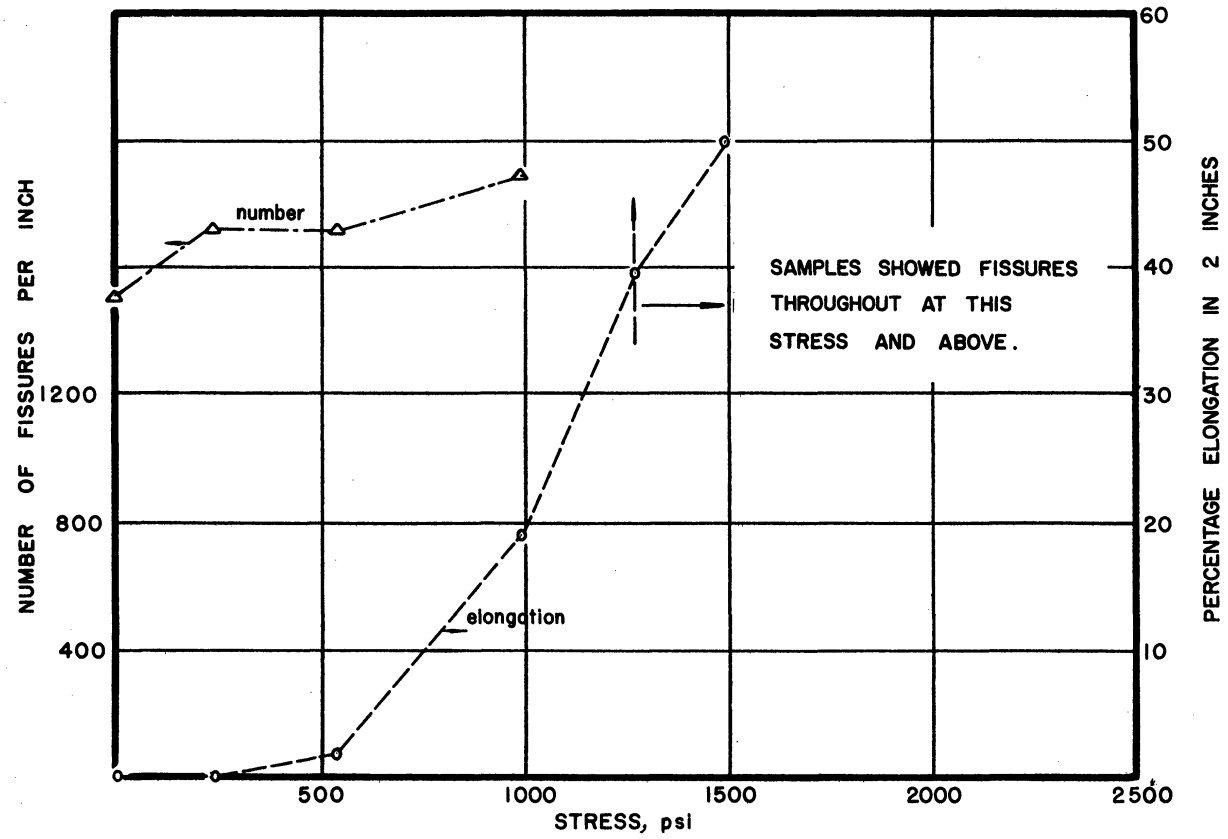

Fig. 84. Summary Penetration-Frequency Curves; Chromel ARM Alloy, Heat A, 1900°F, 100 Hours.

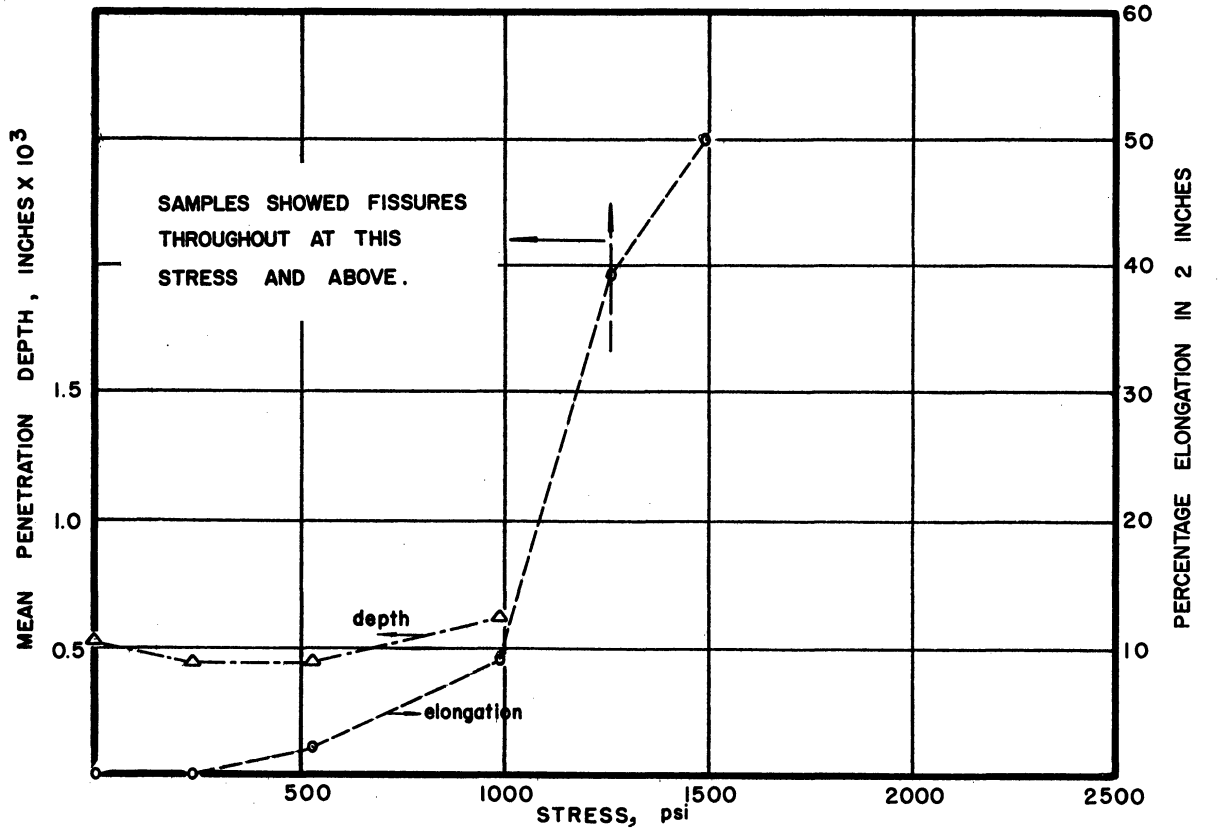

Fig. 85. Summary Penetration Depth Curves; Chromel ARM Alloy, Heat A, 1900°F, 100 Hours.

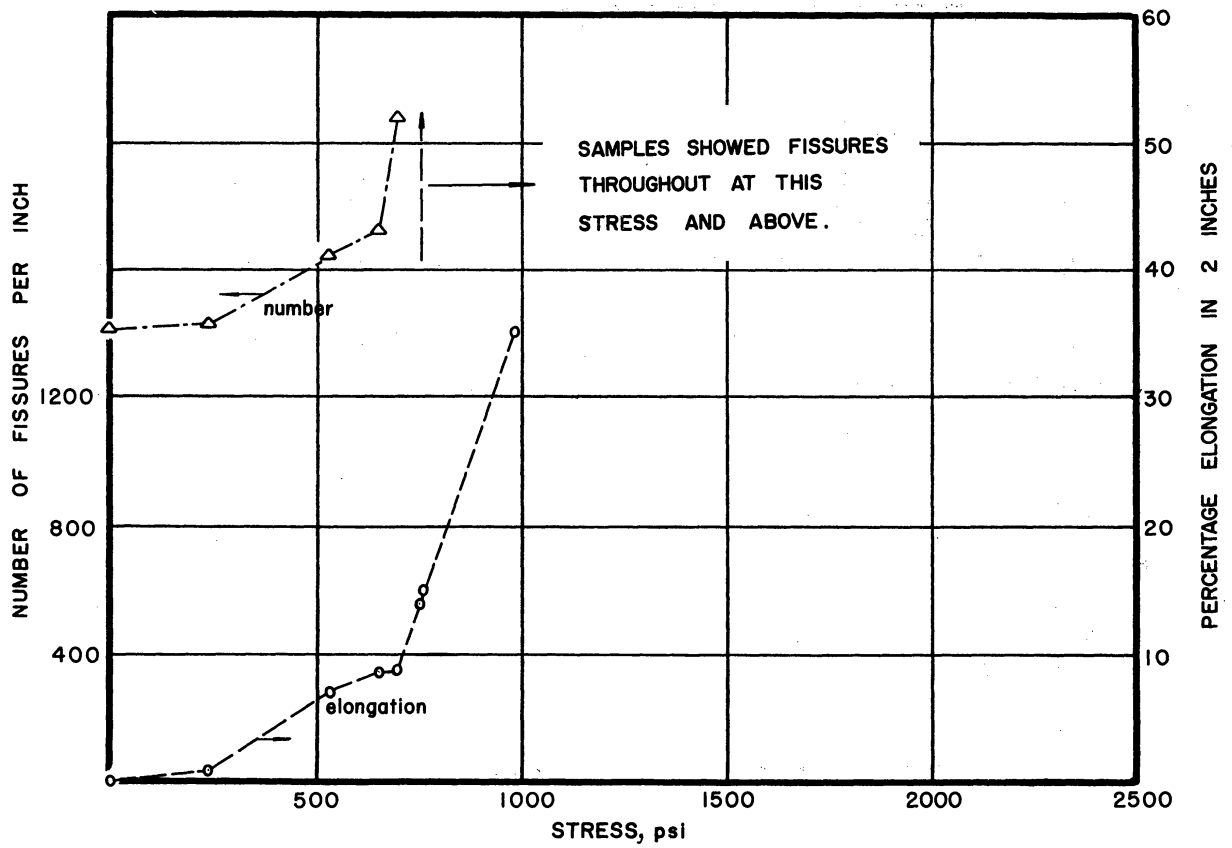

Fig. 86. Summary Penetration-Frequency Curves; Chromel ARM Alloy, Heat A, 2000°F, 100 Hours.

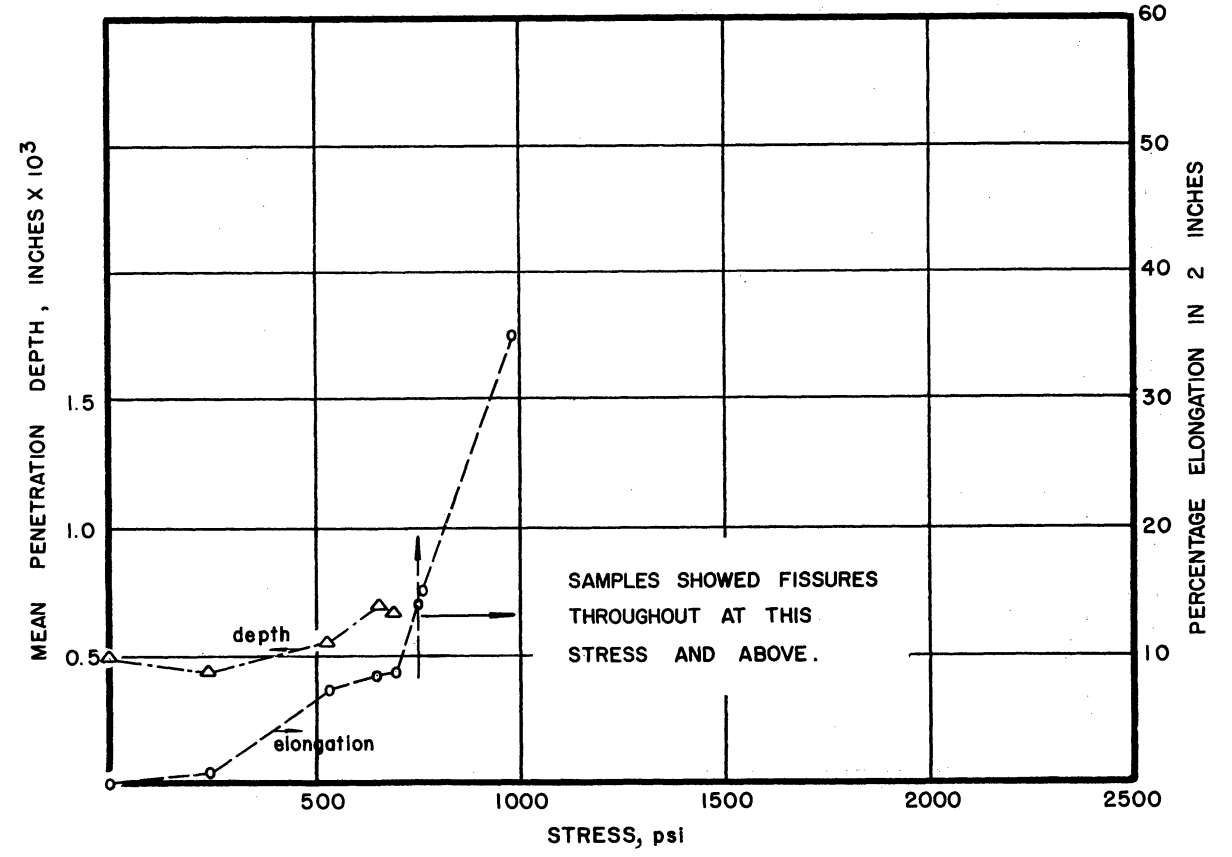

Fig. 87. Summary Penetration Depth Curves; Chromel ARM Alloy, Heat A, 2000°F, 100 Hours.

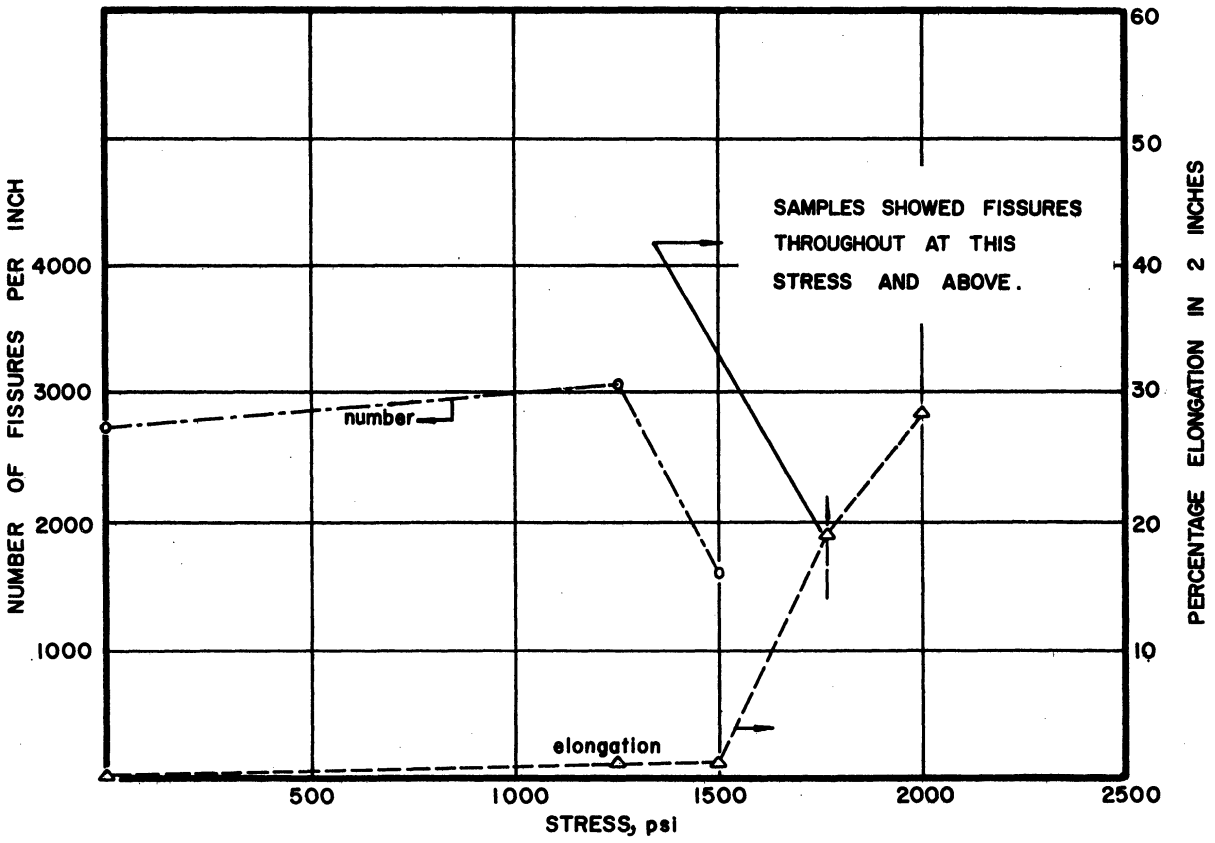

Fig. 88. Summary Penetration-Frequency Curves;
Chromel ASM Alloy, 1800°F, 100 Hours.

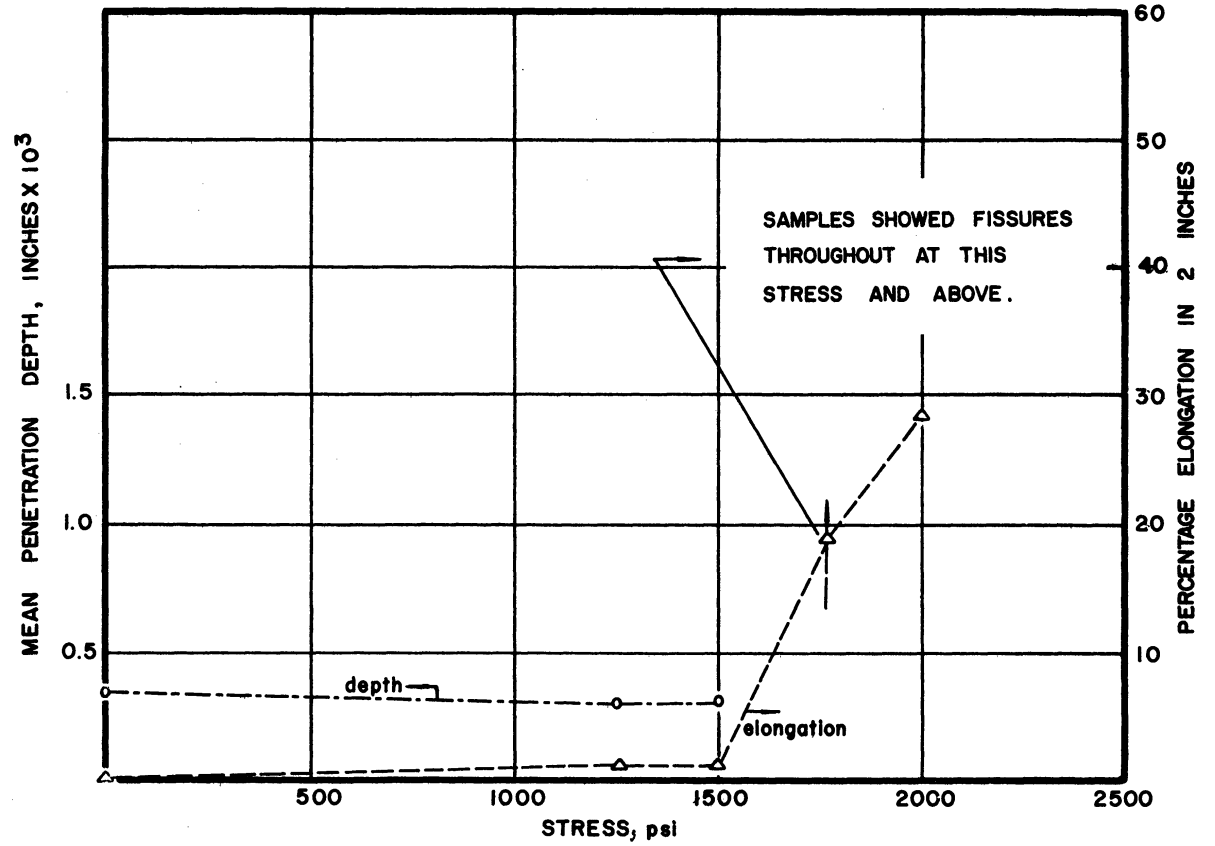

Fig. 89. Summary Penetration Depth Curves;
Chromel ASM Alloy, 1800°F, 100 Hours.

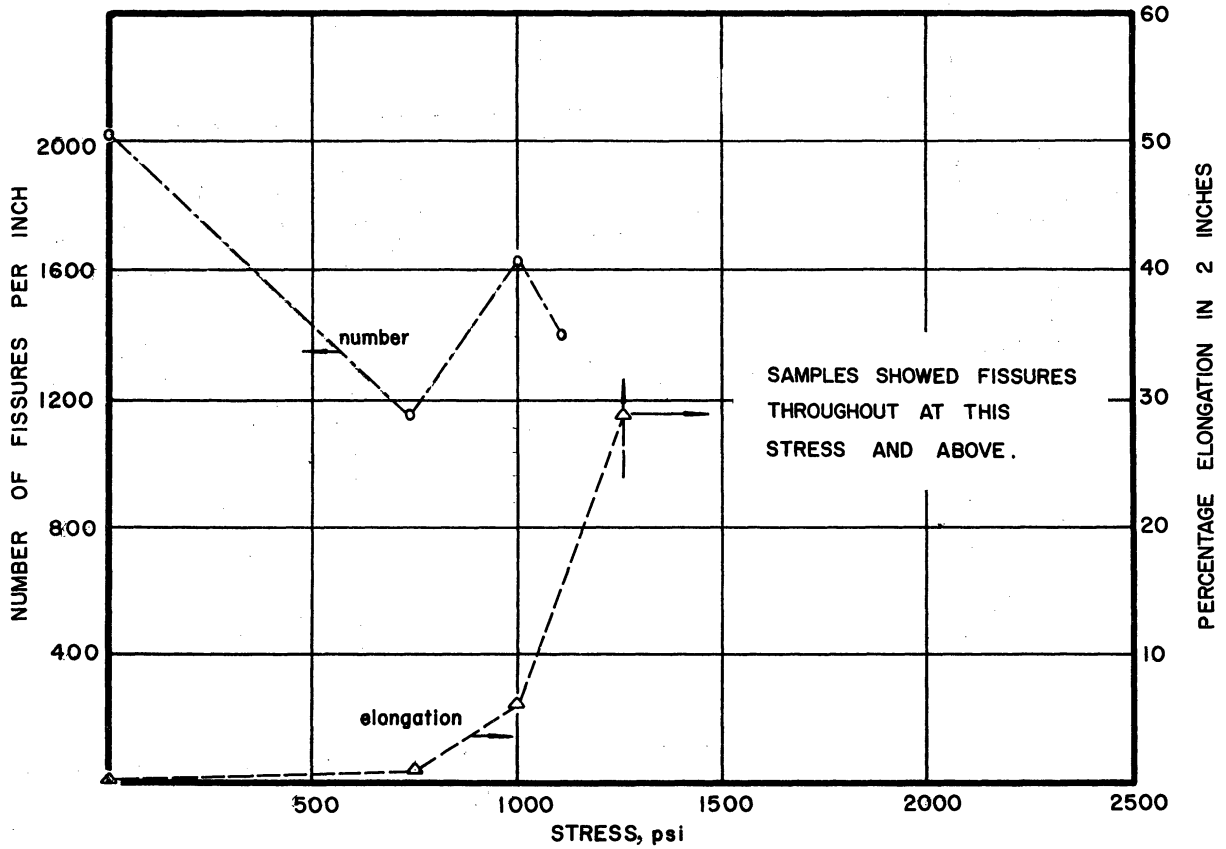

Fig. 90. Summary Penetration-Frequency Curves;
Chromel ASM Alloy, 1900°F, 100 Hours.

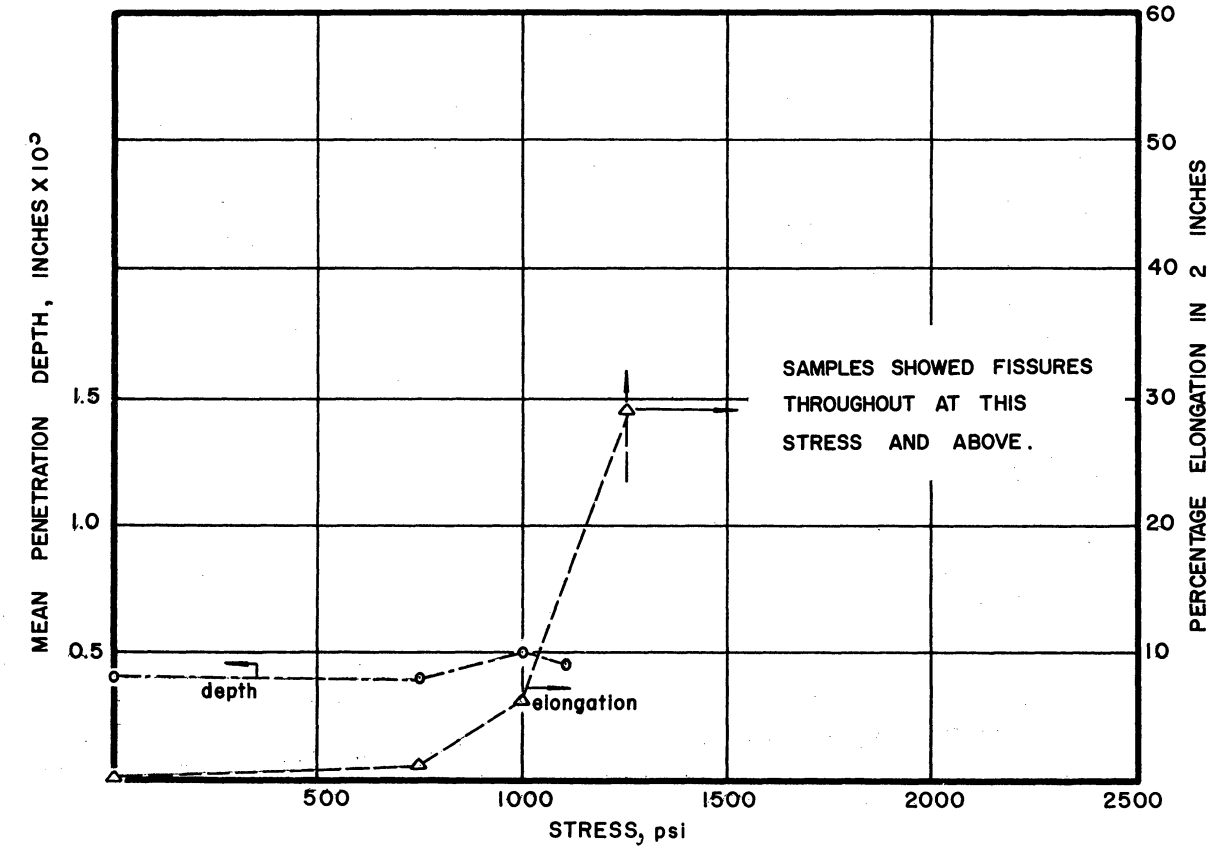

Fig. 91. Summary Penetration Depth Curves;
Chromel ASM Alloy, 1900°F, 100 Hours.

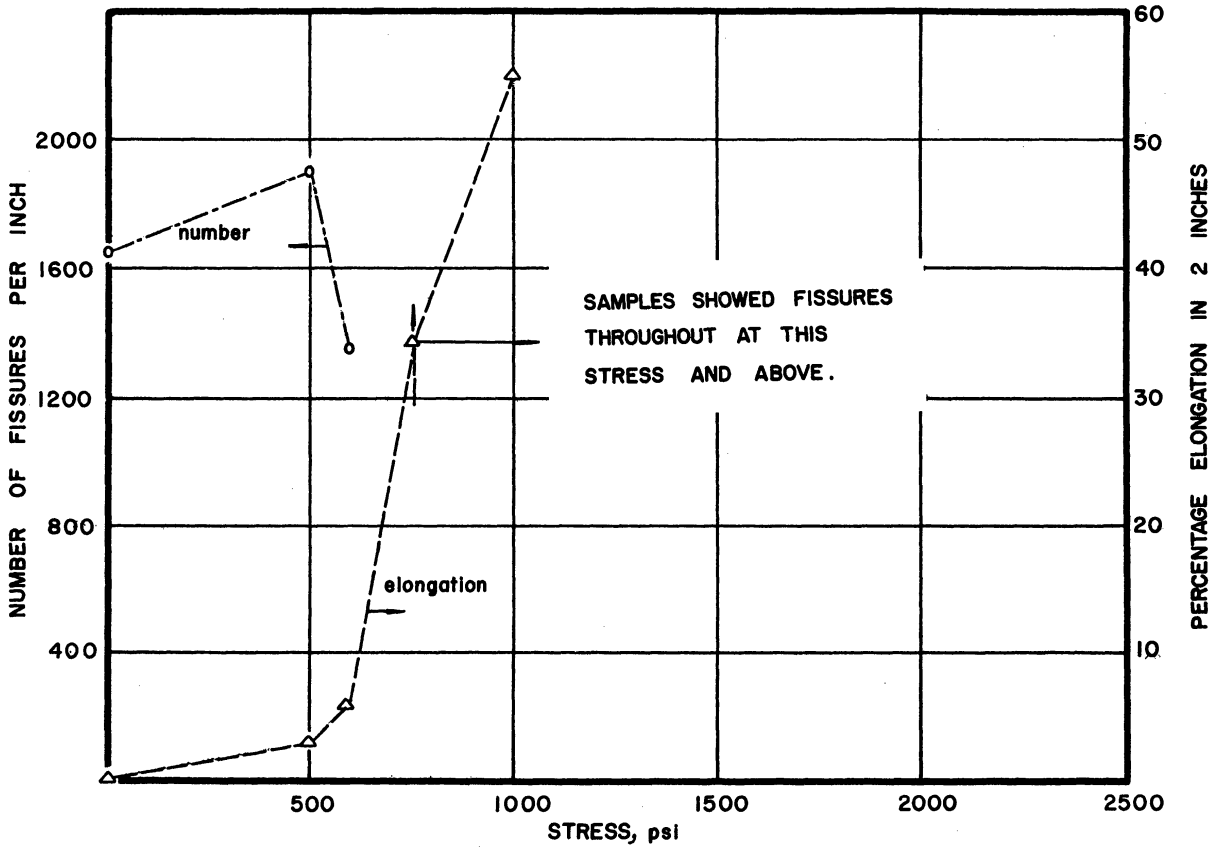

Fig. 92. Summary Penetration-Frequency Curves;
Chromel ASM Alloy, 2000°F, 100 Hours.

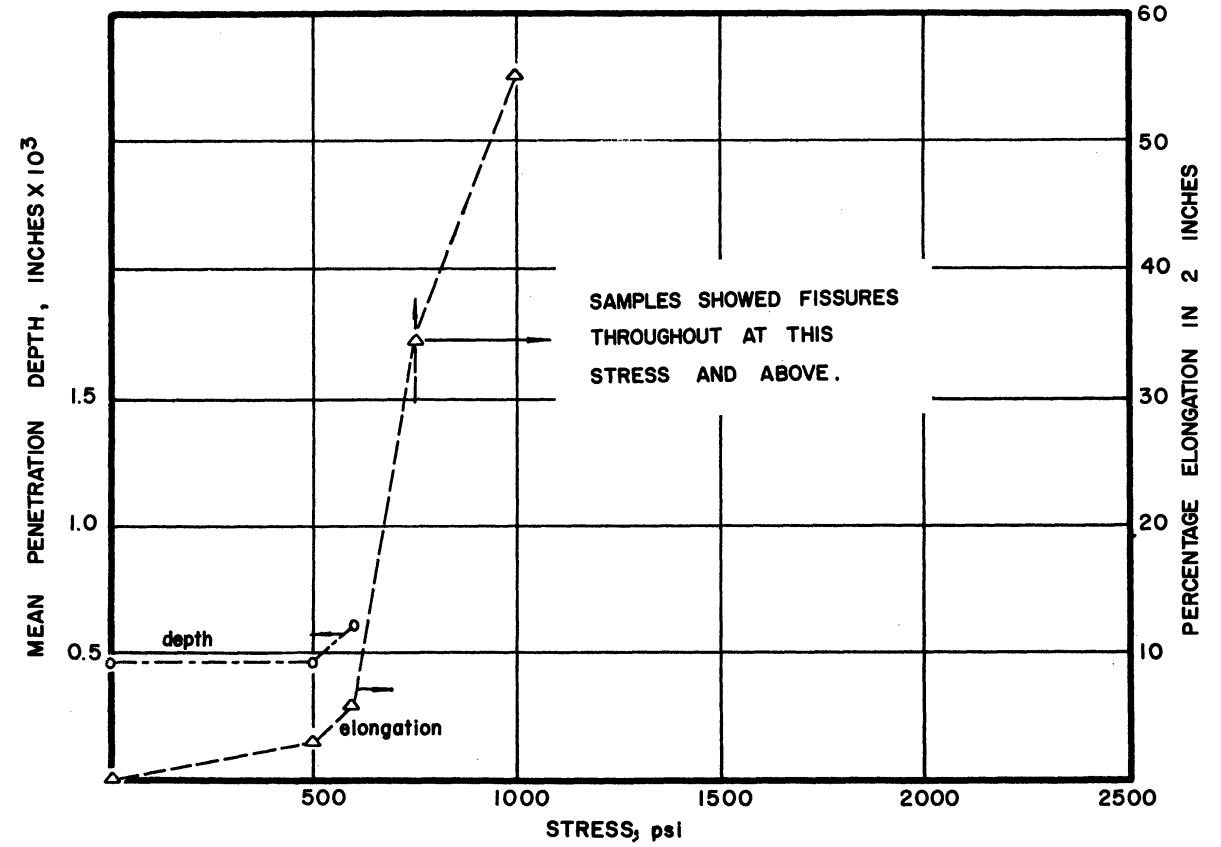

Fig. 93. Summary Penetration Depth Curves;
Chromel ASM Alloy, 2000°F, 100 Hours.

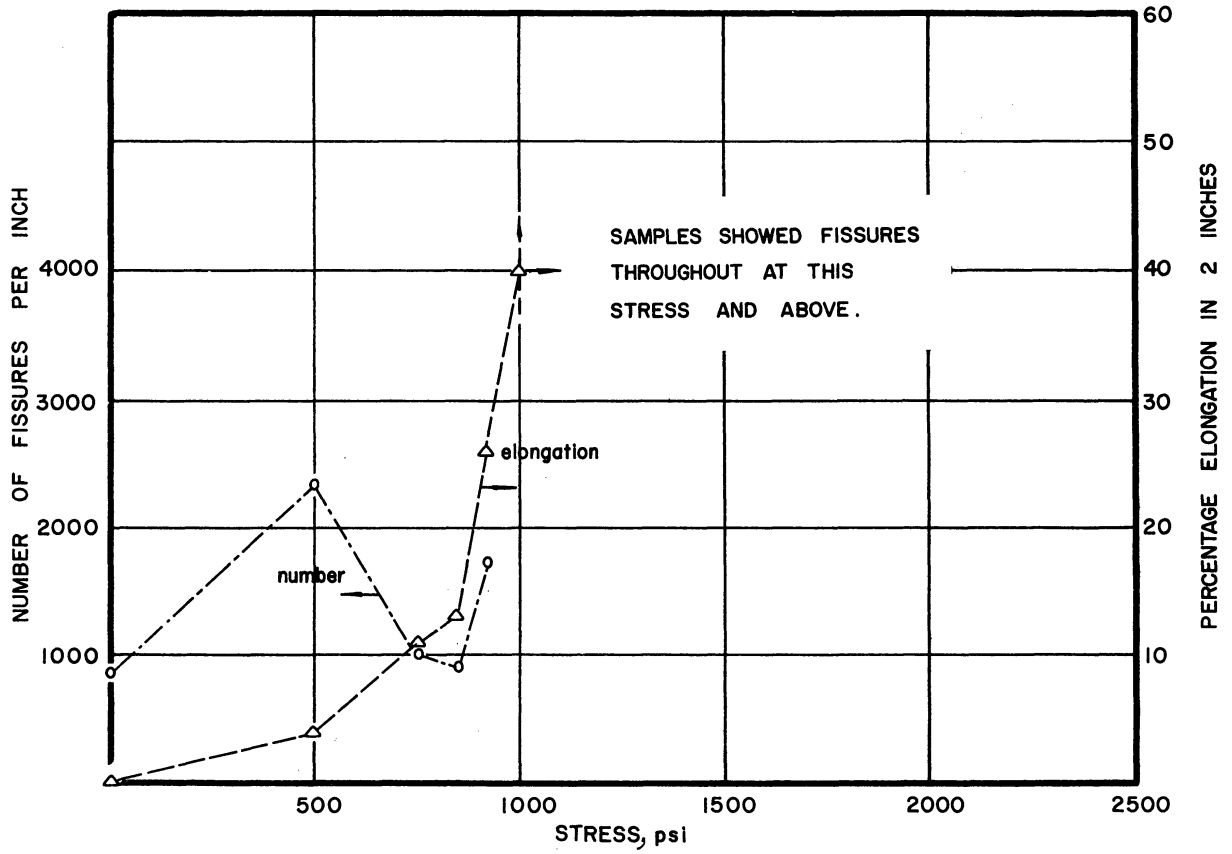

Fig. 94. Summary Penetration-Frequency Curves; Chromel D Alloy, 1800°F, 100 Hours.

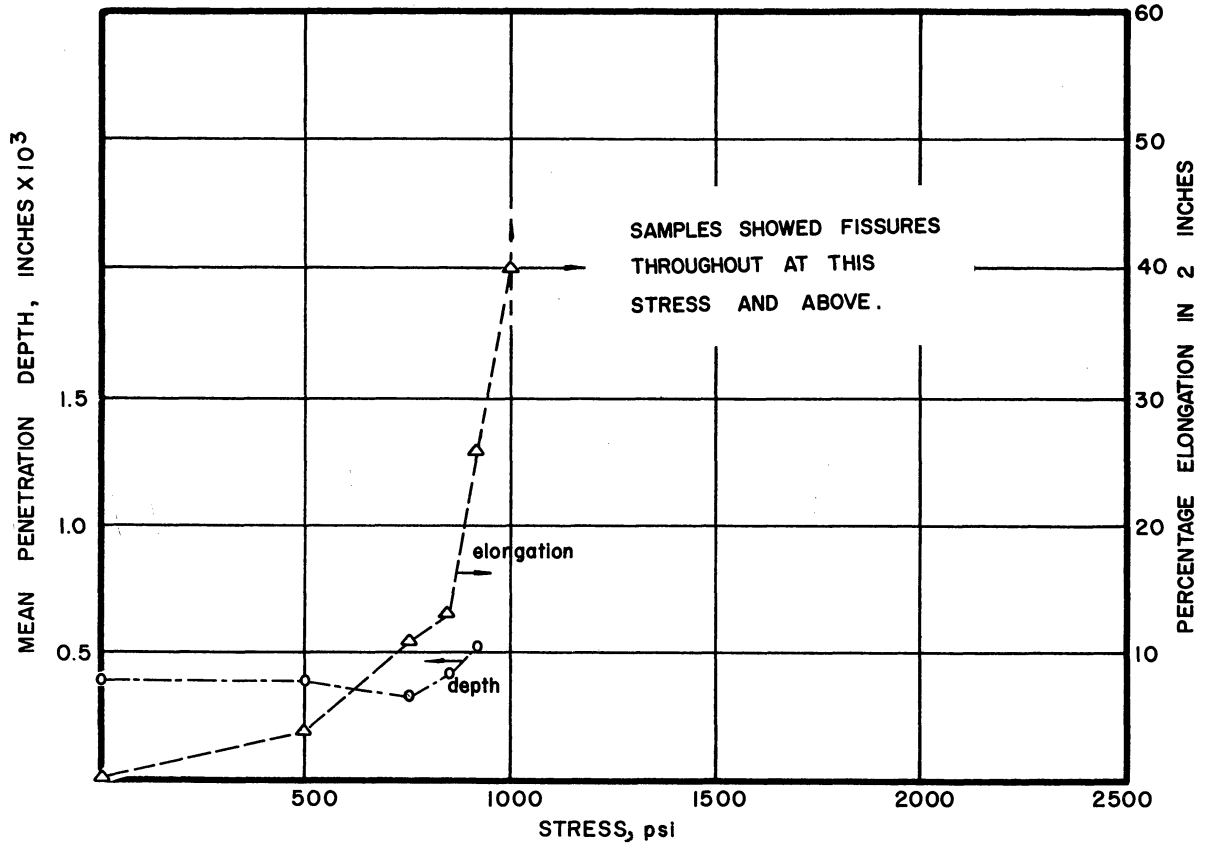

Fig. 95. Summary Penetration Depth Curves; Chromel D Alloy, 1800°F, 100 Hours.

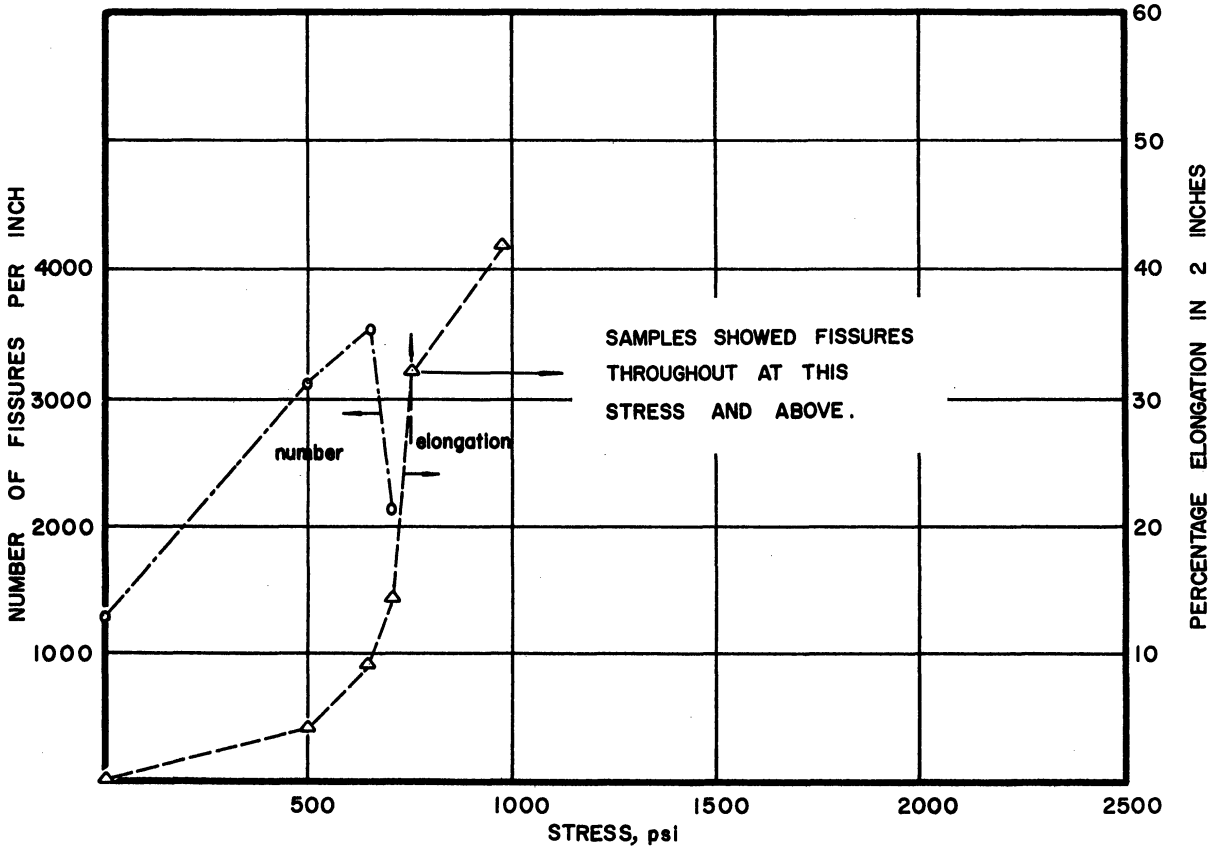

Fig. 96. Summary Penetration-Frequency Curves;
Chromel D Alloy, 1900°F, 100 Hours.

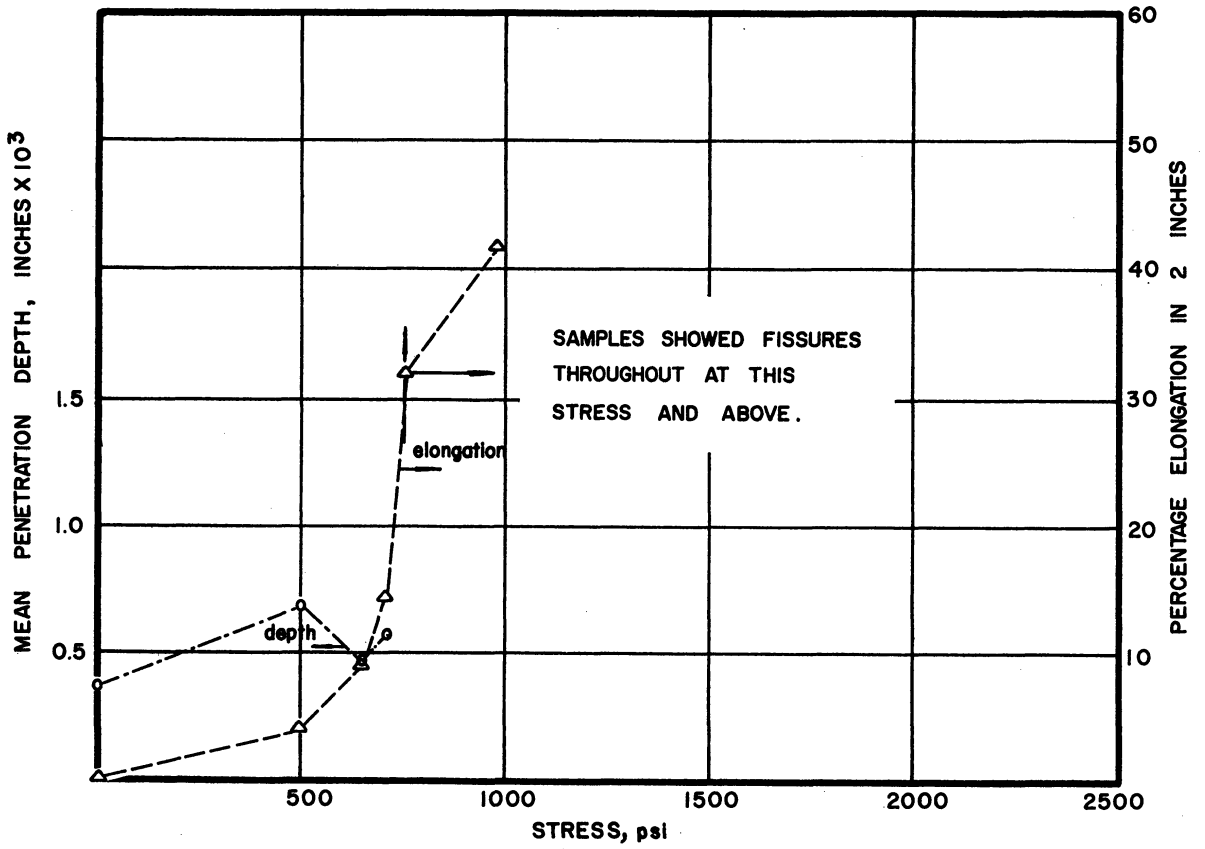

Fig. 97. Summary Penetration Depth Curves;
Chromel D Alloy, 1900°F, 100 Hours.

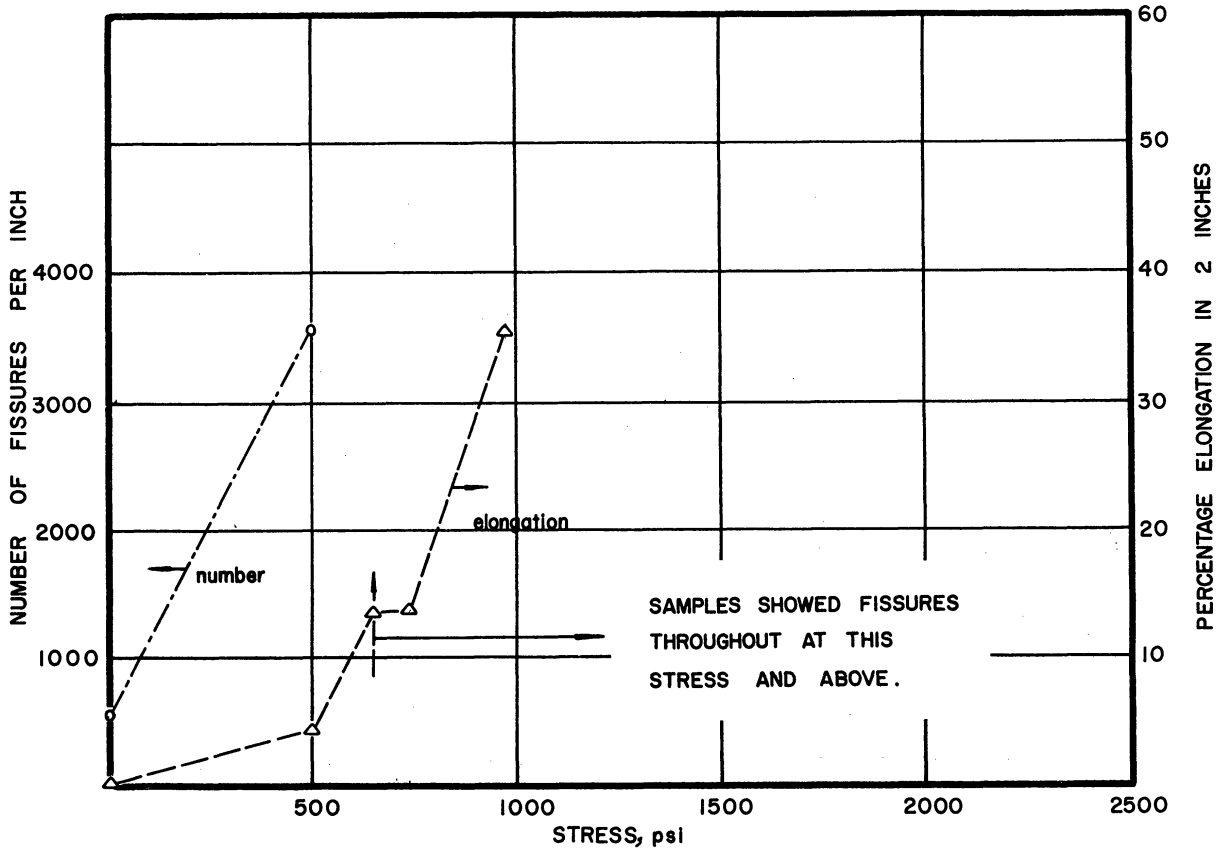

Fig. 98. Summary Penetration-Frequency Curves;
Chromel D Alloy, 2000°F, 100 Hours.

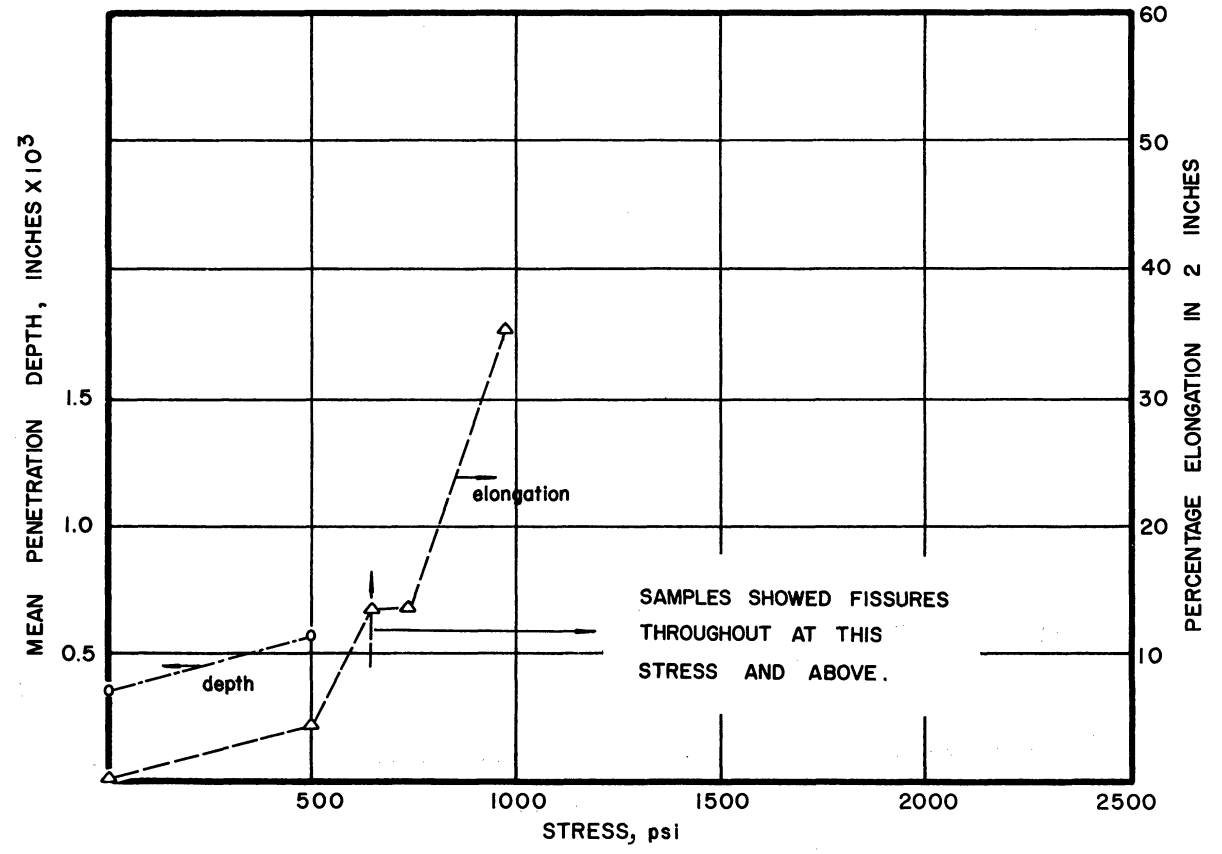

Fig. 99. Summary Penetration Depth Curves;
Chromel D Alloy, 2000°F, 100 Hours.

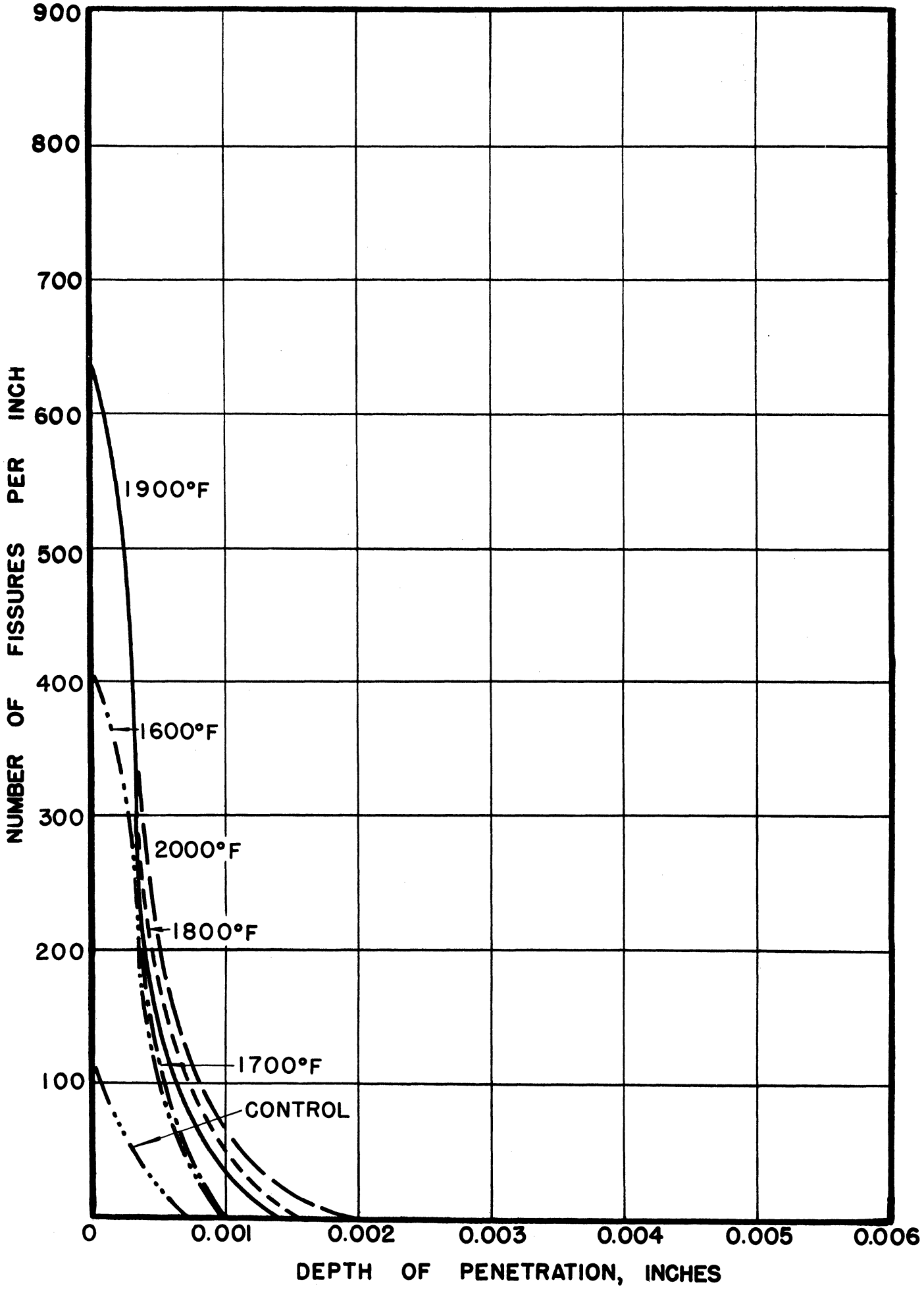

Fig. 100. Penetration vs. Depth Below Surface; Inconel Alloy, Run 30A, 10 Hours.

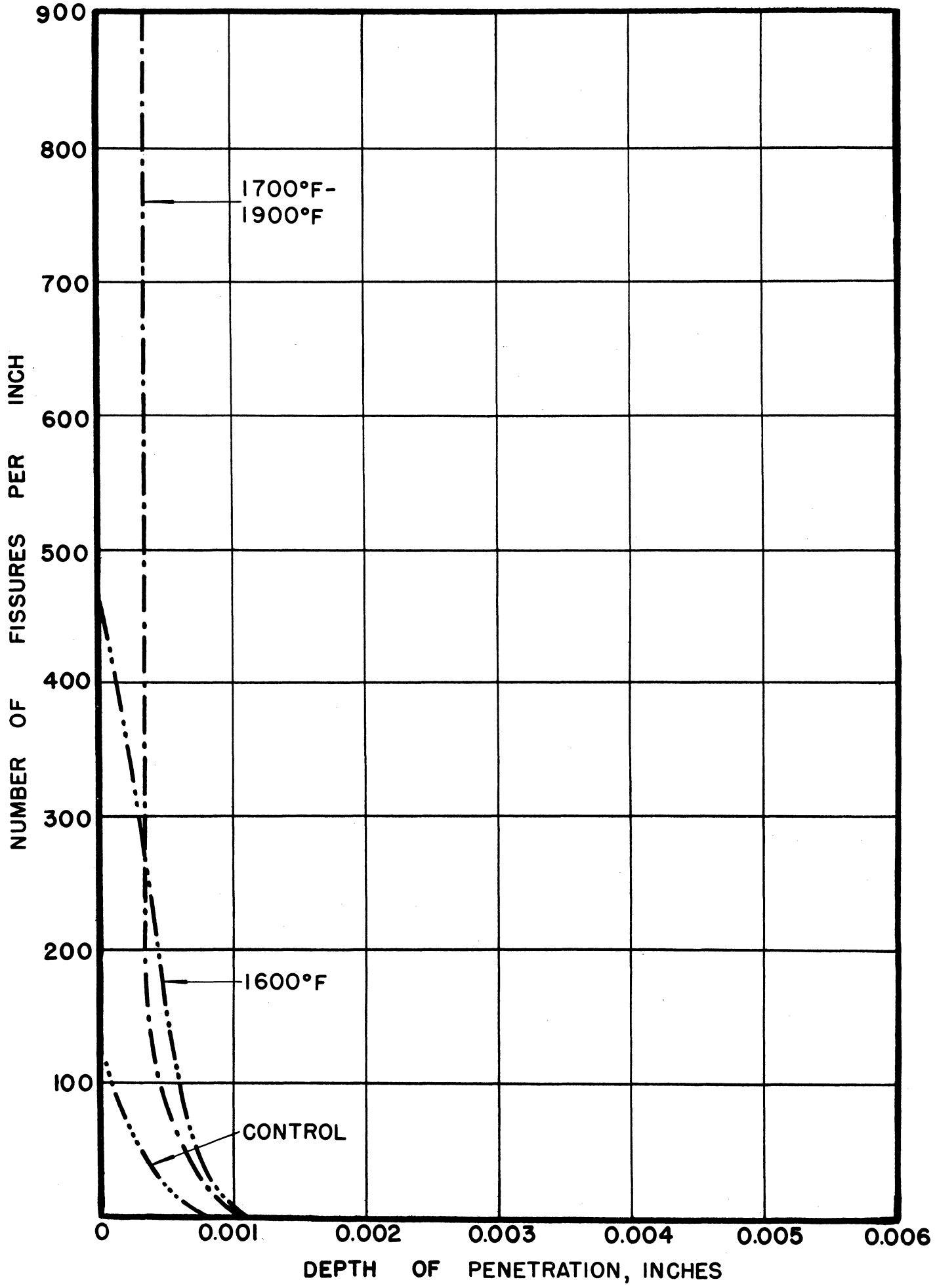

Fig. 101. Penetration vs. Depth Below Surface; Inconel Alloy, Run 30B, 30 Hours.

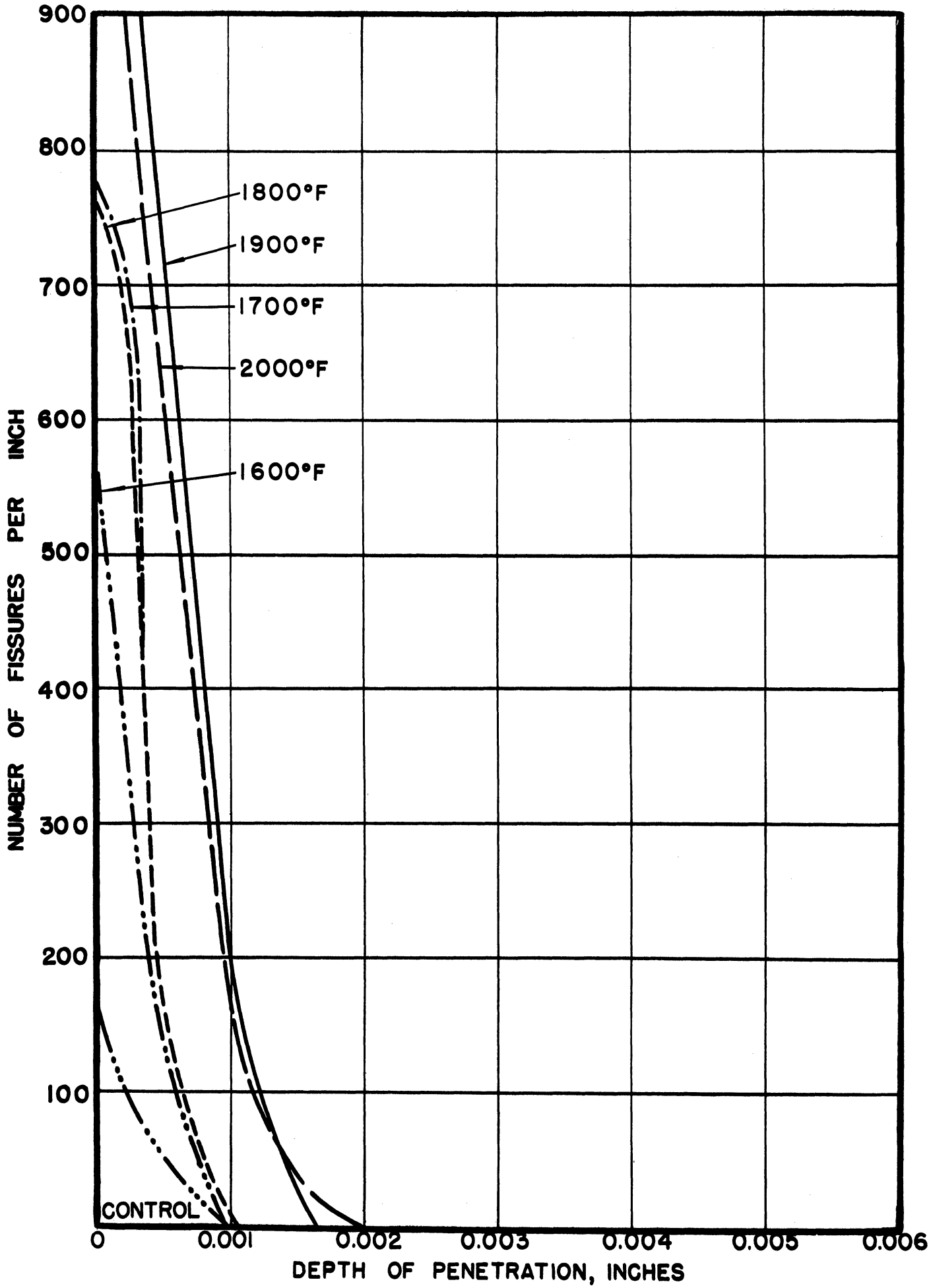

Fig. 102. Penetration vs. Depth Below Surface; Inconel Alloy, Run 30C, 100 Hours.

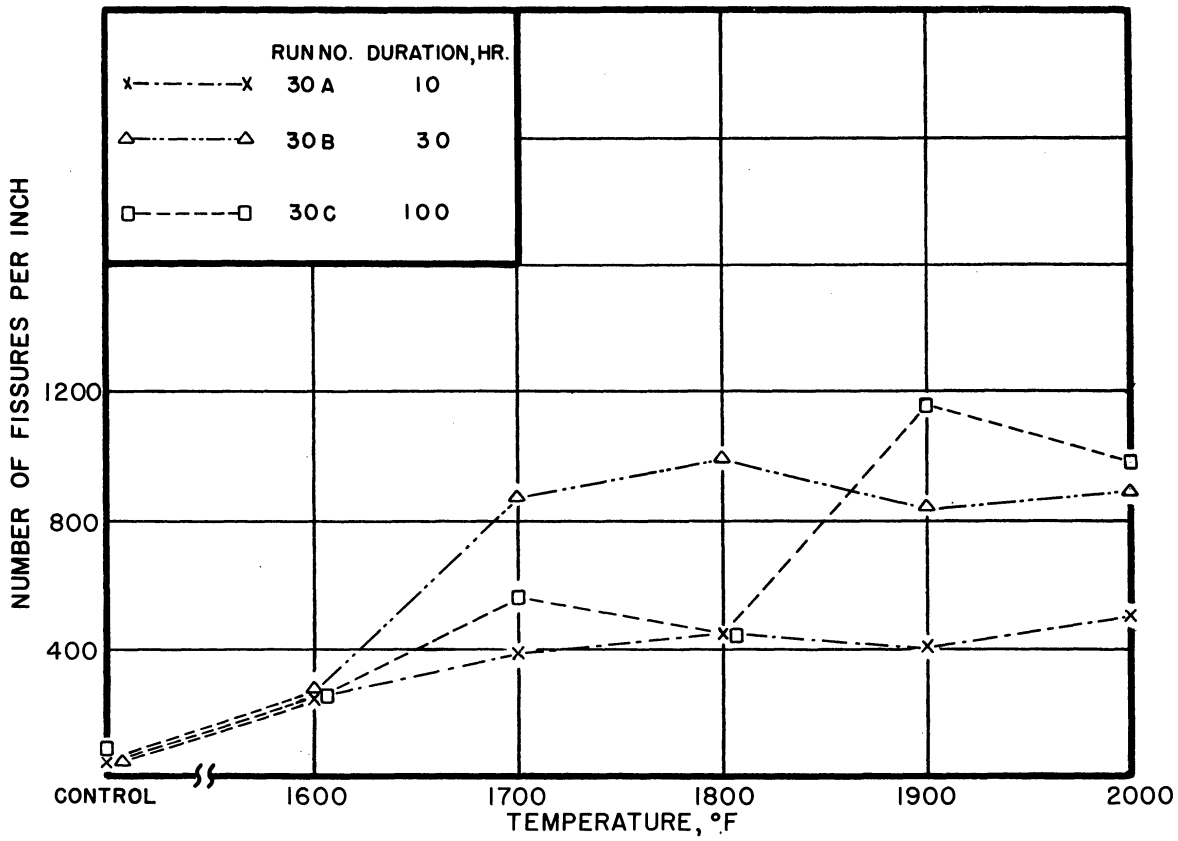

Fig. 103. Summary Penetration-Frequency Curves; Inconel Alloy, Effect of Time.

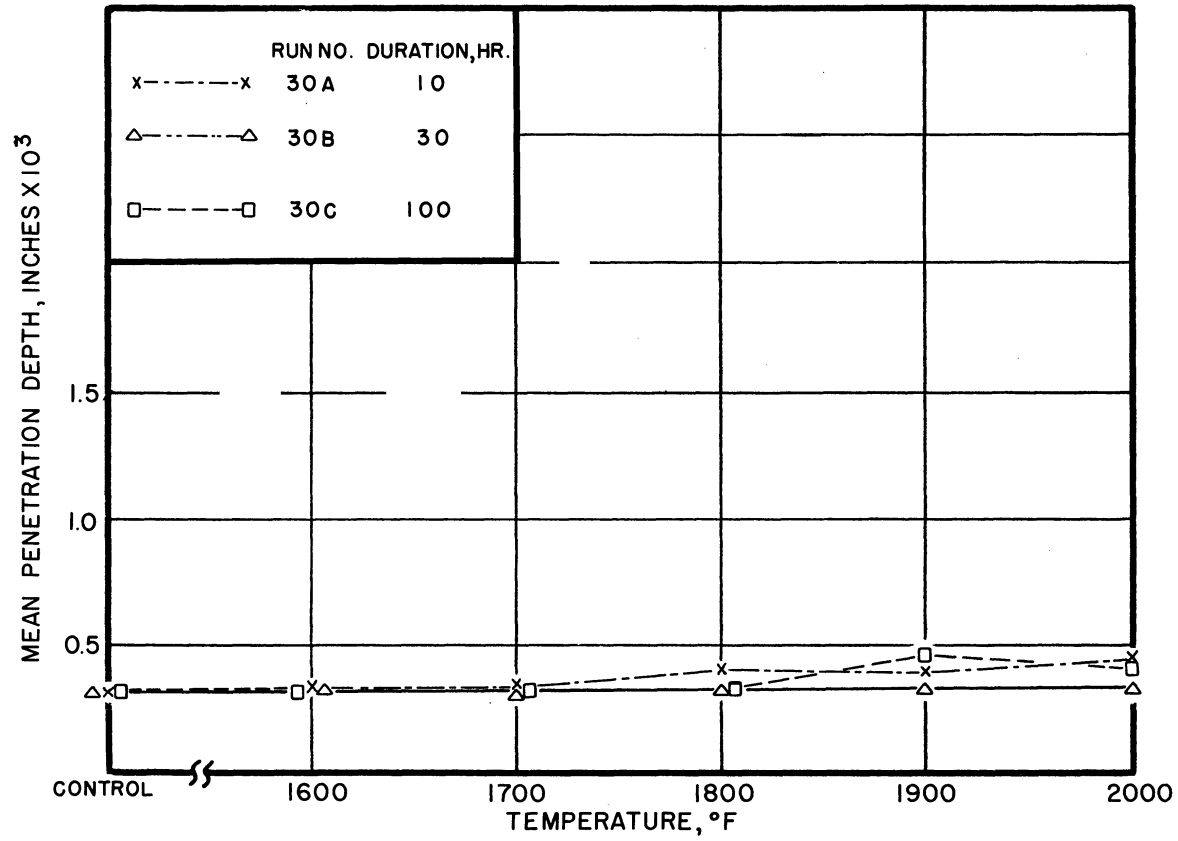

Fig. 104. Summary Penetration Depth Curves; Inconel Alloy, Effect of Time.

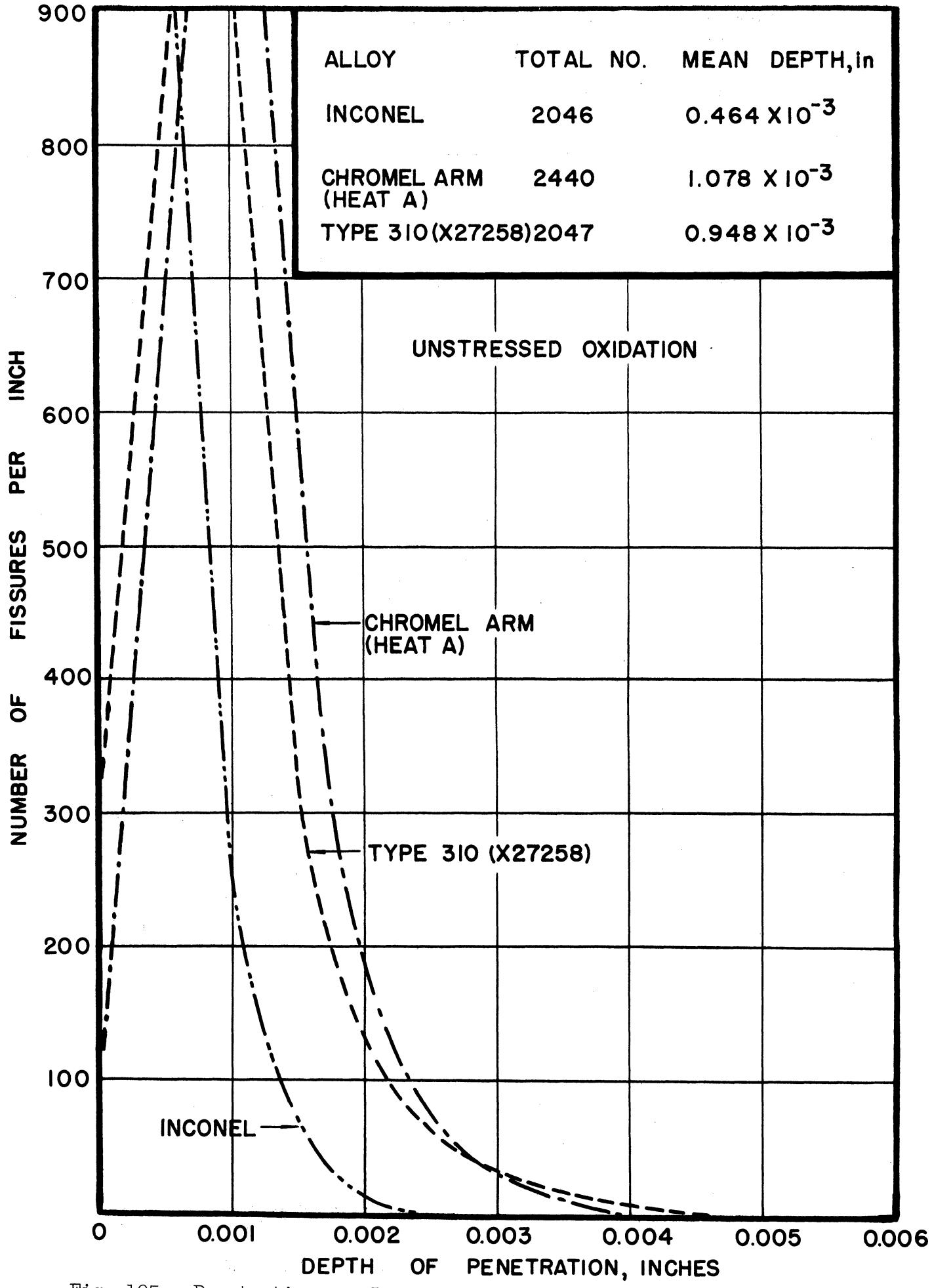

Fig. 105. Penetration vs. Depth Below Surface; Inconel, Chromel ARM, and Type 310 (Heat X27258) Alloys, 1900°F, 500 Hours.

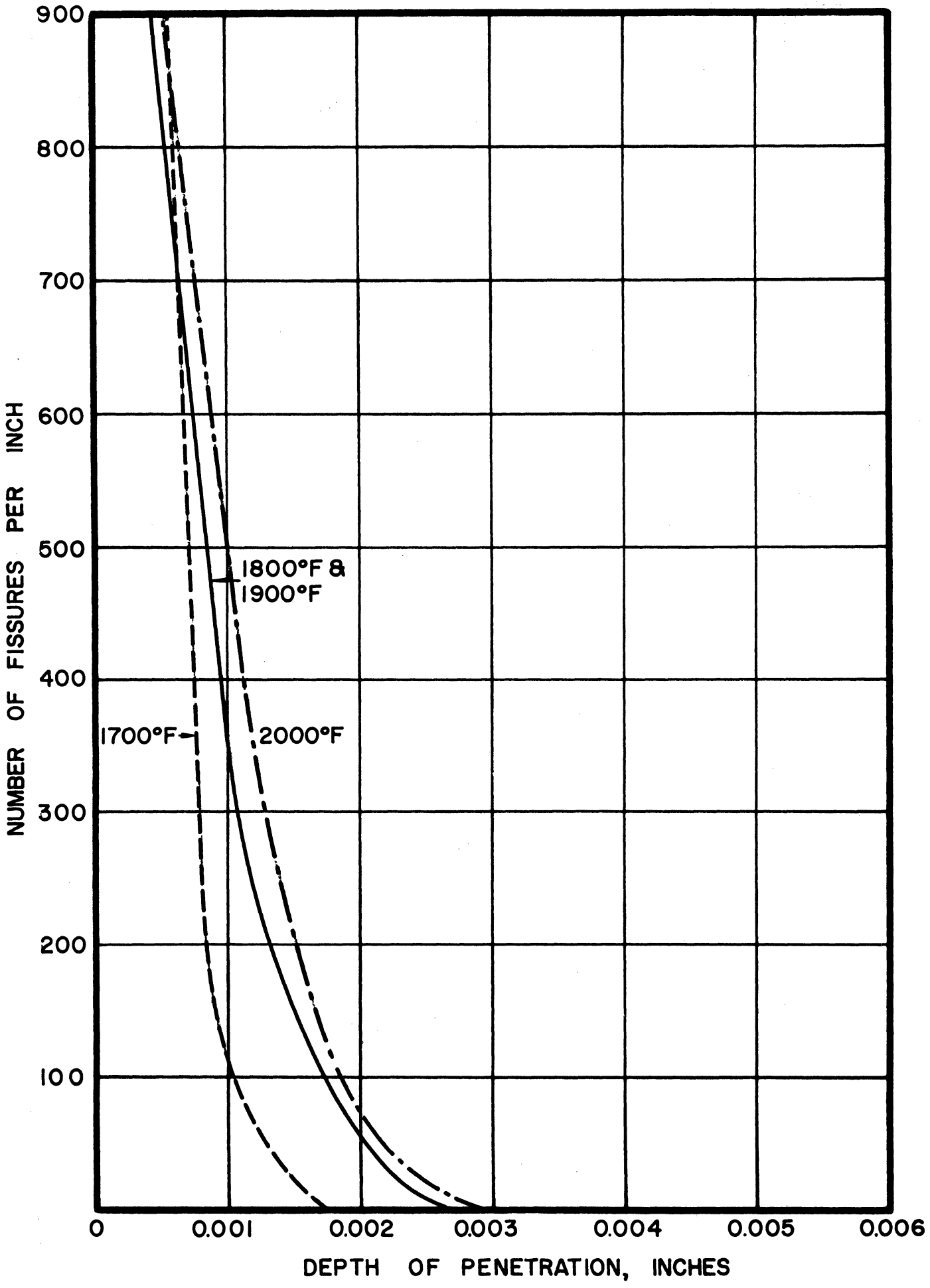

Fig. 106. Penetration vs. Depth Below Surface; Type 310 Alloy, Heat X46572, Dewpoint = +60°F, 100 Hours.

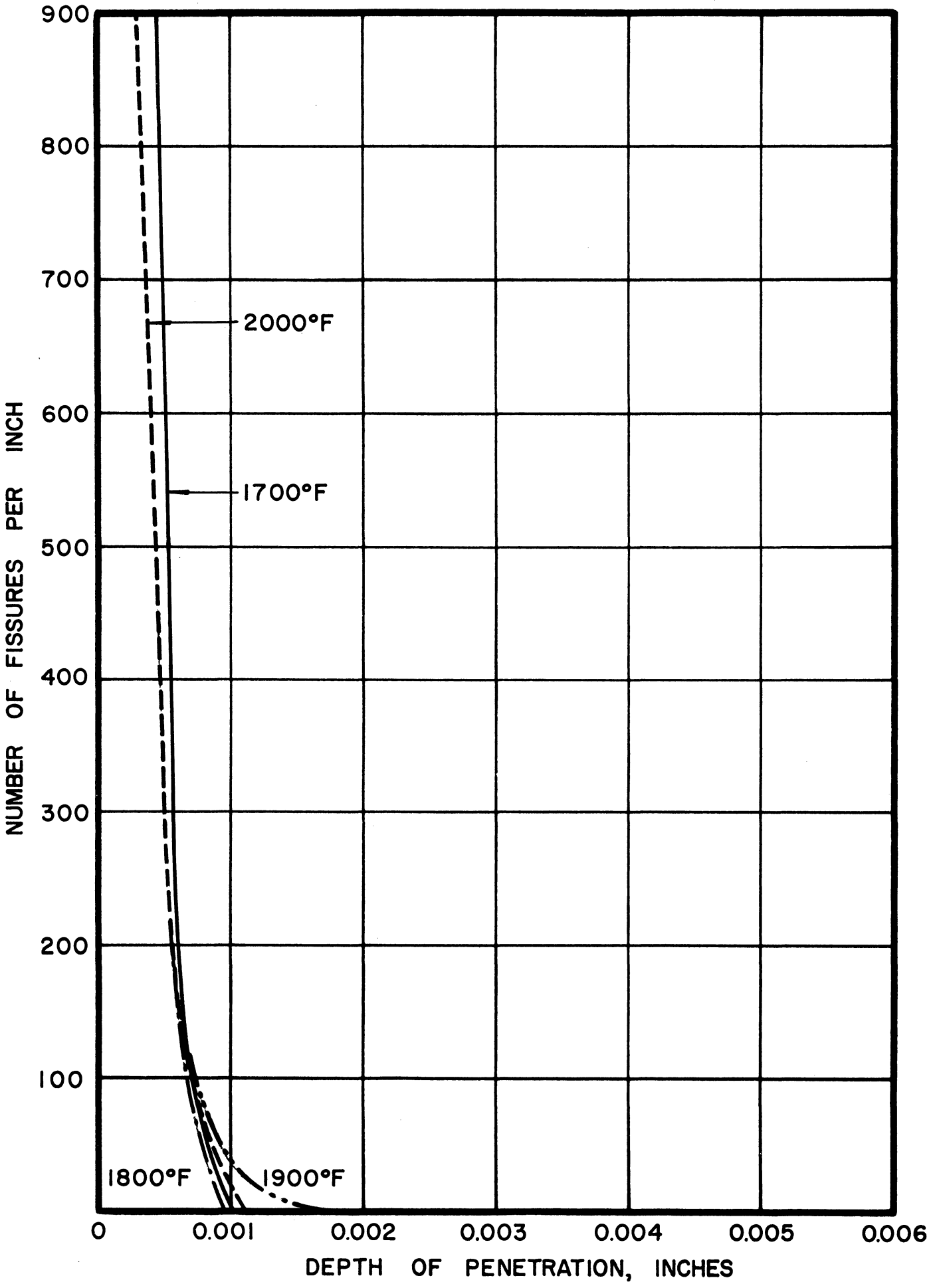

Fig. 107. Penetration vs. Depth Below Surface; Type 310 Alloy, Heat J10, Dewpoint = +60°F, 100 Hours.

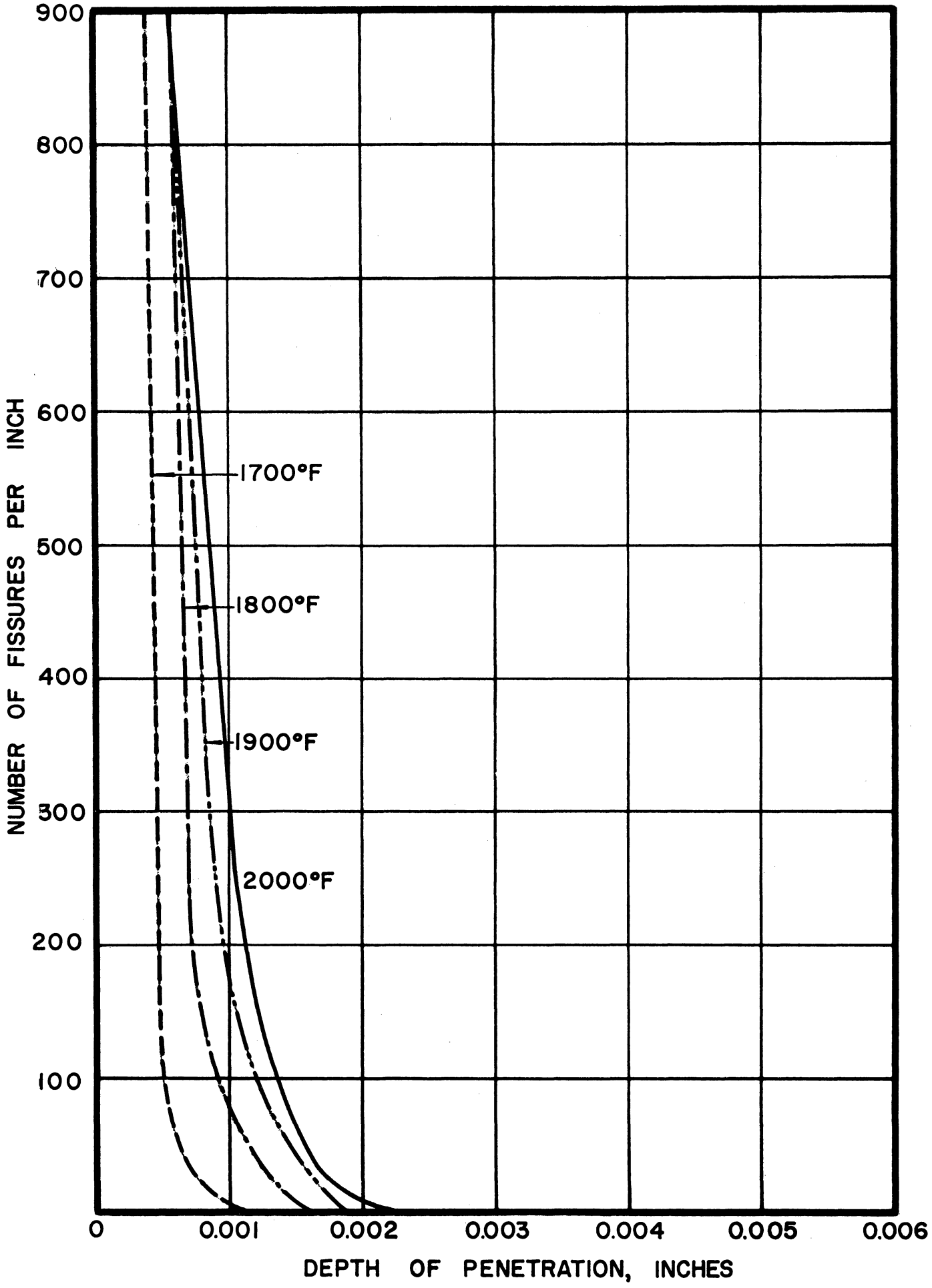

Fig. 108. Penetration vs. Depth Below Surface; Chromel ASM Alloy, Dewpoint = +60°F, 100 Hours.

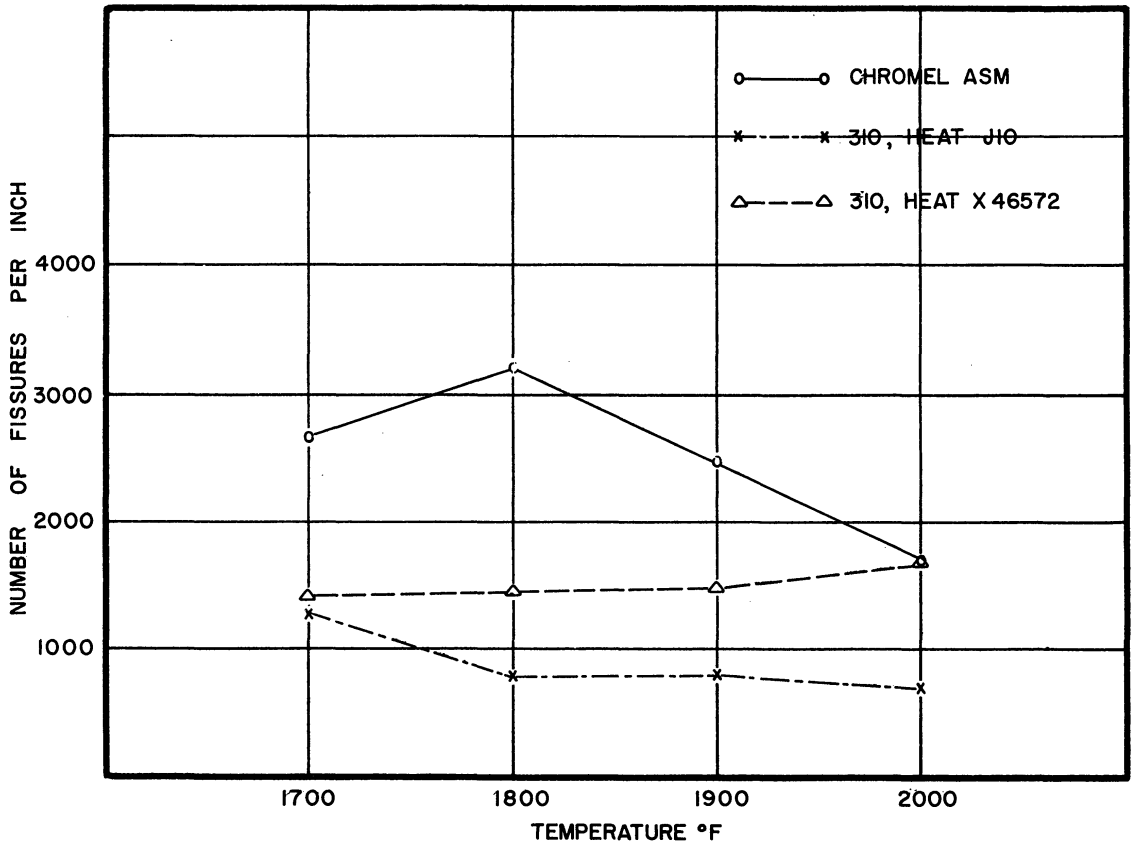

Fig. 109. Summary Penetration-Frequency Curves; Chromel and Type 310 Alloys, Dewpoint = +60°F, 100 Hours.

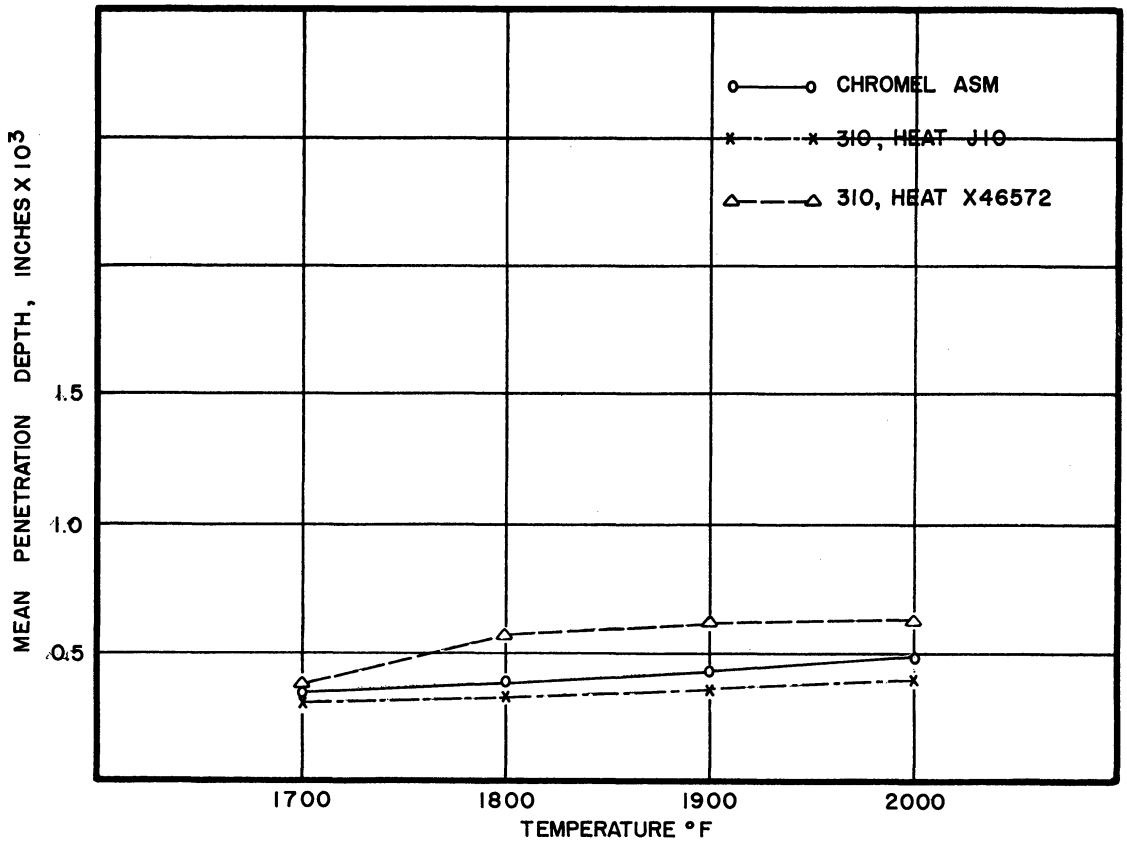

Fig. 110. Summary Penetration Depth Curves; Chromel and Type 310 Alloys, Dewpoint = +60°F, 100 Hours.

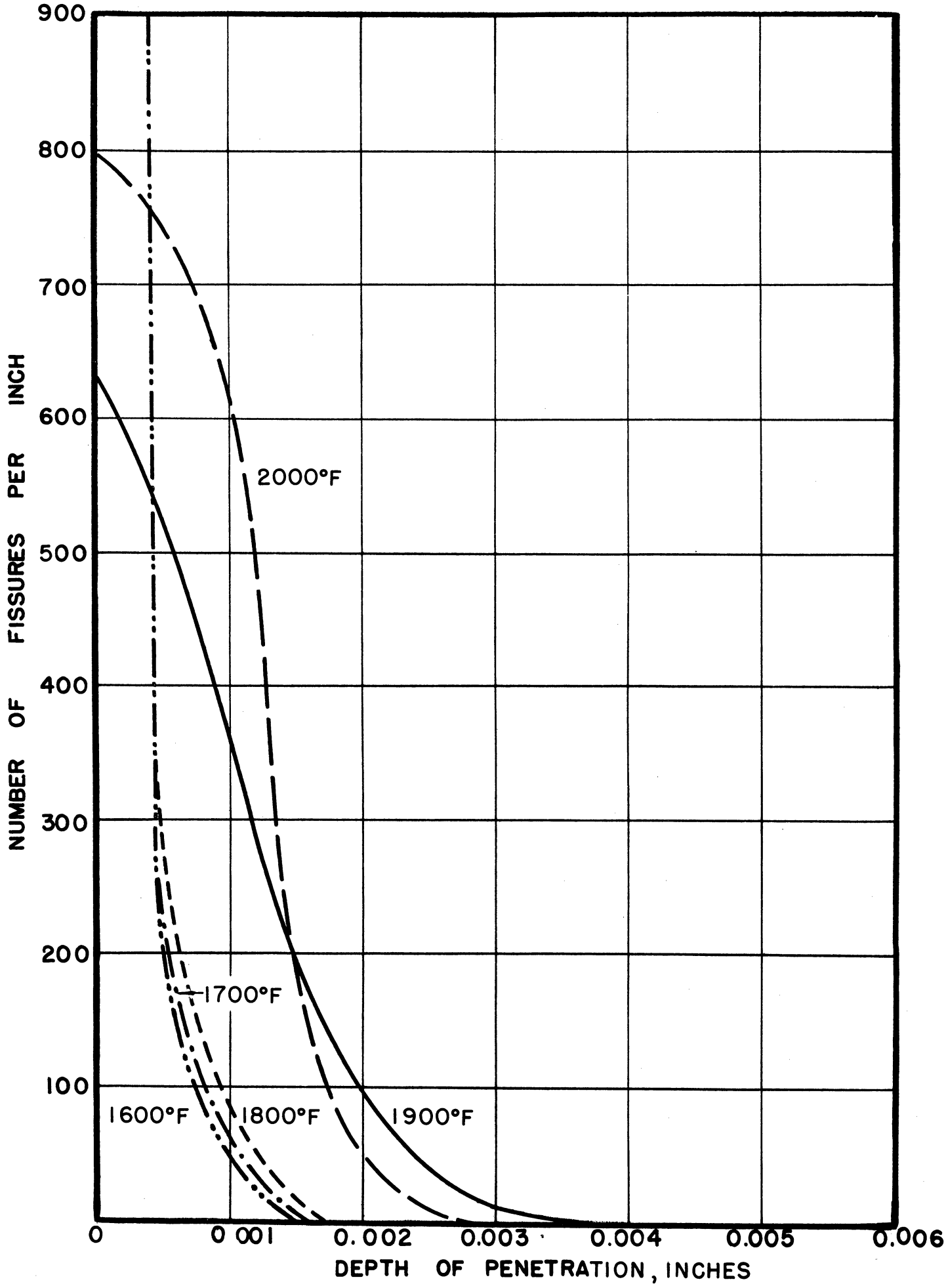

Fig. 111. Penetration vs. Depth Below Surface; Type 310 Alloy, Heat 31372, As-Received, Run 33.

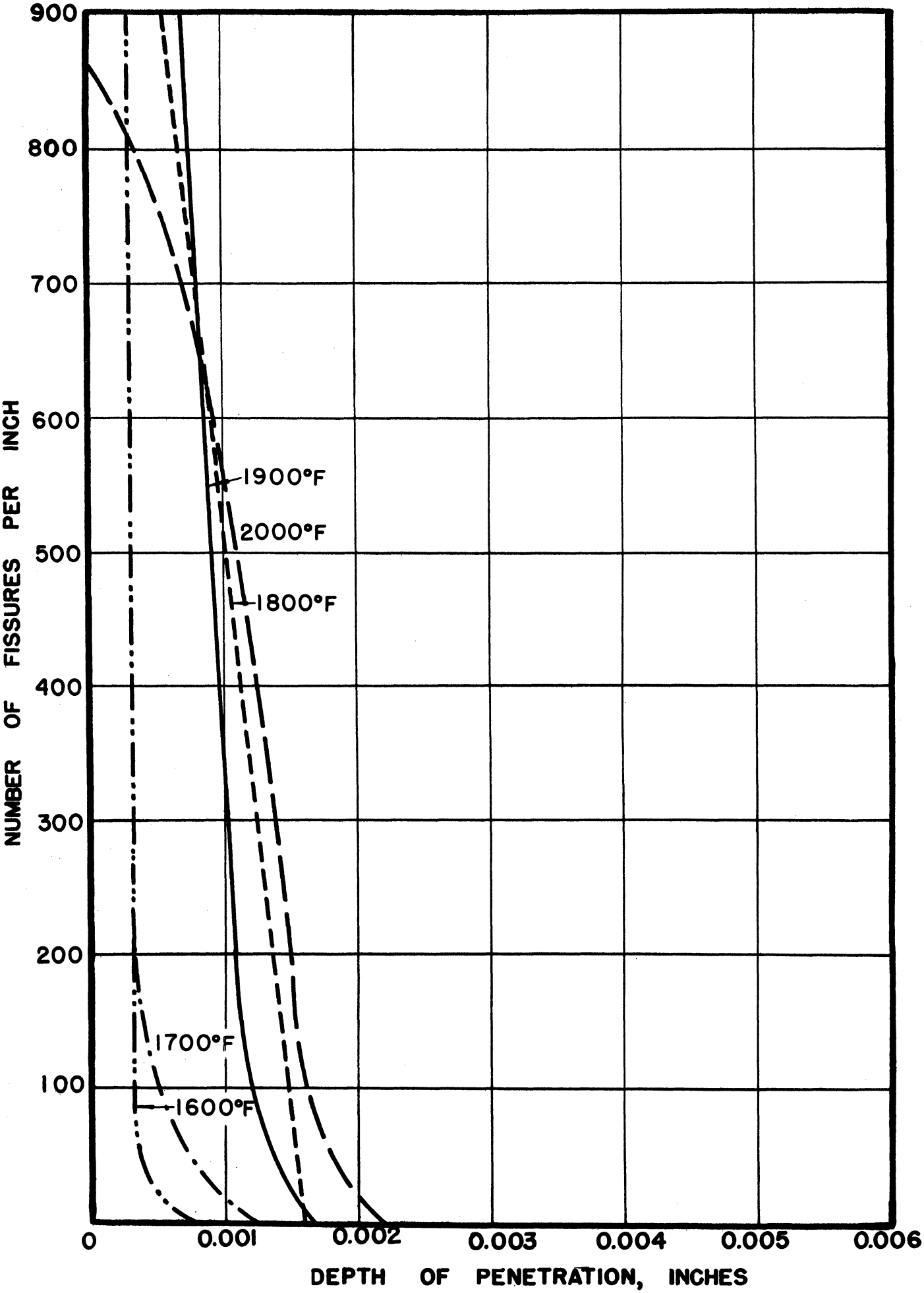

Fig. 112. Penetration vs. Depth Below Surface; Type 310 Alloy, Heat 31372, Reduced 97% and Annealed, Run 33.

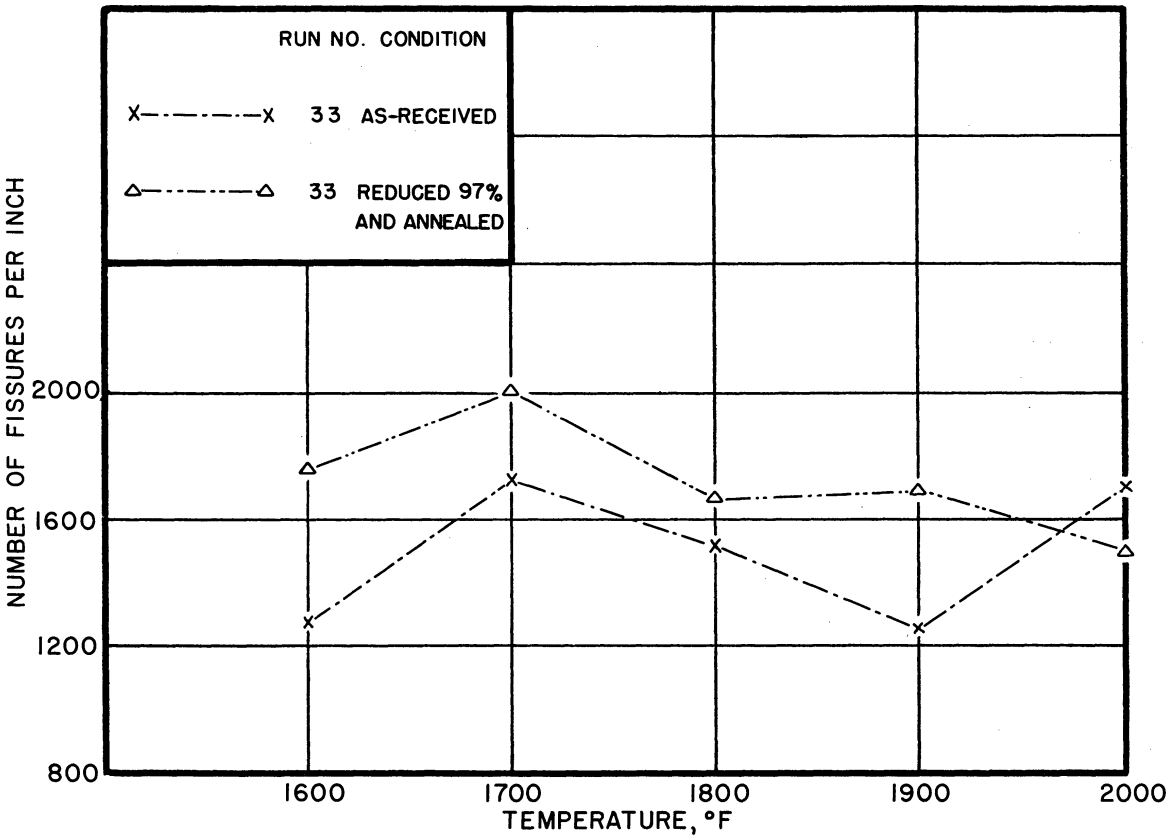

Fig. 113. Summary Penetration-Frequency Curves; Type 310 Alloy, Heat 31372, 100 Hours, Effect of Preferred Orientation.

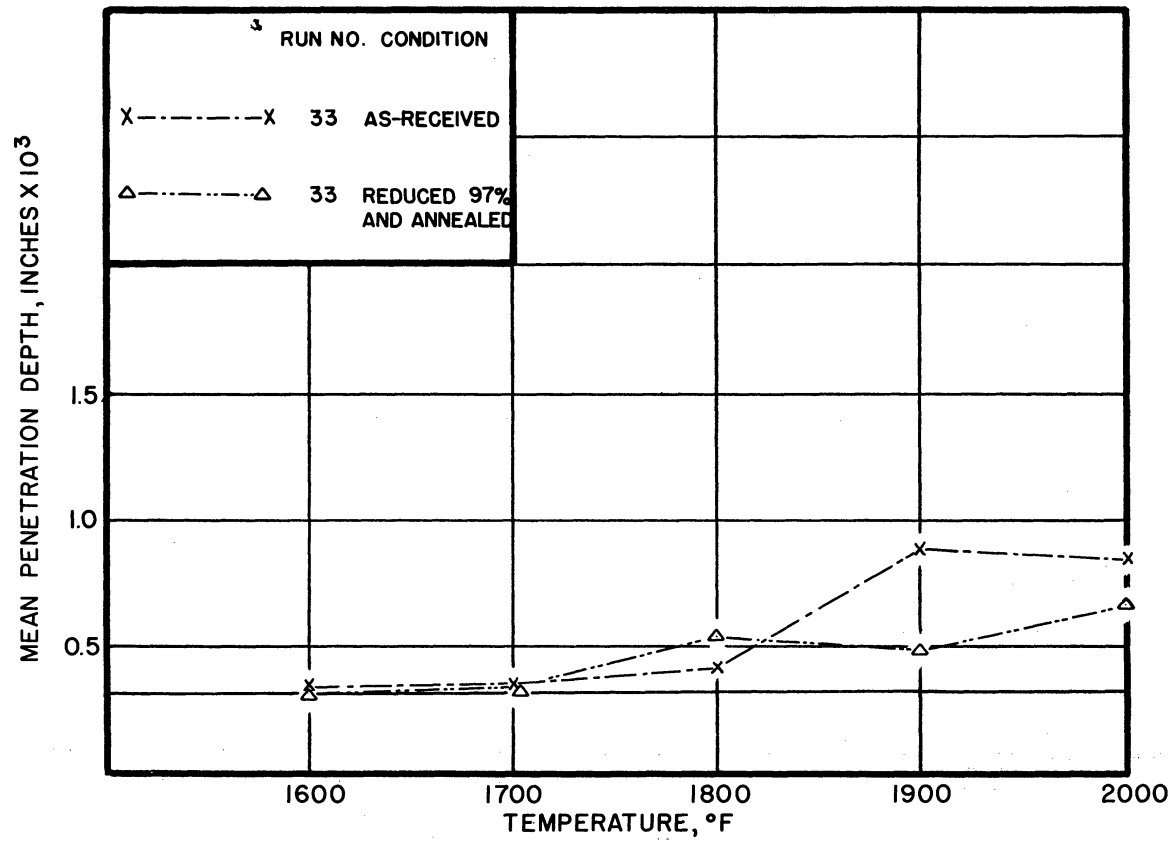

Fig. 114. Summary Penetration Depth Curves; Type 310 Alloy, Heat 31372, 100 Hours, Effect of Preferred Orientation